Foreshore Morphodynamics from Shore-based Marine Radar

On a Stretch of Sylt Beach

L. Lange

in collaboration with
Helmholtz-Zentrum Geesthacht

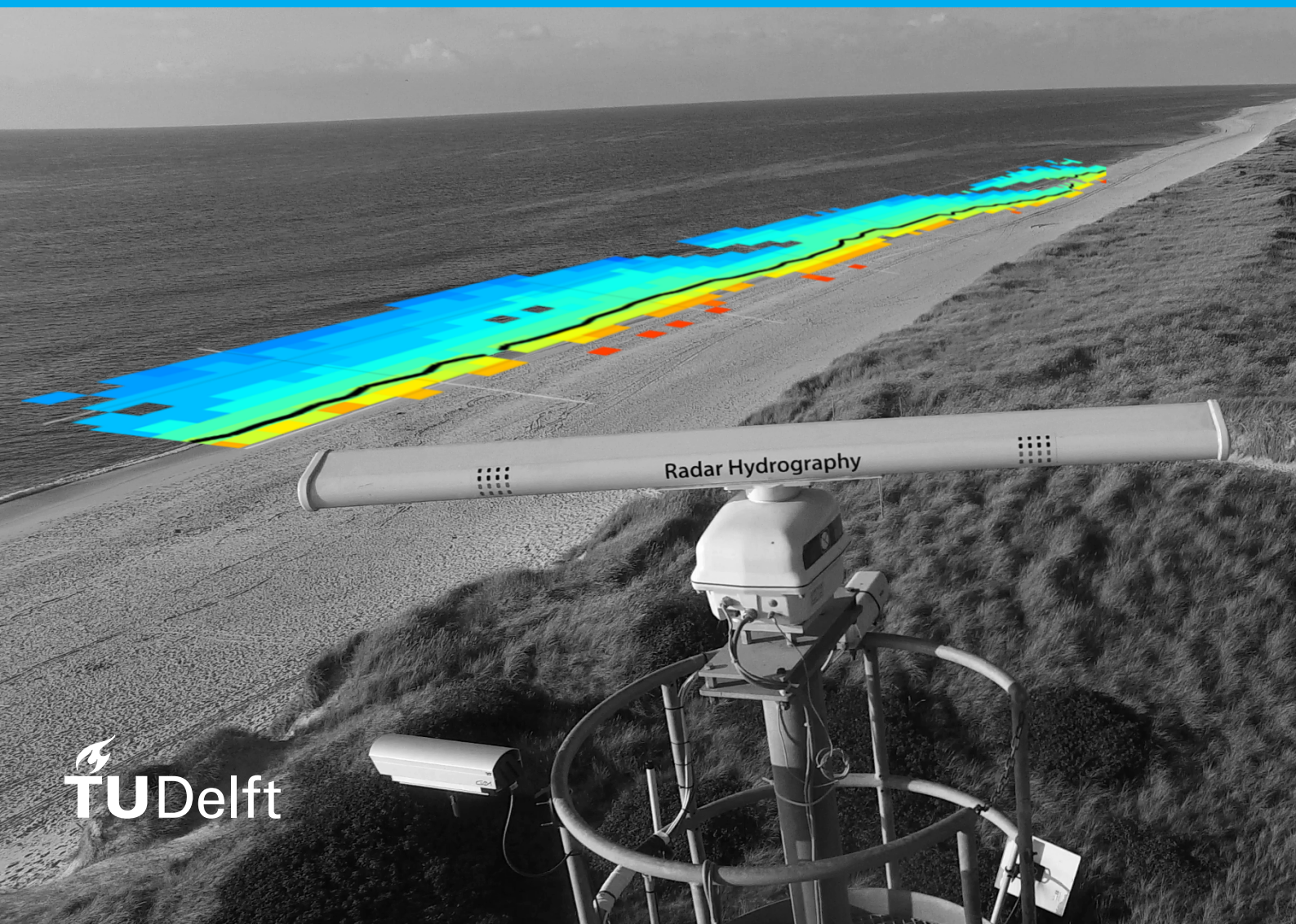

TU Delft

Foreshore Morphodynamics from Shore-based Marine Radar

On a Stretch of Sylt Beach

by

L. Lange

to obtain the degree of Master of Science
at the Delft University of Technology,
to be defended publicly on Wednesday March 6, 2019 at 13:00.

Student number:	4512022	
Project duration:	April 19, 2018 – March 6, 2019	
Thesis committee:	Prof. dr. ir. Stefan G. J. Aarninkhof,	TU Delft
	Ir. Tjerk J. Zitman,	TU Delft
	Dr. ir. Freek J. van Leijen,	TU Delft
Daily supervisors:	Dr. Jochen Horstmann,	Helmholtz-Zentrum Geesthacht
	Dipl.-Ing. Michael Streßer,	Helmholtz-Zentrum Geesthacht

An electronic version of this thesis is available at http://repository.tudelft.nl/.

Cover image: b/w background image by Radar Hydrography group (KOR), Helmholtz-Zentrum Geesthacht, colored overlay based on radar data of this study, not georeferenced, arranged as artistic impression

TU Delft

Contents

List of Figures

List of Tables

List of Symbols and Abbreviations

α	cross-shore beach slope, smoothed over 45 m; beach slope [-]
β_f	upper shoreface beach slope, between 0 and 2 m+MSL; beach slope [-]
$\bar{I}$	time series of mean backscatter intensities
ζ	water level [m+MSL]
d	bed level [m+MSL, m+CD]
g	gravitational acceleration [m/s^2]: $g = 9.81$
H	wave height [m]
H_0	deep water wave height [m]
H_s	significant wave height [m]
L_0	deep water wave length [m], estimation from linear wave theory: $L_0 = (gT^2)/(2\pi)$
R	cross-correlation coefficient [-]: $-1 \leq R \leq 1$
T	wave period [s]
T_p	peak wave period [s]
z	z coordinate, positive upward [m+MSL, m+CD]
BH-CRS	Bunker Hill Coordinate Reference System
BSHcmod	BSH operational circulation model
CD	Chart Datum
CSV	Comma Separated Values (file format)
GIS	Geographic Information System
GLONASS	transliteration: Global Navigation Satellite System (operated by Russian Federation)
GNSS	Global Navigation Satellite System (any satellite-based navigation system with global coverage)
GPS	Global Positioning System (operated by United States of America)
HDOP	Horizontal Dilusion of Precision
HZG	Helmholtz-Zentrum Geesthacht
LiDAR	Light Detection and Ranging
LKN.SH	Landesbetrieb für Küstenschutz, Nationalpark und Meeresschutz Schleswig-Holstein
MHHW	Mean Higher High Water
MHW	Mean High Water
MLLW	Mean Lower Low Water
MLW	Mean Low Water

radar	Radio Detection and Ranging
RDB	Radar-Derived Bathymetry (based on TWA, unreliable parts are filtered)
RTK	Real Time Kinematic
TR	Tidal Range
TWA	Temporal Waterline Approach (by Bell et al. [2016])
UHF	Ultra High Freguency
UTC	Coordinated Universal Time

Abstract

Bathymetry strongly affects nearshore hydrodynamics that drive sediment transport. However, recent bed level information is not always available, especially not simultaneously resolved in space and time. Time series of radar backscatter images can be used to retrieve bed levels in the intertidal area with the so-called Temporal Waterline Approach (TWA) by Bell et al. [2016], yielding a two weeks average bathymetry at spatial resolutions in the order of a few meters. Bed levels are estimated for each radar cell individually by correlating temporal patterns of wet-dry transitions from the radar with hypothetical patterns found in the water level record for different tidal levels.

In this study data recorded by a marine X-band radar located at Bunker Hill station (Sylt, German Wadden Sea island) is used to improve TWA, validate the improvement as well as to show its potential in application. A survey was conducted in May 2018 to provide ground truth. Two modifications are made, that improve robustness and reliability of TWA's output by adding a second threshold and semi-automating the quality procedure. Root mean square error between radar-derived bathymetry (RDB) and ground truth for the intertidal area is 43 cm (bias 12 cm) on a 7.5 m squared grid. Sensitivity analysis of four parameters (i.e. vertical resolution, inclusion of wave induced effects on water level, length and position of analysis window, thresholds in quality check) reveals, that TWA is most sensitive to the choice of thresholds. Sensitivity analysis is utilized to tune TWA to achieve full coverage of the intertidal area (zero coverage elsewhere) with sufficient accuracy. Additionally it is found that at costs of accuracy the period for which averaged bed levels are retrieved can be shortened from 14.5 to 8.3 days. This is promising, because RDB potentially is able to observe short-term changes in the order of a few days (e.g. storm events).

To demonstrate the value of the improved TWA for bathymetry surveys in intertidal areas the method is applied to a 3.2 km stretch of beach in front of Bunker Hill station, capturing the beach state variations in the course of 2017. During wind sea dominated season (winter) a ridge-runnel type of beach is present, that changes to a skewed transverse bar and rip system during swell dominated season (summer). The method is sufficiently accurate and robust for application and proves its potential to reveal new insights, e.g. indications on how the transition between two beach states evolves. In coastal science RDB could serve as a tool to improve existing theories by providing detailed information, that reveals underlying processes. In coastal engineering it fills gaps in monitoring schemes, for example to evaluate effects of nourishment strategies.

Preface

During my Bachelor thesis I used a hydrodynamic numerical model to investigate the limits of sea weed growth in the Wadden Sea. Theoretically I could have known beforehand, but I happened to only realize when I was almost done, that already by definition of resolution in space and time my task was determined to fail (at least with respect to the study goal I euphorically set off with initially). Challenged by a tremendous lack of data: only two years out of ten were covered, anything can be interpolated with that. Since then I believe there must be other ways than assuming a patchwork of decades of bathymetry as representative for one modeller-chosen instant in time. Although less accurate – or maybe only less established – radar technologies have the advantage of all year round any minute operation, downtimes only due to maintenance, repair and heavy rainfall. Is it possible to fill the gaps in numerical modelling with that and actually come to use the 100 % capabilities of our today's numerical models? As I experienced it, reliability of model output is limited less due to insufficient programming or mathematical description of natural phenomena (or computational power, come to that), but rather due to limitations in the input we are able to provide. Causing a lot of effort in calibrating over and over again.

I took this as starting point for my motivation for this Master thesis. Of course the answer to that is way beyond a thesis and therefore it boiled down to the conflict between data we are able to acquire (limited by costs mostly, not necessarily technology) and the phenomena we want to investigate. The shortcomings I experienced during my Bachelor thesis showed that most of the bathymetric data is outdated or not detailed enough, either in space or time or both. Common practices are established based on this prerequisite of inconsistent data – and they work well enough for, for instance, everyday engineering work at the coast. Yet several decades of scientific work are spent to get one consistent data set. So I took out in this thesis to find, if radar actually proves its potential to fill some of the gaps.

In that I would like to thank my daily supervisors Michael Streßer and Jochen Horstmann, for treating me more like a scientist than a student and the often rather political discourse about science. The latter especially important to mention, because usually it is not considered a part of scientific training – but always should be. My daily supervision extended even further and I'd like to thank all members of Radar Hydrography for their interest in my work and troubles, as well as their support with ideas, look-ups, information and hardware (be it hard drives or ancient GPS devices). Come to that, I seized as much as possible of the opportunities a research center like HZG has to offer. I could not only attend seminars from other disciplines, but was also welcomed to join any internal meetings, which I actively did. All this extra-curricular activities went at costs of my precious thesis time, and I'm thankful for the patience and supportive feedback my committee had for me.

I deem the whole journey through my thesis a meaningful outlook for a PhD project. Not only method-, troubles- and content-wise, but also with respect to the social side of science, that is communicating (with various means and in various contexts) with those who were neither officially nor inofficially involved with my thesis. Any time Christian Winter asked me to show my progress, it boosted my motivation. The same holds for the (mainly digital) conversations with his student Sebastian Hein, who worked on a similar project like mine in the exact same area. He was the one who pointed me at the possibility to track nourishments. I was also given the opportunity to join a get-to-know meeting for studies conducted on Sylt. As often as possible I took the challenge of presenting my work to an audience and I'm glad that I was given this opportunity not only by the Institute of Coastal Reasearch (HZG), but Ludwig-Franzius-Institute (Leibniz Universität Hannover) as well.

Last but not least, I was lucky to mainly be in charge myself of the data I needed. Yet, I was glad that Arfst Hinrichsen (LKN.SH) and Thorger Brüning (BSH) – whenever I called for it – gave easy and fast access to any additional data I required. To anyone who considers working with radar data I'd like to recommend the extensive knowledge base of radartutorial.eu, like it was recommended to me when I started with my thesis.

L. Lange, Kiel, February 13, 2019

1

Introduction Why Marine Radar May Reveal New Insights

The coast and coastal zone are popular for living, recreation, sports and food. But attracted people and their properties are at risk. People are dragged offshore by rip currents and drown. Houses and agricultural areas are flooded during storm surges or being destroyed by big waves. Those threats are met by various strategies. Coastal protection measures are designed to protect the coast from flooding and wave impacts. Coastal engineers and scientist make a joint effort to combine the human need for safety and our responsibility to leave nature undisturbed where possible. Disruption of equilibrium state is minimized by taking into account the variable nature of the coastal zone, which is connected to coastal processes evolving on large and small scales, in space and time. Often this requires data that resolves small scales of space and time simultaneously, to feed an empirical analysis or a numerical model for example.

Numerical models become common in coastal engineering practice and coastal science and they are already more advanced in their capabilities than the ability to use them. Limitations today are for instance found in definition of boundary and initial conditions. Methods to survey those quantities are limited – mainly due to costs, but also by physics. Current survey schemes are usually sufficient for large scale investigations. But with the availability of small scale data models can advance and for example investigate processes in highly inhomogeneous regions. Detailed information in time as well as in space is prerequisite in such investigations. Bathymetry is an important input in sediment modelling. Gradients in sediment transport cause erosion and accretion, which is a potential threat to humans living at the coast and one reason for the relevance of sediment modelling. Established methods of mapping are either limited in their temporal or spatial resolution. Most schemes monitor only once a year (e.g. LiDAR, echosounding) but cover a large area with high resolution up to 1 m grids and accuracy in the order of centimetres in height. Higher sampling frequencies often can only be achieved by reducing spatial resolution and extent, which eventually results in point measurements of time series. To account for this lack in information usually interpolation is used or models are run prior to the actual investigation, which introduces interpolation errors and uncertainties. Instead marine (or nautical) radar proves to be a promising survey method for mapping an area with a sufficient spatial resolution and at the same time resolve temporal scales down to hours. Stive et al. [2002] point out that small spatial scales are linked with short temporal scales and conclude that it is important to have measurements that capture both at small scales (see their Table 1a and b). This comes at costs of spatial coverage, which cannot go beyond the radar range and commonly is in the order of a few kilometres.

Before empirical analysis methods or numerical models are employed it has to be tested if radar-derived quantities contain the required information. This work therefore investigates the potential of radar-derived bathymetry in tracking foreshore phenomena either natural like storm events or anthropogenic like nourishments, as well as for identifying beach states in the course of one year from time series of radar-derived bathymetries. If this kind of information is contained in radar-derived bathymetry, this reflects its potential to serve not only as a device to observe and investigate foreshore morphodynamics, but also as a tool to numerical modelling.

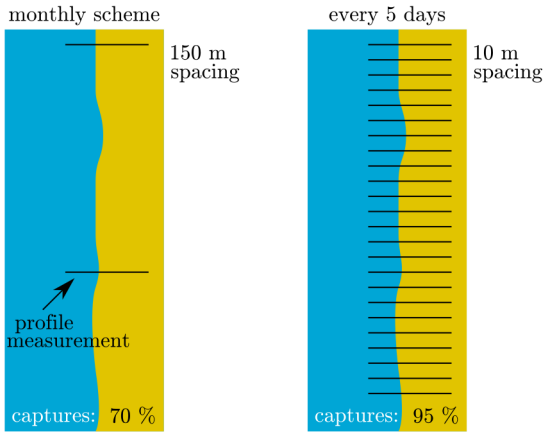

Figure 1.1: temporal and spatial scales of a monitoring scheme determine how much variability is captured **source:** visualization based on values from Blossier et al. [2016]

1.1. State of the Art in Monitoring Coastal Zones

Monitoring of coastal zones is performed in various ways on various spatial and temporal scales. Mapping bed levels of subtidal and intertidal areas is commonly used to gather data for nourishment design as part of coastal protection measures. This study focuses on the intertidal area. Established schemes to map it are airborne laserscans (LiDAR), echosounding from ship (during high tide) and land-based GPS surveys. All three of them are capable of spatial resolutions in the order of 1 m and better, with accuracy of bed levels in the order of centimetres, but they are labour-intensive and costly. Which is why monitoring schemes often do not reach better sampling frequencies than a few times per year. For most of them also environmental conditions play a role (wind, waves, rain), which additionally limits their actions to non-storm seasons. These shortcomings can be overcome by a marine radar operating at X-band frequency, mounted to a shore-based station (e.g. Bell et al. [2016]), a platform (e.g. Carrasco et al. [2017]) and even to a moving vessel (e.g. Bell and Osler [2011]). Current monitoring schemes on Sylt (profiles up to four times a year) provide information about roughly 45 % of shoreline variation, whereas monitoring every two weeks captures more than 80 % [Blossier et al., 2016]. Fig. 1.1 visualises the effort in increasing the captured variability up to 95 % by means of profile measurements. A monthly scheme with profiles 150 m apart is already uncommon, because it is a lot of work. To capture even higher morphological variability not only the temporal interval has to be refined, but the spacing of the profiles as well, which comes close to a two-dimensional measurement. A marine radar collecting images every hour for ten minutes can provide a map of the intertidal area every two weeks (e.g. Bell et al. [2016]). Besides that other methods have been developed for marine radars to monitor the coastal zone. Methods are based on instantaneous backscatter intensities, on averaged intensities or their standard deviations. Time series of instantaneous radar images are used to retrieve sea states (wave spectra) (e.g. Nieto Borge et al. [1999]), to identify individual waves and their properties (e.g. Nieto Borge et al. [2004]), to retrieve current fields and subtidal bathymetry (e.g. Bell [1999], Friedman [2014], Holman et al. [2013], Senet et al. [2008]), to estimate wind gusts or track activity of mammals (e.g. McCann and Bell [2017]). Whereas mean (time averaged) intensities are used for wind field retrieval (e.g. Dankert [2003]), bathymetry retrieval (e.g. Bell et al. [2016]), or localisation of submerged bars by localising the bar induced breaker zone (e.g. Ruessink et al. [2002]). Standard deviations of backscatter intensities can be used to extract bathymetries in a similar procedure like Bell et al. [2016] present for mean backscatter intensities. A project with this objective preceded this study at Radar Hydrography group (HZG). Some marine radars are equipped to receive coherent signals (coherent or coherent-on-receive). Next to intensities they record speeds of the scatterers, too, so-called Doppler speeds. Doppler speed is physically different to the mechanism behind intensities and therefore the combination of both allows comparison (validation) of the same events recorded within one device, which usually is not possible. This way calibration of individual radar stations may become obsolete [Horstmann et al., 2015]. The Doppler radar is not used in this study, but further studies may prove it as another source for bathymetry retrieval (amongst other possibilities to use Doppler speeds). It is

Figure 1.2: want to measure vs. able to measure – How does it come together?

promising because it may serve as a tool to detect orbital velocities of surface gravity waves. Because of costs and increased complication in interpretation dopplerised radars are not commonly in use.

Marine radar operating at X-band has already been used successfully to map subtidal areas. Intertidal areas are mapped with established methods at the costs of either few points in space or low sampling frequencies. Marine radar collects both, spatial and temporal information at high rates. Its capabilities should be used to investigate common hydraulic engineering questions, like sediment transport on the foreshore. Radar techniques have high potential in resolving more details of coastal processes, and therefore offer a unique opportunity to reveal new insights in known processes.

1.2. Study Objective and Concept

A link (i.e. method) has to be found between the processes to be studied and the possibilities offered by devices to measure those. Fig. 1.2 contrasts the foreshore processes with radar output. Despite scientific work showing examples for successful and feasible application of marine radar the attention given to radar techniques in monitoring coastal zones is low. Investigations made during this study therefore aim at answering two study questions:

1. What is the added value of operating shore-based X-band marine radar?
2. How does the distinct channel-shoal pattern of Sylt develop in the course of one year?

This report begins with presenting the Theory of Radar Technology and Morphodynamics (Chap. 2). Those two fields are combined within this study to tackle the two study questions above. The following chapter introduces the Study Area and Data Availability (Chap. 3). Chapter Methods (Chap. 4) describes in detail how foreshore bathymetry is derived from time series of radar images. This serves a basis for morphodynamic analyses. It is followed by a Validation and Discussion of Radar-derived Bathymetry (Chap. 5). A survey was conducted to collect ground truth. On this basis not only a validation is performed, but also a sensitivity analysis of the method. The latter is quite important, because the method has been published recently and so far no more applications of it are known to serve as reference on how to apply it in another study area. The first study question is analysed in Chapter Applications (Chap. 6). Here the evolution of beach states in the course of one year is extracted from radar-derived bathymetry. Chapter Discussion (Chap. 7) deals with the two study questions and Chapter Conclusions and Outlook (Chap. 8) finalizes this study with a wrap-up of the work and a glimpse on follow-up projects.

2

Theory of Radar Technology and Morphodynamics

2.1. Backscatter Measured by Marine Radar

2.1.1. Radar Technology in General

An active remote sensing technique like radar is characterized by transmitting defined electromagnetic waves and receiving their reflections off surfaces (so-called backscatter). The received signal consists of uncalibrated backscatter intensities, often denoted with the unit dB. Passive remote sensing techniques are limited to receiving only. They record electromagnetic waves that are present, like optical cameras that capture waves from the visible light spectrum. Polarized antennas are used to transmit and receive. Either transmitting and receiving capabilities are both vertically (VV), or both horizontally (HH) polarized, or a combination of both (HV or VH) [Streßer, 2014]. HH polarization is more commonly used than VV. X-band refers to a frequency range of 8 to 12 GHz [ITU-R, 2015, TABLE 4] (i.e. 3.75 to 2.5 cm wave lengths).

2.1.2. Bragg Scattering Measured by Shore-based X-band Marine Radar

For X-band marine radar at moderate grazing angles backscatter is predominantly related to an interference effect called Bragg scattering, that occurs between the transmitted electromagnetic waves (e.g. λ=3.2 cm) and sea surface roughness elements with $\approx \lambda/2$ (e.g. 1.6 cm), so-called Bragg waves [Carrasco et al., 2017]. Therefore backscatter intensities strongly depend on wind, that is sufficient to produce enough Bragg waves [Trizna and Carlson, 1996]. Bragg waves are modulated by tilt and hydrodynamic conditions (e.g. surface currents, wind drag, orbital motion of waves) [Carrasco et al., 2017]. This modulation patterns are visible in the backscatter and can be analysed to retrieve for instance sea states. Additionally the backscatter contains shadowing effects. For low grazing angles (so-called grazing incidence) geometrical shadowing becomes more important [Nieto Borge et al., 2004]. This effect increases with range. For VV polarization shadowing is more pronounced than for HH, which relates to the diffraction of the radar beam behind a shadowing wave crest (see for instance Figure 1 of Plant and Farquharson [2012]). At grazing incidence and HH polarization effects like wedge scattering (mechanism described by Lyzenga et al. [1983]) and micro breaking are more dominant than for VV [Carrasco et al., 2017]. Sudden increase to extreme values (i.e. 'spikes') in the received signal are another (non Bragg) effect, which is referred to by 'sea spikes'. The combination of Bragg scattering and sea spikes is also referred to as sea clutter [Bell et al., 2016], which is distinct from target detection for example. The cause for sea spikes is under debate and more than one mathematical definition exists. Bell et al. [2016] contribute sea spikes in their data to breaking and steep waves, which is shared by most scientist. See Section '6.6 Spiking' by Lee et al. [1995] for in-depth discussion on spiking events and definitions and Jessup et al. [1990] for an experimental investigation.

The radar itself is located above the sea surface. The resulting angle with the sea surface is called grazing angle. See Fig. 2.1 for a definition sketch. Distinction is made between low, moderate and high grazing angle ranges (grazing angle varies with distance to the radar). Shadowing is one effect that is related to grazing angles (for an investigation of geometrical and partial shadowing see for example

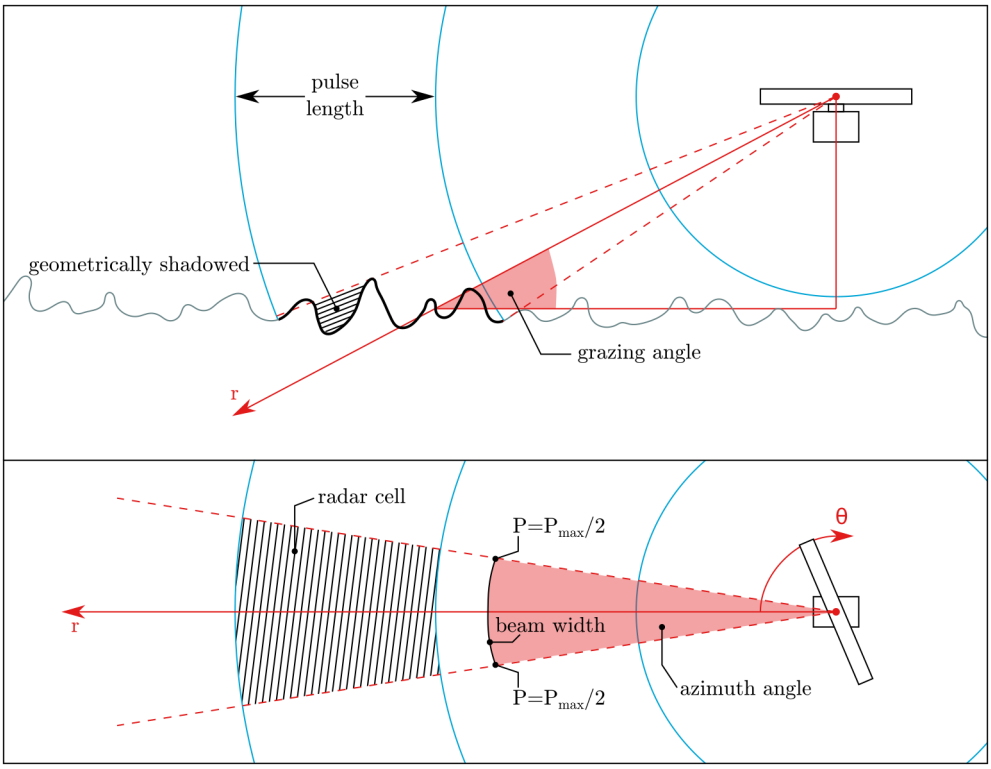

Figure 2.1: definition sketch of radar scattering **top:** (cross-shore) side view **bottom:** topview **P:** power ∝ backscatter intensity

Plant and Farquharson [2012]). The radar beam in the bottom panel of Fig. 2.1 is simplified as a beam bounded by straight lines, but physically it is rather drumstick shaped. The beam width is defined as the azimuth between the points, where the power is half of the maximum power. It determines amongst others the spatial resolution.

The rotating radar collects data in polar coordinates (range r and angle θ in bottom panel of Fig. 2.1). For practical reasons (e.g. computational efficiency on equidistant grids) those are converted to Cartesian coordinates. Radar cell size depends on sampling frequency and beam width, which can be influenced with the operational mode, but is also limited by the radar hardware. Bell et al. [2016] use squared cells of 3.75 m, whereas the Bunker Hill radar operates at 7.5 m. The further away the less (polar) datapoints are available to make up one (Cartesian) cell. This is why information far away from the radar tends to be more smeared, even over more than one cell, than close to the radar. Another range dependent effect is the power decay, which some applications correct for. Furthermore in order to obtain information in the horizontal plane, it may be neccessary to correct for antenna height (see grazing angle in Fig. 2.1). For low grazing angles in relation to the scales of the study objective the antenna height correction may be neglected. Especially in studies that aim at retrieving bed levels antenna height correction would have to be applied iteratively, since the bed levels for which shall be corrected are unknown prior.

Due to the nature of the radar beam and receiving procedure the output constitutes a continuous geographical field, which is intrinsically different from measurements constituting point clouds. This field of data becomes especially useful, if it can be related to geographical coordinates. Like camera images, radar images are georeferenced with the help of objects with known coordinates, that are identified in the backscatter image. It is however less straightforward than for camera images, because only one quantity (i.e. intensity) is available, which makes identification of objects and matching them correctly more difficult.

2.1.3. Interpreting Backscatter Maps

Radar backscatter images require more interpretation than for instance camera images. The latter is more intuitive, because it is what everyone observes on a daily basis. Camera images may consist of

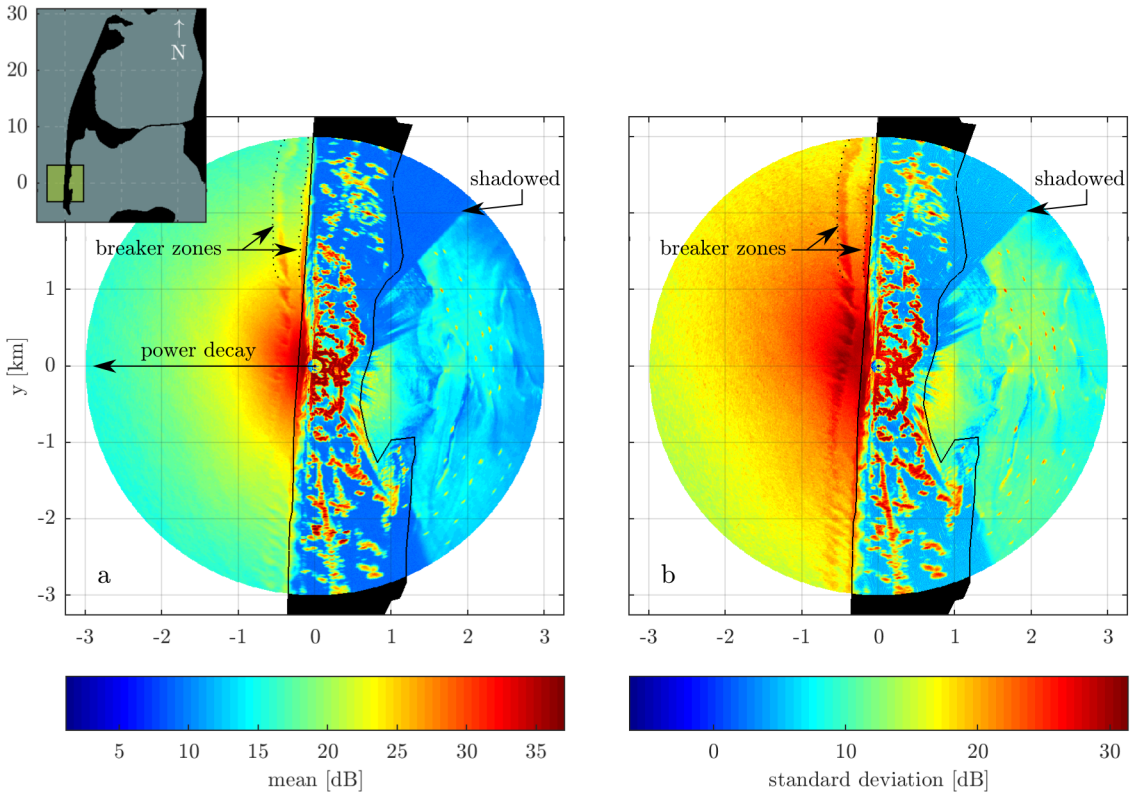

Figure 2.2: examples of radar images and their interpretation **a** mean **b:** standard deviation **data:** radar record covering about 10 min from May 16, 18:00, 2018

three color channels, brightness and saturation, whereas a radar image only shows intensities, from low to high. In order to distinguish different surfaces it should be known prior which kind of environment is monitored, e.g. if mostly land, or sea. This way lines of high intensities can be narrowed down to a vessel, over a truck. Furthermore radar backscatter intensities are amplified, either logarithmically (e.g. Bell et al. [2016]) or linearly (e.g. [Carrasco et al., 2017]). In both cases high returns increase even more. For the logarithmic amplifier high returns increase (relatively) more than for low returns, whereas it is the same amplification for all returns in a linear amplifier. The latter therefore should produce less intense sea spikes.

The following rules are basic to the interpretation of images from X-band shore-based marine radar. On the scales observed with a rotating radar (order of seconds for one rotation and roughly spatial scales in the order of couple of meters) land usually does not move, whereas coastal waters are well variable on such scales (e.g. wave motion). Therefore a look at time series (i.e. standard deviation of intensity in one cell over time) can reveal areas of land and water. Other examples for large variations in intensity are passing vessels, (spatially) moving breaker zones or tidally driven variations of the waterline. Next to variation in the signal also mean backscatter intensities are related to certain surfaces. Such statements are qualitative. Low mean intensities are observed for parts of the land, however some objects yield very high returns (see Fig. 2.2). Returns from water surfaces strongly depend on wind speed and direction. The more wind, the higher the returns.

Wind strongly influences the information visible in radar images. If wind speeds are too low, such that water surface does not yield enough roughness elements to produce significant Bragg scattering, radar images do not contain enough information for a reliable interpretation. At X-band frequency rain is detected and therefore also used for weather radars. For applications in the coastal zone rain events can render radar images useless, due to changes in sea surface roughness induced by rain drops [Braun et al., 2002]. One radar may produce interference patterns with a second radar. Those show as certain patterns in the radar image. Such artefacts can hinder the analysis procedure. Other unwanted appearances of objects for studies in the coastal zone are people, birds and other animals.

Often those are averaged out in mean images. Objects like mounted buoys or piles remain. Because of the approximately sphere shaped sent signal of the radar very high objects, like a radio mast, may appear closer or farther away in the radar image than in reality. This effect is negligible for the water surface, which is approximately a plane and any water movements (e.g. waves, tides, other water surface deflecting processes) are small in comparison to heights that would be needed to cause a shift visible on a grid with a resolution in the order of couple of meters. A radio mast of about 165 m above radar, about 2 km away from the radar was estimated to appear shifted by maximum two cells.

This section introduced rules to interpret backscatter images from shore-based marine radar operating at X-band frequency purely based on considerations from radar physics. Additional information can be gathered based on the characteristics of the area covered. Coastal zones are strongly influenced by hydrodynamics, which in turn alter the morphology. The resulting morphological features, like bars, channels and the beach itself, show as distinct features in radar images, when dry during ebb. In turn morphology alters hydrodynamics during flood. Those modulations of ocean surface waves is visible in radar images, too. Understanding of hydrodynamic and morphodynamic processes is therefore crucial, when observing coastal zones with a radar. The following section provides an overview of these processes.

2.2. Morphodynamics on a Mixed-energy Coast

Nomenclature in coastal zones is not standardized. [CEM, 2002a] therefore seek scientists to precede their work with a sketch and definitions, which is provided in the first section of this chapter. The next two sections sketch hydrodynamics and morphodynamics at stake as well as their link. This is concluded with detailed information about aspects that serve as basic knowledge to the study.

2.2.1. Definition of the Coastal Zone

The coastal zone is the transition zone between land and sea, that is under direct influence of marine processes. The extent of the transition zone strongly depends on field of application/research, researcher or study objective. For this study it is referred to definitions given by CEM [2002a]. CEM defines the landward boundary at the highest reach of strongest storms. The seaward boundary is set at the continental shelf break, which is distinguished from shoreface by its slope [CEM, 2002a]. Alternative seaward boundaries are for example the deep water limit for waves in linear wave theory or depth of closure. Water is deep, if no effect of waves on the sea floor is present, i.e. they are fully dispersive, which approximately is the case for relative depths d/L of 0.5 or larger (classification limits presented in CEM [2002b], their Table II-1-1). Depth of closure is used in the definition given by Kraus et al. [1998] for two reasons. Their definition is optimized for wave-dominated coasts with pre-dominantly cross-shore sediment transport and its intention is to serve as engineering tool for nourishment (beach-fill) designs [Kraus et al., 1998]. Aragonés et al. [2018] alternatively list a geological perspective based on sediment cores on depth of closure [Wallace et al., 2010] and an analytical approach based on linear wave theory (including full range of relative depths, and not only shallow water) [Ortiz and Ashton, 2016]. Aragonés et al. [2018] present a fourth approach in which they utilize the cross-shore grain size distribution to estimate depth of closure.[1] Deep water limit, depth of closure and even the continental shelf break are linked via processes at stake. For each of them another process is most dominant, which is site-specific and depends on the study objective at hand, too. Waves are one main driver for sediment transport in the coastal zone. Depth of closure therefore coincides roughly with deep water limit, where in deep water only weak (tidal) currents are available to transport sediments (low sediment transport). For this study rather depth of closure is of interest, as depicted in Fig. 2.3. Note, that coast is the onshore, dry part, next to the coastal zone. Between the shoreface and the coast lies the shore. It extends from mean lower low water (MLLW) line up to the highest reach of storms, somewhere at the foot of the dunes, which marks the coastline. Inbetween is the mean higher high water (MHHW) line, which marks the foreshore. The foreshore is also known as intertidal zone or area, as will be investigated in this study. Anything below MLLW is subtidal.[2] Waves approaching the intertidal area are already shoaling. They enter the intertidal area mostly breaking, which is therefore almost entirely surf zone. Note, that

[1] See Introduction part by Aragonés et al. [2018] for history of depth of closure formulations.

[2] Several publications exist that derive bathymetries from radar images in subtidal areas, e.g. Bell [1999], Friedman [2014], Holman et al. [2013], Senet et al. [2008]. This study focusses on the intertidal area instead, based on work of Bell et al. [2016].

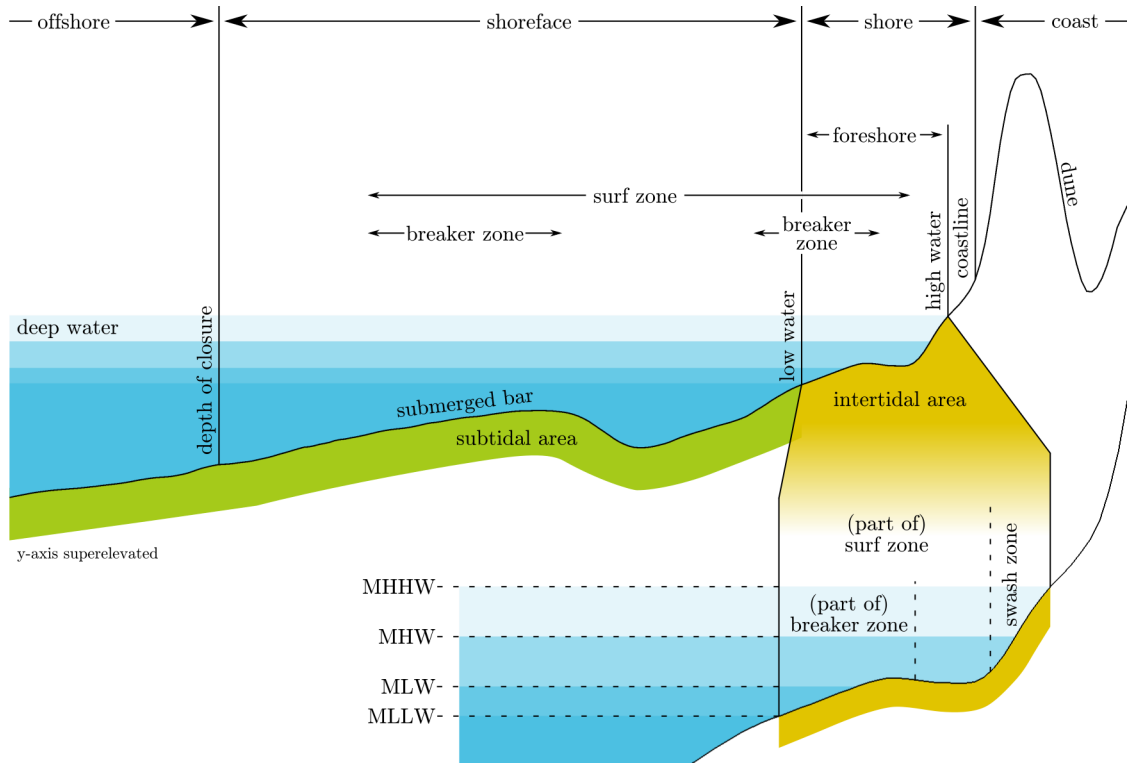

Figure 2.3: subdivisions of coastal zone (sideview) **ambiguity:** boundaries vary with tide, waves, wind and other forces **data for illustration:** profile from echosounding and GPS, Sept 2016, water levels from Westerland pile (see also Tab. A.3) **source:** based on nomenclature and definitions of CEM [2002a], profile from echosounding and GPS, Sept 2016, water levels from Westerland pile (see also Tab. A.3)

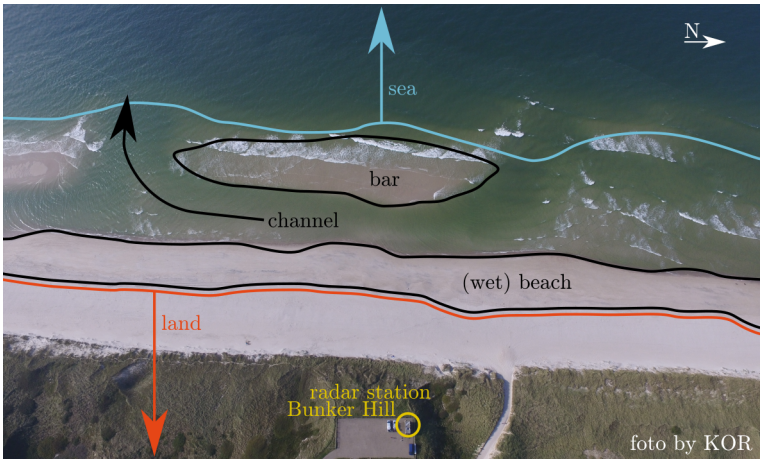

Figure 2.4: morphological features in the coastal zone (topview) **captured:** Oct 2015

the term nearshore refers to the shoreface. This study therefore describes foreshore morphodynamics (as opposed to nearshore morphodynamics from radar for subtidal areas). With this subdivisions the respective transformation of waves is mirrored, which allows to dedicate certain processes to certain subdivision. For all subdivisions given in Fig. 2.3 holds, that the limits are never strict and usually vary over time and are additionally blurry for each time step. Relative depth for instance is a measure that relates to an individual wave. Even if a mean wave length is used, this still implies that some of the waves are affected by the bottom earlier than this, and some just later (since there is never a regular sea state). Alternative subdivisions of (sandy) coasts are available. Each serves another purpose with respect to the problem at hand, as for example light penetration depth for ecological studies.

This study focuses on soft coasts with fine to coarse sand. In general sandy coasts exhibit dynamic behaviour on scales down to hours and even shorter, because of the mobile nature of small grains (as opposed to rocky coasts). Morphological features are governed by this. Fig. 2.4 shows characteristic features present in the coastal zone of mixed-energy coasts to define the nomenclature used in this study. Other names for bar are ridge or shoal. The channel that lies between a bar and the (wet) beach, thus runs parallel to the coast, can also be referred to as runnel. A channel separating two bars exhibits a strong offshore directed current and is called rip (channel). A waterline describes the line the current water level causes on land. A shoreline often is set at MSL or the mean tidal level, but may also be an isoline of arbitrary level, that is handy for the case at hand. Within this study beach refers to wet beach. Runnel and rip are only used, if their distinct characteristics are important. The length of a bar is measured parallel to the coast, whereas its width is measured in cross-shore direction.

2.2.2. Brief Introduction to Hydrodynamics at Stake: Tide and Waves

A mixed-energy coast is shaped by tidal and wave forcing alike. Riverine input is absent or marginal (relatively). At the coast tides manifest as periodic water level changes with accompanying currents. Usually tides are described whether water levels peak once (diurnal) or twice (semidiurnal) a day (i.e. period). Additionally tidal range (i.e. at first guess twice the amplitude) is used to indicate its magnitude. Tides are commonly described by a sum of so-called tidal constituents, each consisting of a sinusoidal wave with various periods and amplitudes. The set of periods (ranging from half a day to years) is given by astronomical relations, e.g. time it takes for the moon to orbit the earth. The main constituent originates from the moon's gravitational force and is tagged with an 'M' for 'moon'. The part that causes the semi-diurnal effect is referred to with 'M_2 tide'. Similar applies for instance for sun-related effects, that would be for instance S_2 tide. The M_2 tide has a period of about 12 hours and 25 min, which is usually referred to as one tidal cycle. Amplitudes for each constituent are strongly affected by local conditions, e.g. geometry. Diurnal and semi-diurnal effects are described by combining certain tidal constituents. Another important effect is the neap-spring cycle. It is a modulation of the daily tidal signal with a period of 14.76 days [Kvale, 2006]. It shows as periodically decreasing and increasing tidal range. Due to Coriolis the tidal wave circulates around so-called amphidromic point. At Sylt for instance the tidal crest first reaches the southern tip and then travels northwards along the west coast.

The definition of waves in this study is restricted to surface gravity waves, especially wind sea (locally generated) and swell (generated in distant wind event), thus periods of couple of seconds up to 20 seconds. Like the tide, waves are described by period and wave height (i.e. roughly twice the amplitude), too. Waves are generated by wind. Fetch and duration of a wind event govern the wave properties, roughly the following holds: the longer and/or farther the wind blows the longer and/or higher the waves. In engineering applications and in research often, too, the scales are such that individual waves are not of interest. Instead sea states are described with statistical measures. Commonly used is the significant wave height H_s, which denotes the mean of the upper third of individual wave heights. The mean period $\bar{T}$ is defined on the full set of waves. Records of individual waves usually contain water level elevations. With methods like zero down crossing individual waves are detected and respective individual periods and wave heights are determined. If no record of individual waves is available sea state properties can also be extracted from wave spectra, as for instance provided by some buoys. Research describes several relationships between the spectra's moments and time series based measures (see for instance Holthuijsen [2007]). The peak period T_p is defined as the period of maximum energy in the spectrum. It is slightly lower than the mean period. Other periods are defined based on the spectral moments. Each of them comes with distinct properties, for instance T_{m01}, which is the inverse of the mean frequency and less affected by high frequency noise than other spectra derived periods. An in-depth description of waves is found in Holthuijsen [2007].

To classify coasts Hayes [1979] focus on coasts without major river influence. He relates tides and waves as parametrized by mean tidal range and mean wave height (see Hayes [1979] their Fig. 15.). The mixed-energy coast is of relevance to this study. Its properties are determined by overall equally important tidal and wave forces. Throughout the course of a year the dominance of one over the other may vary. By this definition it is possible that the coast changes its energy state within the course of one year. This strongly depends on the seasonality of forcing in that area.

The area of interest in this study lies between the depth of closure and the highest point reached by water on the shore, because this is the morphodynamically active part. The waterline moves periodically with the tide in horizontal and vertical direction. Its position is determined by the tidal motion, as well as the geometry of the beach. Additionally its position is altered by wave forcing, which causes run-up as well as wave set-up. Waves furthermore transition during their progression from deep water to the shore. Effects on the wave's shape are shoaling and breaking (let aside refraction, diffraction and reflection). Its path is altered by refraction and diffraction, which also may alter the shape of the wave (over non-uniform bottom). The combined wave action over the geometry of the sea floor causes currents in the water column. Those lead to rip currents, undertow and shore parallel currents. The interaction of time- and space-dependent current fields caused by tides and waves determines sediment transport rates. Non-equilibrium sediment transport in turn changes morphology, which again alters hydrodynamics. This is why hydrodynamics and morphodynamics form a coupled system.

2.2.3. Brief Introduction to Morphodynamics at Stake: Sandy Coasts

Hydrodynamics drive morphodynamics and vice versa, i.e. hydrodynamic forces alter beach morphology and morphodynamics alter hydraulics. This kind of coupling forces a system to converge towards an equilibrium state (both static or dynamic are possible). A sandy coast may consist of several morphological features, that change through the course of a year or at the occurence of single events. Starting point of morphological change is mobilized sediment. Locally mobilized sediment may cause erosion. Sediment mobilized in other places and transported to the local spot may result in accretion, if it is deposited there. Mobilization of sediment depends on the thresholds that initiate motion. Different models for initiation of motion exists. Some deal with individual grains, whereas others base their models on sediment properties like the median grain size. Approaches are similar in their general concept, i.e. that balance of forces (e.g. shear, pressure) varies with the flow observed above the sea floor. They differ in the way the problem is solved, which amongst others goes back to disciplines at stake as well as the problem at hand (basic research or engineering application). Parameters governing the mobilization and transport of sediment are grain size and shape, exposure, flow magnitude, turbulence level, grain and water density. In the coastal zone grains are predominantly mobilized by turbulence induced by flow reversal (back and forth motion of wave orbital velocities) rather than by flow magnitude. This yields a cross-shore distribution of mobilization potential, based on wave height (increases and then reduces towards the shore) and relative water depth. Mobilized sediment moves vertically based on a balance of settling velocity and turbulence. Usually sediment concentrations increase towards

the bottom. Therefore undertow is very efficient in transporting sediment offshore [Niemeyer, 1992]. Undertow is a return current that is wave related [Svendsen, 1984]. Due to a net onshore mass transport in waves water piles up on the shore. This is balanced by a return current near the bottom, the so-called undertow. Its magnitude decreases with distance from the shore. Eventually it is too weak to keep sediments suspended and they are deposited on the shoreface [Niemeyer, 1992]. Undertow increases with increasing wave forcing, and therefore is stronger during winter (i.e. storm or wind sea dominated season). In winter beach profiles develop milder slopes and the intertidal area appears to loose sediment (i.e. shoreline moves onshore), because sediments are deposited in subtidal areas. During summer (i.e. no storm or swell dominated season) undertow is less strong and the net onshore transport induced by the wave motion dominates. Sediment deposited at the submerged bar is mobilized by long, low waves and transported onshore. Beach profiles steepen and even a berm may form. Sediments deposited as berm may eventually leave the coastal zone and enter the dune system [Bendixen et al., 2013]. Orientation of depositional features strongly is affected by the incidence of waves. If the dominant wave direction is orthogonal to the shore rip will have the same alignment and bars appear parallel to the shore. Whereas for oblique incidence, rips also form at an angle. Bars look similar to spits, because they are connected to the shore at one side. These effects originate from wave-induced longshore currents, which can be explained by radiation stress theory. Usually the rate of change in morphology is slower than the rate of change in wave direction. It is therefore a characteristic determined by the dominant wave direction.

Sediment transport can be classified differently. By its result (erosion and accretion), by its cause (waves, tide), by its direction (cross-shore, shore parallel) or by its scales (short-term, long-term; instantaneous, averaged). Storms move sediments on scales of days (abruptly), and are an example for natural causes for sediment transport, whereas nourishments are anthropogenic. An example for gradual change is the periodic change from winter to summer profile and vice versa.

2.2.4. Detailed Description of Basics to this Study

This section describes how run-up and wave set-up are estimated and introduces the concept of beach states.

Run-up and Wave Set-up Irribarren and Nogales define in 1949 the later called Irribarren number ξ (Eq. 2.1). Its intended use is to determine, if waves are breaking on a slope or not by defining $\xi_c \approx 2.3$ as critical value (acc. to Battjes [1974]).

$$\xi = \frac{\tan \alpha}{\sqrt{H/L_0}} \tag{2.1}$$

As can be seen, ξ depends on the beach slope α and the wave steepness H/L_0 with wave height H and the deep water wave length L_0. The latter is estimated from wave period T with linear wave theory for deep water:

$$L_0 = \frac{gT^2}{2\pi} \tag{2.2}$$

Battjes [1974] picks up at that point, goes one step backwards and argues that it can only be said, that a critical value ξ_c is proportional to ξ, but not necessarily $\xi_c \approx 2.3$. He further describes which aspects of breaking waves are governed by the Irribarren number, amongst others wave set-up, run-down and run-up. Stockdon et al. [2006] advance this knowledge into an empirical formula that combines run-up and wave set-up as 2 % exceedance value [Stockdon et al., 2006, Eq. 19]

$$R_2 = 1.1\left(0.35\beta_f\sqrt{H_0 L_0} + \frac{\sqrt{H_0 L_0 (0.563\beta_f^2 + 0.004)}}{2}\right) \tag{2.3}$$

for intermediate beaches ($0.3 < \xi < 1.25$) with foreshore beach slope β_f (same as α) and deep water wave height H_0. The rmse of this empirical estimation is denoted with 38 cm [Stockdon et al., 2006]. Note, that R_2 is only dependent on beach slope, and wave steepness, which form the Irribarren number. Blossier et al. [2016] derive shorelines for a 1.3 km long stretch of beach located within the range of the study area of this work (see Chap. 3) by means of a video monitoring system. Eq. 2.3 is part of their water level model. A similar approach as in Eq. 2.3 is presented by Aarninkhof et al. [2003]. It is

applied to four sites as part of the water level model in a video-based approach as shown in the work of Plant et al. [2007]. Battjes [1974] lists quite some assumptions needed to conclude that run-up and wave set-up are goverened by ξ. Those are not elaborated in detail here. Note, that the assumption of a plane beach ahead the other assumptions does not hold for the study area of this work.

Beach State A refined set of beach states is first defined by Wright and Short [1984]. It is a parameter that summarizes depositional characteristics of a shore. A shore is then classified into certain groups of beach states, each of it related to a distinct morphology. There is for instance the ridge-runnel system, as can be found on Sylt during winter. Usually beach states are derived as an averaged quantity, and therefore characterize a certain strip of coast for more than a year. In this study the definition of beach state is brought down to smaller time scales and therefore the evolution of beach states can be presented (which is only possible because of the high temporal resolution of the method used in this study).

3

Study Area and Data Availability

3.1. Study Area Bunker Hill

Sylt is a German barrier island in the southern North Sea. It is close to the Danish border and thereby the most northern island of Germany (Fig. 3.1). There is no significant influence by a river (as opposed to tidal and wave influence). Net sediment transport offshore is directed northwards, following the tidal motion. Sylt has developed as two splits due to diverging sediment transport close to the coast. The northern half experiences approximately a northward net sediment transport, whereas the southern half experiences a net southward transport. Schematics of net sediment transport are presented in Figure 16 in Ehlers [1988] or Fig. 3. in Ahrendt [2001]. Sylt is threatened by retreat, which starting in 1984 is met by nourishments [Ahrendt, 2001]. Losses are in the order of 1.2×10^6 m^3/year to 1.4×10^6 m^3/year of which about 0.4×10^6 m^3/year (30 %) are lost to the south [Ahrendt, 2001, AWL, 1997]. Nourishments are carried out yearly by Landesbetrieb für Küstenschutz, Nationalpark und Meeresschutz Schleswig-Holstein (LKN.SH). Shoreface as well as beach nourishments are conducted [LKN.SH, 2017, 2018]. Efforts are made to increase the efficiency of nourishments based on concepts within the framework of Building with Nature, for instance within the subproject BaseWad as part of Interreg North Sea region partnership[1].

Hayes [1979] refines the class of mesotidal coasts into three subgroups. Sylt lies in the low-mesotidal range, thus between 1 to 2 m (Fig. 3.2, for definition of class boundaries see Tab. A.2) and has a semi-diurnal tide (see for instance Fig. 32. in Davies [1980]). Tidal gauges at List and Hörnum are located at the sheltered (east) side of Sylt. Tidal gauge Westerland is located on the exposed (west) side. At Hörnum the tidal range is increased probably due to reflections. The variation of the tidal range along Sylt's west coast should be within the limits of those three, as also indicated by literature (e.g. Figure 8 in Ehlers [1988], Fig. 33. in Davies [1980]), authorities (e.g. LKN.SH) and the operational model from Bundesamt für Seeschifffahrt und Hydrographie (BSH). Sylt is furthermore located in a medium wave energy environment, with predominantly wind sea ($\overline{H_s} = 1.1\,m$ and $\overline{T_p} = 7\,s$, for more details see Tab. A.1 and Fig. A.4) and matches the classification as a "[s]torm wave environment" in Fig. 27. of Davies [1980]. The coast thus classifies as **mixed-energy coast**. Tides and waves both contribute to the shape of the coast, yet for the case of Sylt waves dominate (most of the time). The sediment transport caused by wave action overrules the transport induced by tidal motion. The classification of mixed-energy with wave-dominance is a good starting point to investigate morphology and dominant transport mechanisms. Davis and Hayes [1984] clarify that the relation between wave and tidal energy is important, not the absolute values themselves. This concept is dealt with in more detail throughout the morphodynamic analysis in Chap. 6. Due to seasonality of wind there is also a seasonality in wave characteristics, mainly winter and summer related[2].

Bunker Hill is a platform at about 20 m+MSL, located on the southern tip of Sylt. The radar itself is about 26 m+MSL. The orientation of the shoreline of the southern tip is tilted with respect to north by about 3°. The study area at Bunker Hill is restricted by the maximum range of the radar located at Bunker Hill (about 3 km radius). The covered sea on the exposed side of Sylt is free of fixed objects,

[1] `northsearegion.eu/building-with-nature`
[2] or as it is stormy and non-stormy season related

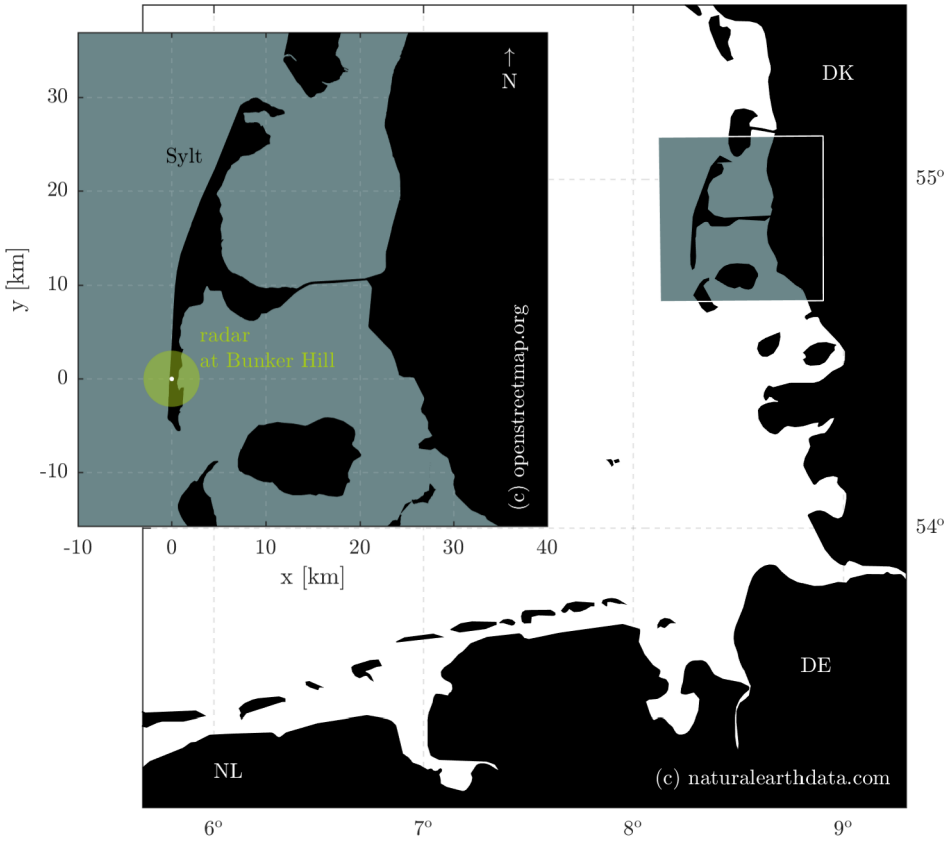

Figure 3.1: study area on Sylt with radar station at Bunker Hill **close-up:** Bunker Hill is located on the west coast on the southern tip of Sylt **overview:** location of Sylt in the German Bight (southern North Sea) **data:** based on openstreetmap.org and naturalearthdata.com

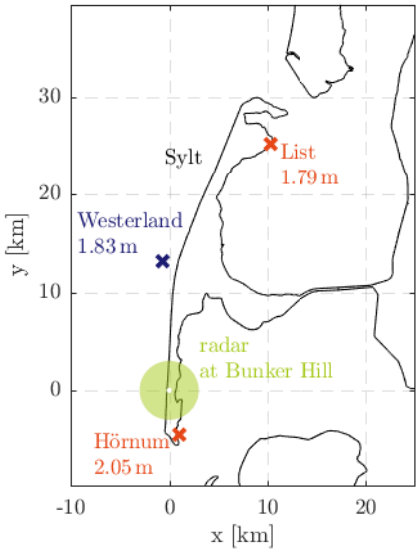

Figure 3.2: mean tidal range from three tidal gauges located at Sylt **purple:** 2006 to 2015 operated by LKN.SH **orange:** 2004 to 2013 operated by WSA Tönning **data:** tidal range as difference between MHW and MLW (for data see Tab. A.3)

Figure 3.3: impressions of Sylt beach close to Bunker Hill **left:** dunes and beach, foto taken from Bunker Hill platform **right:** channel and shoal, about 1 km south of Bunker Hill platform **captured:** May 15, 2018, close to low water

except for one buoy that occasionally is fixed south east of the radar location. A local coordinate reference system is used (Bunker Hill Coordinate Reference System, BH-CRS). Its origin is the radar itself, x-axis is pointing east, y-axis north. Coordinates of the radar are given in Tab. 3.1. It is based on UTM zone 32N (EPSG:5555) and has the same geographical properties. Fig. 3.3 gives an impression of the beach at Bunker Hill. The radar was set up in 2013 and is operated by the department of Radar Hydrography of Helmholtz-Zentrum Geesthacht (HZG).

The morphology is homogeneous for most of the part covered by the range of the radar. The profile configuration usually is intermediate with a ridge-runnel pattern for oblique waves, according to the schematics of Wright and Short [1984, their Fig. 2.] (recited in Fig. A.1). Additionally a submerged bar is present about 500 m offshore (Fig. 3.4, also shown by Fig. A.2), as observed for dissipative beaches. Therefore two breaker zones are present in front of Bunker Hill. The slope of the beach (approximately above MSL) is around 0.11 (slopes from ground truth May 2018 in Fig. 5.15, Blossier et al. [2016] found 0.13 from measurements in April, June, October and November for the same area). The channel-shoal system (approximately below MSL) has milder slopes quite below 0.07. Sediment on the exposed (west) side ranges from fine to coarse sand (based on Figure 11, Zeiler et al. [2014],

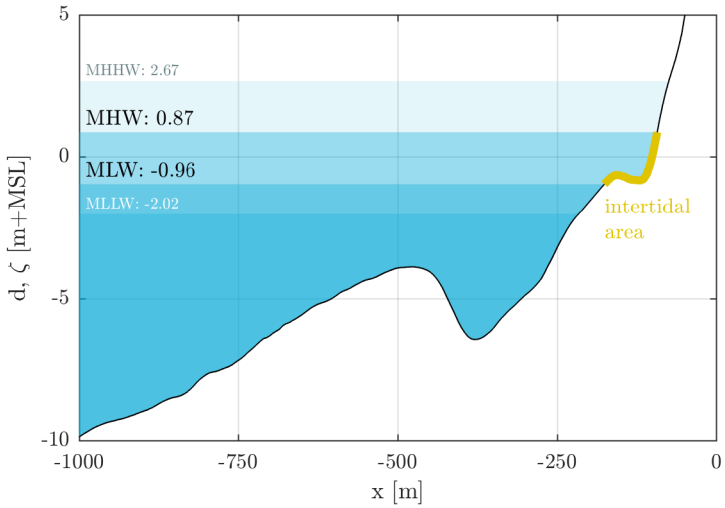

Figure 3.4: beach profile at Bunker Hill with submerged bar and ridge **data:** profile from echosounding and GPS, Sept 2016, water levels from Westerland pile (see also Tab. A.3)

AufMod project[3]). Surf similarity parameter is about $\overline{\xi}$=0.99 for 2017 (σ=0.63, see Fig. A.5). Breaker types are thus predominantly plunging, with tendency to spilling (classification from Battjes [1974]).

3.2. Data Coverage

This section lists data sources used in this study. A map with positions of all instruments, as well as a table with their respective data sets are provided (Fig. 3.5, Tab. 3.1). Any time stamps in this work are given in Coordinated Universal Time (UTC).

[3] www.kfki.de/de/projekte/old_aufmod

#	instrument	output	purpose	period
1	radar at Bunker Hill	uncalibrated backscatter intensities	input for TWA in:	
		$I = f(x, y, t)$	application (Chap. 6),	Jan 5 to Nov 2, 2017
			validation (Sec. 5.2) and	May 9 to 23, 2018
			sensitivity (Sec. 5.3)	May 1 to 26, 201
2	BSHcmod	water level (modelled)	input for TWA in:	
		$\zeta = f(t)$	application (Chap. 6),	Jan 5 to Nov 2, 2017
			validation (Sec. 5.2) and	May 9 to 23, 2018
			sensitivity (Sec. 5.3);	May 1 to 26, 2018
			phase shift to 5 (Sec. A.3.1)	Apr 25 to May 25, 201
			ground truth (Sec. 5.1)	Apr 16 to May 31, 2018
3	GNSS (RTK)	bathymetry $d = f(x, y)$	ground truth (Sec. 5.1)	May 15 to 17, 2018
4	Westerland buoy	wave height, period and direction	wave environment (Sec. 3.1)	Dec 1, 2016 to Nov 30, 2017
		H_s,T_p,T_{m-10},$\theta = f(t)$	wave run-up (Sec. 5.3.2)	May 9 to 22, 2018
			ground truth (Sec. 5.1)	Apr 16 to May 31, 2018
5	Westerland pile	water level	tidal range (Tab. A.3)	2006 to 2015
		$\zeta = f(t)$	visualisation (Tab. A.3)	2006 to 2015
			phase shift to 2 (Sec. A.3.1)	Apr 25 to May 25, 2018
6	List tidal gauge	water level $\zeta = f(t)$	tidal range (Tab. A.3)	2004 to 2013
7	Hörnum tidal gauge	water level $\zeta = f(t)$	tidal range (Tab. A.3)	2004 to 2013
8	echosounding + GPS (RTK)	cross-shore profile $d = f(y)$	visualisation (Sec. 2.2.1 and Sec. 3.1)	Sep 22 to 26, 2016

Table 3.1: data sets used in this study **#:** numbers can be found in Fig. 3.5 **output:** only output used in this study is listed

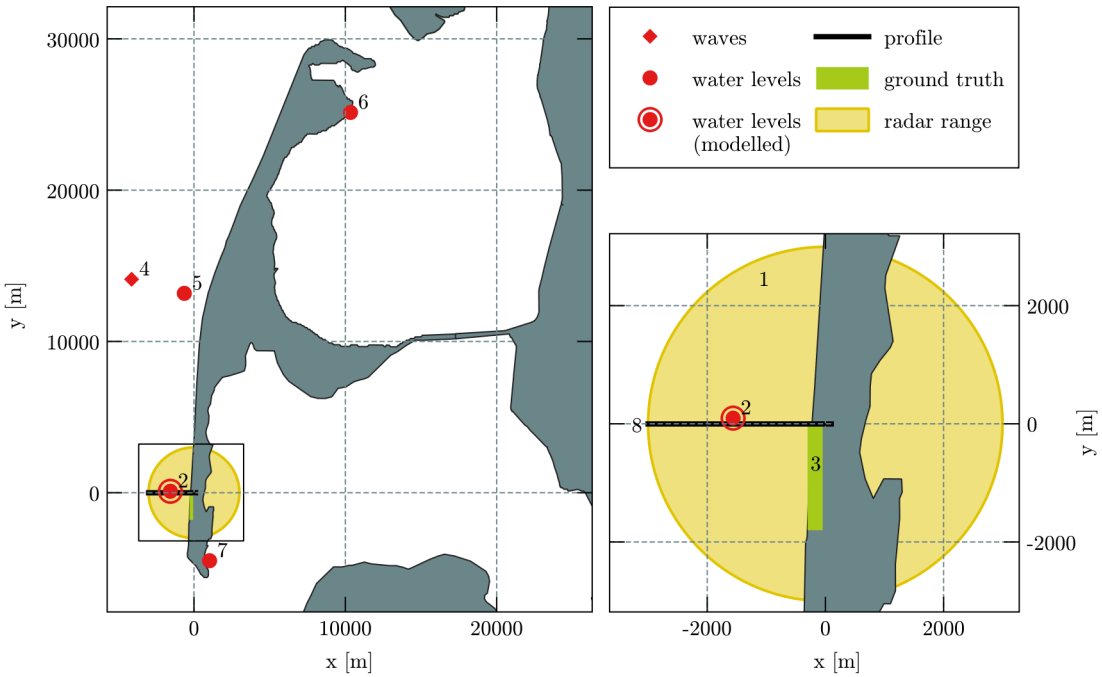

Figure 3.5: map of instruments used in this study **numbers:** refer to entries in first column of Tab. 3.1 **source:** background map based on openstreetmap.org

4

Methods Bathymetry Retrieval from Radar

Bell et al. [2016] aim at developing a robust method to derive bathymetries from radar images. For decades now scientists have tackled the problem of retrieving shorelines from images (mostly photographs). Setting a threshold to determine whether a pixel is covered by water or dry has been one answer so far and is manifested in various approaches with differing complexity and automation algorithms. It is a case-sensitive technique and prone to bias. Bell et al. [2016] do not solve this problem, but reformulate the task from another perspective: the problem is shifted from the spatial to the temporal domain. By the costs of limiting temporal resolution (instead of snapshots it is looked at periods) it offers an automatable algorithm to detect not just a shoreline (i.e. iso depth contour), but to cover the intertidal area. Their attempt is based on radar images (backscatter intensities). It is supposed that the same concept could be applied to photographs as well – to the benefit of finer spatial resolution, but smaller extent.[1] The basis for this work are bathymetries from radar images derived with the so-called Temporal Waterline Approach (TWA). To answer the questions formulated as study objective single bathymetries are analysed with respect to their morphological features. By combining these results with process understanding (Chap. 2) the morphodynamic evolution is hypothesised.

This section starts with describing the general concept of the Temporal Waterline Approach by Bell et al. [2016] and its implementation in the scope of this study. Details and adjustments are presented afterwards. Most important adjustment made improves the quality check by adding a second threshold. It is found that both thresholds are crucial for the performance (sufficient accuracy vs. full coverage of intertidal area) of the Temporal Waterline Approach. Furthermore the extensive knowledge gathered throughout the sensitivity analysis unveiled a rule of thumb for the estimation of the otherwise subjectively chosen thresholds in the quality check. The last section (Sec. 4.6) summarizes this chapter.

4.1. Temporal Waterline Approach

The Temporal Waterline Approach (TWA) works on a single location, i.e. cell (or pixel, in analogy to photographs), on the scale of tidal cycles. To retrieve a full bathymetry a loop has to be run over all cells applying TWA to each of them. TWA thereby is made of two main steps. Expressed in pseudo-code:

[1] Statements by Stefan G. J. Aarninkhof and Michael Streßer, oral discussion during progress meeting for this thesis, Apr 19, 2018

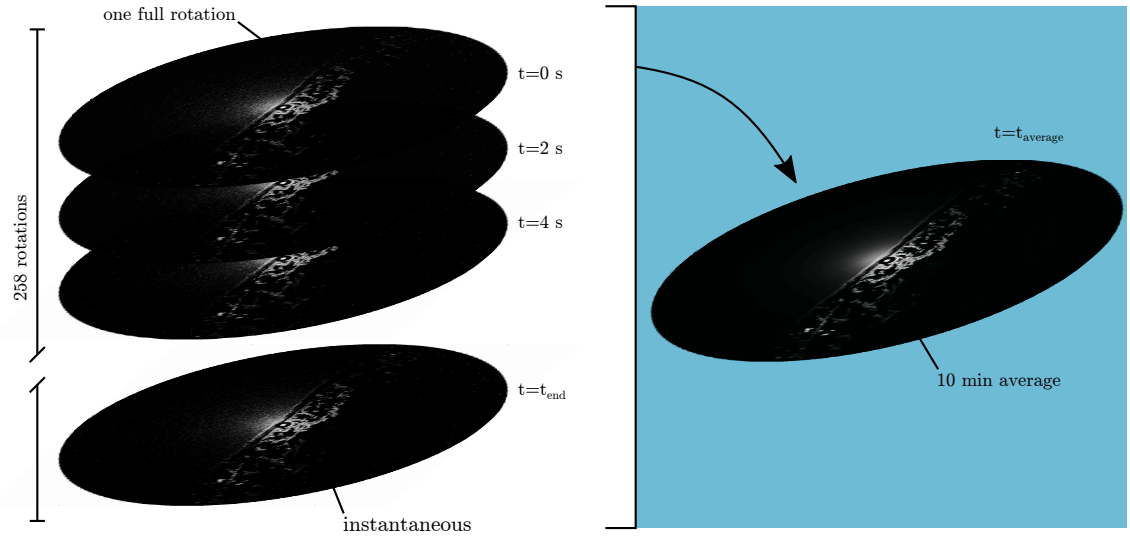

Figure 4.1: from time stack of radar images to 10 min average **left:** radar time stack – a single radar record of about 10 min lengths captures 258 rotations with the operational mode used at HZG **right:** averaging over all 258 rotations yields a 10 min average, which is similar to a time exposure image **data:** May 5, 2018, 13:00 to 13:09

```
for each cell do  TWA
                  |- 1 retrieve bed level
                  |    |- find steep gradients in radar
                  |    |- for each possible bed level do
                  |    |      find intersections with water level
                  |    |- match radar and water level patterns
                  |    |- find best match
                  |    |» bed level
                  |- 2 check quality
                  |    |- quality of match
```

Radar images are recorded by a GEM X-band (9.41 GHz) marine radar with VV polarization. The radar used in the original work is HH polarized, but uses the same frequency. HH polarization yields higher returns for sea spikes, e.g. breaking events, whereas Bragg scattering yields similar returns in both polarizations [Jessup et al., 1990, Lee et al., 1995, Ruessink et al., 2002]. For the performance of TWA VV polarization may be beneficial over HH polarization, because non-Bragg scattering like sea spikes is less pronounced. The radar operates with a pulse repetition frequency of 2000 Hz and samples each pulse with 20 MHz (pulse length of 50 - 70 ns). This results in cell size of 7.5 m in range. Maximum range is 3.26 km. One rotation takes about 2 s.

1 retrieve bed level:

In the operational mode of HZG the radar runs about once or twice per hour and then records instantaneous backscatter intensities for approximately 10 min (records with less than 8 min are discarded, more than 10 min is cut to 10 min). Each 10 min record is averaged (Fig. 4.1), yielding a time series of 10 min averages (denoted by $\bar{I}$) with each time step about 30 min or one hour apart. To maximize the outcome it is recommended to cover a full neap-spring tidal cycle with the time series. This time series is the basic input to TWA.

A single cell is picked and its mean backscatter intensities are extracted (Fig. 4.2). Note, that at

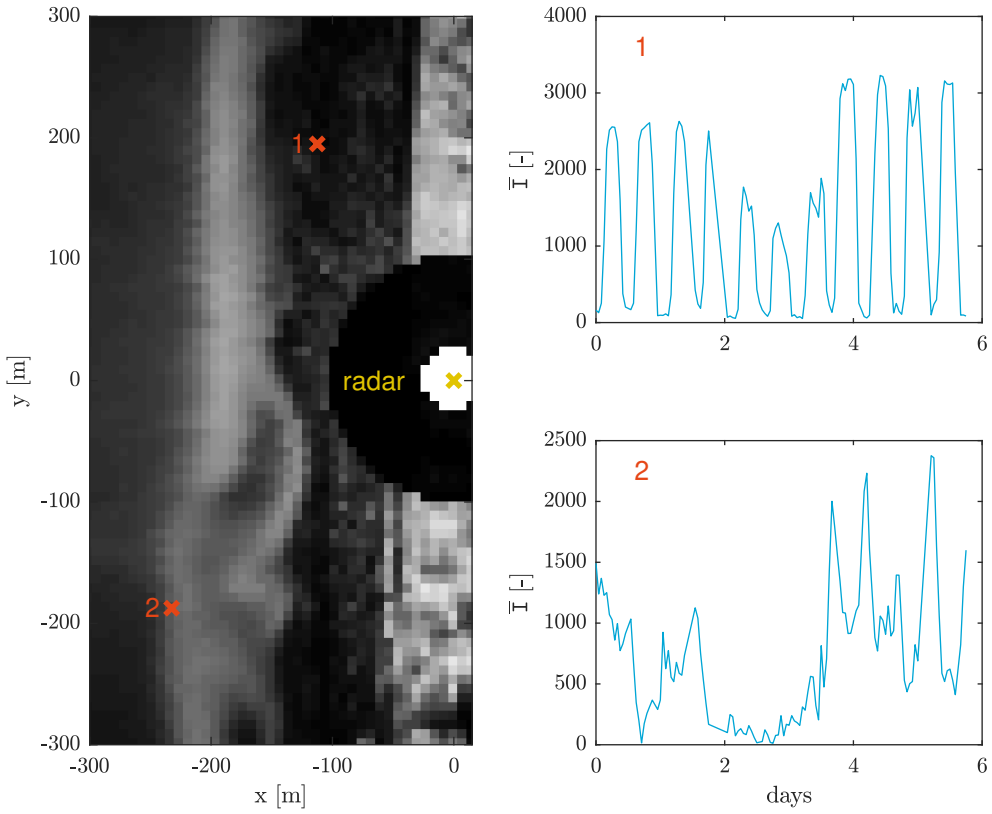

Figure 4.2: example records of $\overline{I}$ over time at two locations **left:** to show the two locations a part of the first image (May 20, 2017, 0:00) of $\overline{I}$ is shown, 1 is located at the upper boundary of the intertidal range (beach), 2 at or below the lower boundary of the intertidal range **right:** $\overline{I}$ over time at the two example locations **data:** May 20, 2017, 0:00 to May 25, 2017, 19:00

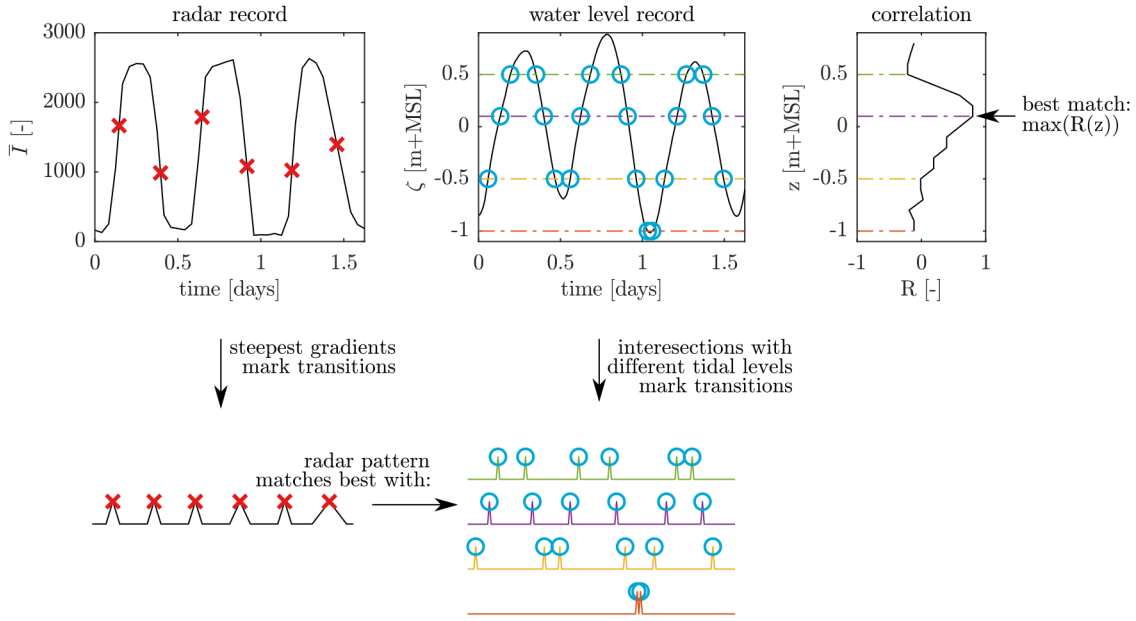

Figure 4.3: concept of Temporal Waterline Approach, application to a single cell **top row (from left to right):** based on $\overline{I}$ (red crosses) and ζ (blue circles) patterns of transitions from wet to dry and vice versa are detected. For the water level record various possible transition patterns are possible, depending on the actual bed level (that is yet unkown and to be found). The comparison (normalized cross-correlation) of those patterns results in a set of bed levels z connected to a $R(z)$ value. The best match is found by $\max(R(z))$ and points at the most likely bed level z. **bottom part (from left to right):** transition pattern of radar record gets correlated with the various possible transition patterns of the water level record. In this example the second pattern best resembles the pattern of the radar record. **data:** May 20, 2017, 0:00 to May 21, 2017, 16:00

location 1 the tidal frequency clearly is visible, whereas at location 2 it seems to be present in the second half, but hidden in the first half. Part of the time series of 1 is used in Fig. 4.3 to explain the method.

The main notion of TWA is, that **rapid changes in time in mean backscatter intensity denote transitions from wet to dry and vice versa**. Although this notion proves to be wrong in some cases (e.g. it also detects the change from breaking to non-breaking), it appears that TWA nevertheless is robust against fallacies related to this aspect. Transitions (i.e. rapid changes) in the backscatter time series are mathematically found as peaks in the absolute gradient:

```
t_transitions_radar = peaks of abs( grad( Ī ) )
```

Note that if no transitions are found in the radar record (unlikely yet concept-wise possible) the cell lies outside the intertidal range (thus above or below). Red crosses in the left column of Fig. 4.3 mark the transitions.

The next step is to find the transitions from wet to dry and vice versa in the water level record ζ. The intersections of all possible (hypothetical) d and ζ now mark the transitions.

```
t_transitions_wl = intersection hypothetical bed level with ζ
```

Blue circles in the centre column of Fig. 4.3 indicate intersections. Assume the bed level d was 0.5 m for the cell marked as location 1 in Fig. 4.2 above, indicated by the green horizontal line. The intersection pattern found for this bed level does not match well with the pattern found for the radar record (red crosses, left column). Therefore another bed level is assumed, the arising transition pattern is again compared to the radar pattern, and so on. The comparison of patterns is carried out by means of a correlation coefficient $R(z)$. The best match is indicated by the maximum of $R(z)$ over all hypothetical bed levels (usually the range from lowest to highest ζ in the water level record):

```
d_best_match = d that yields max(R(z))
```

Note that $\max(R)$ is positive given the above notion of rapid changes is not violated. Only few cells have negative $\max(R)$, although many $R(z)$ values are within the range of -0.3 to 0.3. The issue of negative $R(z)$ is part of the discussion on the notion of rapid[2] changes marking transitions.

The procedure is repeated for all cells within the range of the radar, which yields a final bed level d and the related maximum correlation R for each cell (see top row of Fig. 4.4). Unfiltered output of TWA for study area Bunker Hill is shown in Fig. 4.4.

2 check quality:

Further processing is needed to check if the best match found a valid bed level. This is linked to the limitations of this method and described in detail later on (Sec. 4.5). Bell et al. [2016] only use one criterion to filter invalid points. Based on observations in their study area they find, that cells with a R of less than 0.3 [3] are mostly located in submerged parts and therefore do not yield reliable estimates of d. Therefore any bed levels with a $R \leq 0.3$ are discarded (see Fig. 4.6 for an impression of the effect).

Bell et al. [2016] present the accuracy of TWA in relation to the range (see Fig. 23, Bell et al. [2016]). In comparison to a LiDAR survey a RMSE of 0.31 m in the near range increasing to 0.84 m in the far range is found by them. Overall the rmse is in the order of 60 cm. Also bias increases with range, from 0.12 m in near range to 0.59 m in the far range, overall in the order of 40 cm. They discuss their findings in relation to the slopes of the bathymetry and the occurence of pooling water. The robustness of TWA is challenged by amongst other, major changes in wind climate, the breaker zone in calm periods or a rocky floor, which may also cause rapid changes in the radar signal, with a pattern that suppresses the wanted wetting-drying pattern. [Bell et al., 2016]

4.2. Water Level Model

Second most important input next to $\bar{I}$ to TWA is the water level. This is in general the case also for camera-based methods, because they link the 'known' water level to the image derived position of the shoreline. Ideally the water level should include at least tide, wind set-up (or any other large scale phenomena), wave set-up and run-up, in order to resemble the instantaneous water level. Tide and wind set-up are usually captured by tidal gauges or numerical models, whereas data on wave set-up and run-up often is missing or not sufficiently accurate or detailed enough. Instead empirical formulations are used to add water level set-up as well as run-up to a water level measured or modelled somewhere close to the study area. Bell et al. [2016] do not include run-up and wave set-up for their TWA analysis, but use a tide gauge that captures water levels due to tide and meteorological conditions (e.g. wind set-up) (see Fig. 5 (d), Bell et al. [2016]). They find that some of the differences between ground truth and TWA results can be explained due to ignoring run-up and wave set-up. Nevertheless they do not mention why run-up and wave set-up are neglected. It might be related to the complexity of the area, which violates many of the assumptions underlying empirical formulations for run-up and wave set-up, or merely the unavailability of wave data, that is required as input to the empirical formulations. The elevations found with TWA are therefore not absolute bed levels, but relative to the water level. Water levels are assumed homogeneous within the radar range.

4.3. Improvements to the Method

One big difference between the study area from Bell et al. [2016] to the current work is the tidal range. For this work it is about five times smaller and therefore some aspects have not been as important in the orginal description of TWA as they are now for this work. Three additions are made in the quality check, as well as one modification:

[2] In the scope of this work 'rapid changes' happen on a timescale of 10 min.

[3] In statistical terms $|R| < 0.3$ basically is no correlation, but it is still possible to see trends, which is enough for TWA [oral statement by Jörg Seemann].

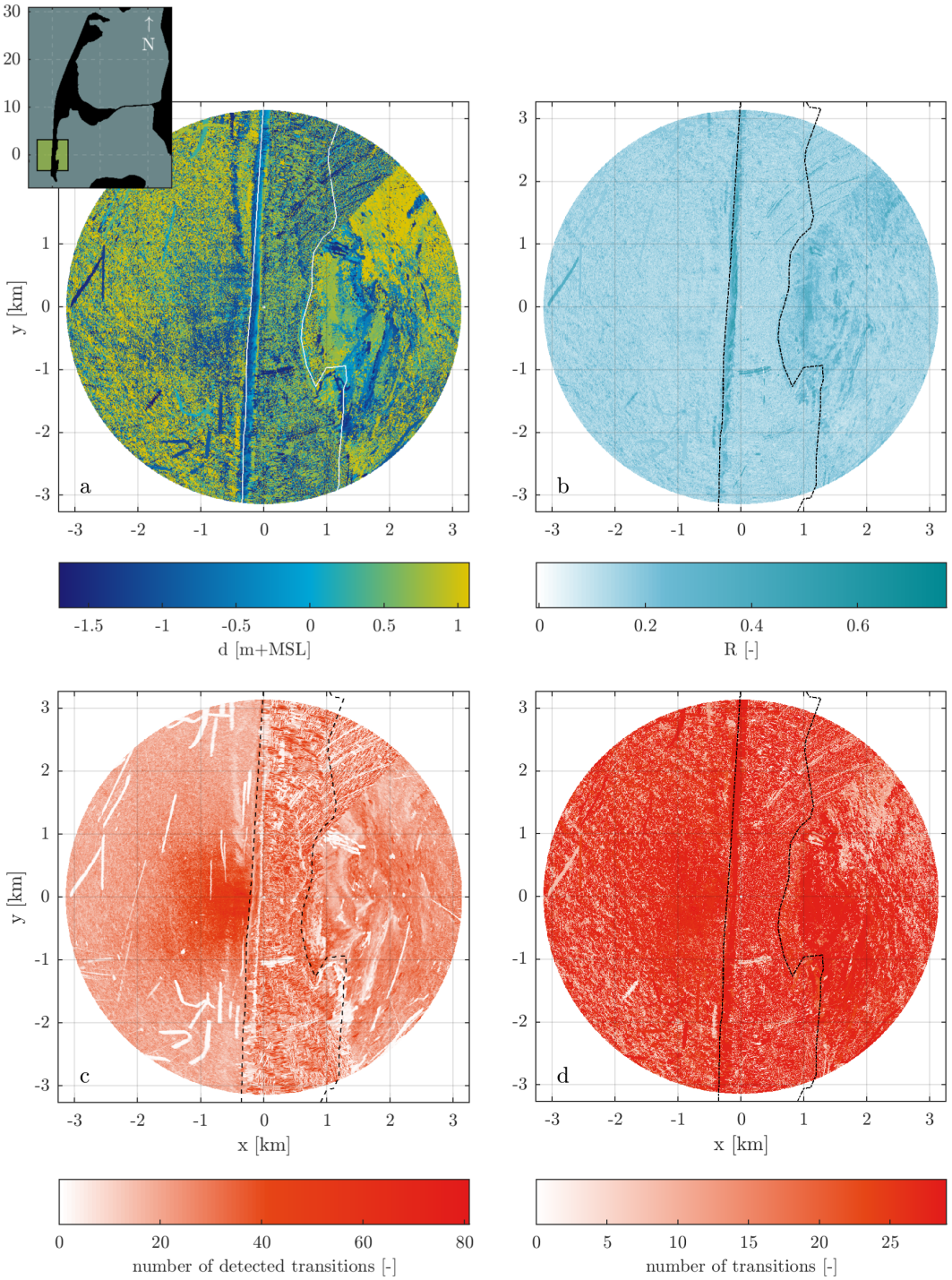

Figure 4.4: output of Temporal Waterline Approach **line:** indicates Sylt's shoreline **a:** bed levels **b:** maximum normalized cross-correlation R **c:** number of transitions detected in radar record **d:** number of transitions in the water level record for which the maximum normalized cross-correlation is found **data:** radar-based data from May 12, 9:00 to May 20, 16:00, 2018, map based on openstreetmap.org

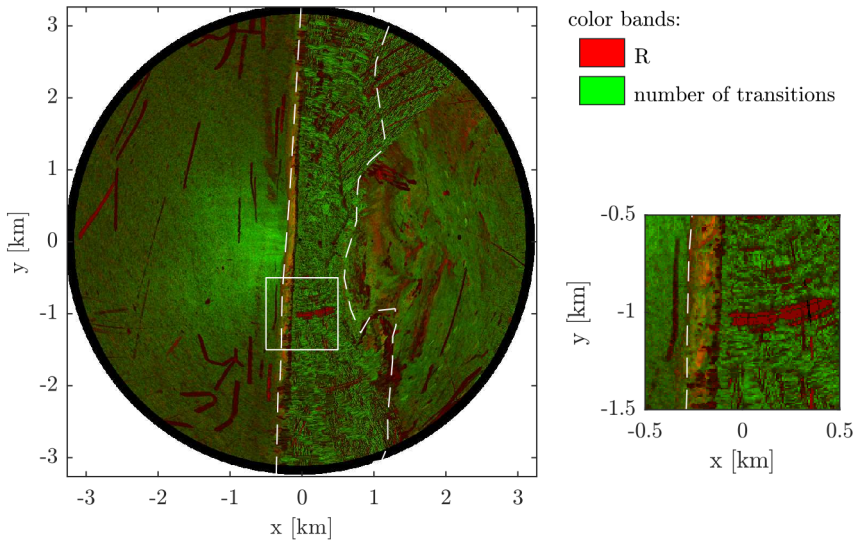

Figure 4.5: need for two filters in TWA **red areas:** high R, low number of transitions, filtered by θ_{trans} **green areas:** high number of transitions, low R, filtered by θ_R **mixed areas:** remain after filtering, see also detail view to the right **data:** radar-based data from May 12, 8:30 to May 20, 15:30, 2018, map based on openstreetmap.org

```
for each cell do  TWA
                  |- 1 retrieve bed level
                  |     |- ...
                  |- 2 check quality
                  |     |- [ADDED] limits of z grid
                  |     |- [ADDED] number of transitions
                  |     |- [MODIFIED] quality of match
                  |     |- [ADDED] remove lonely cells
```

First of all bed levels that are below the minimum water level or above the maximum water level have to be removed (set to NaN or mark in any other way as 'unreliable').

Second, an additional threshold θ_{trans} is introduced.[4] Bell et al. [2016] mention the need for it in their discussion. Fig. 4.5 shows that two parameters (represented in red and green) of TWA govern the non-intertidal areas. Effective filtering thus requires more than just a threshold for R, but one for the number of transitions as well. Mixed areas are untouched by both thresholds. Fig. 4.6 shows the effectiveness of using two thresholds (θ_R and θ_{trans}) instead of one (θ_R) for filtering results of TWA. The left panel presents the result of TWA without filtering. Parts of it look random (i.e. neighbouring cell values are not related), which are the subtidal areas and land mostly. Some cells form consistent patches (e.g. smooth changes of cell value d). Random areas indicate that TWA is not applicable (no tide induced wet-dry transitions). Those cells are intended to be filtered, as presented in Fig. 4.6 (b) for θ_R=$\theta_{R,Bell}$=0.3. Nevertheless the filtering fails in at least two respects, because it implicitly assumes that only random looking (low correlation) areas are invalid. Yet some of the patches left in Fig. 4.6 (b) (e.g. '2nd shoreline' and 'noise (1)') are invalid despite their high correlation. The issue of the '2nd shoreline' arises, because the main notion of TWA is violated. It is therefore more difficult to tackle, than with setting a threshold. The case of 'noise (1)' relates to a second threshold, θ_{trans}, see Fig. 4.6 (c). Fig. 4.6 (d) reduces the threshold for correlation, more cells become visible as well as another kind of 'noise (2)'. Since θ_{trans} represents a preliminary condition to ensure statistical reliability, it is dealt with first. Followed up by investigation of θ_R. For both recommendations are given how to choose

[4]Letter θ will be used to indicate a threshold. Its subscript describes which parameter it relates to.

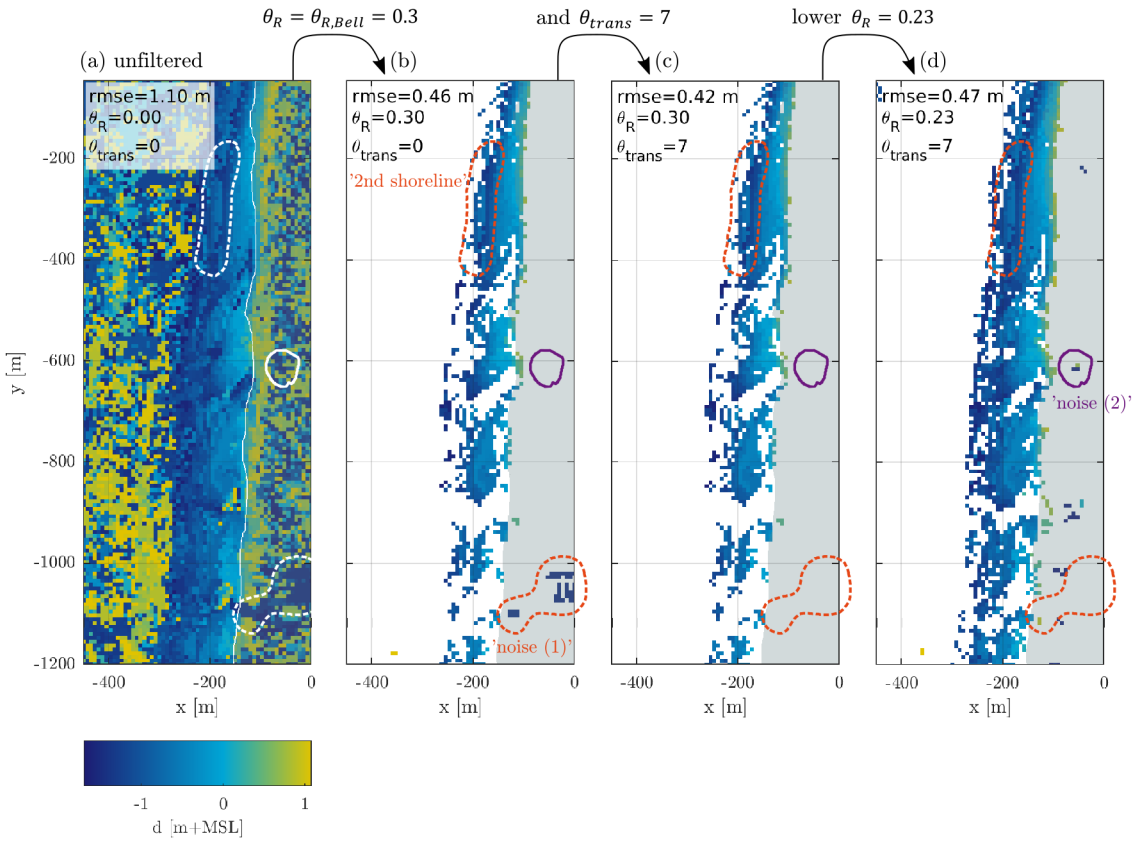

Figure 4.6: effectiveness of two filtering thresholds (instead of one) on RDB **MSL:** white line/grey area indicates mean sea level, land to its right/in grey, sea to its left **a:** unfiltered result of TWA **b:** filtered according to Bell et al. [2016] **c:** additionally cells with too few transitions are filtered **d:** effect of data-based threshold for R **data:** RDB from May 12 to 20, 2018 (16 tidal cycles) and rmse from comparison with and white line extracted from ground truth, May 15 to 17, 2018

respective filtering values.

As described in Sec. 4.1 TWA detects transitions between wet and dry and vice versa. Each cell therefore (theoretically) experiences two transitions per tide, one during wetting, one during drying. The physical maximum of transitions is thus determined by the tidal period (here semi-diurnal) combined with the length of the analysis window. For a window length of 28 tidal cycles (14.5 days) this yields 56 possible transitions. The water level record is influenced not only by various tidal constituents, but meteorological conditions and therefore is not regular. This is why especially for low and high z levels not the possible maximum number of transitions is reached, but only few transitions are present, e.g. a very low mark only falls dry during spring tide combined with winds that benefit a set-down, during the remaining tidal cycles of the analysis this mark is always wet. But with too few transitions it becomes hard to judge whether a detected pattern represents a tidal or random signal. Therefore a second threshold θ_{trans} in addition to the original one (θ_R) is introduced to mark cells as unreliable, that employed too few transitions for the estimation of the cell's bed level. At least eight transitions are required.[5] For analysis windows significantly larger than 2.1 days (yields 8 transitions in a pronounced semi-diurnal environment) it can be handy to choose the threshold larger than 8. The maximum is then defined by the possible (in physical terms) maximum number of transitions[6]. It depends on tidal period and the analysis period T (given in days). Transitions from wet to dry and vice versa occur twice per tide. The limits for θ_{trans} are:

$$8 \leq \theta_{trans} \ll 3.87\,T \tag{4.1}$$

For this study θ_{trans} is set to:

$$\theta_{trans} = \max(8;\ 0.97\,T) \tag{4.2}$$

The factor of 0.97 resembles quarter of the physical maximum of number of transitions within the analysis period. This implies that any window length should be at least as long as containing 32 transitions, thus about 8.3 days, or else θ_{trans} has to be decreased accordingly.

Third, Bell et al. [2016] aim at developing a reliable and robust algorithm to derive bathymetry from radar images. The proposed filter mechanism opposes this aim. The filtering threshold θ_R=$\theta_{R,Bell}$ is set to 0.3, based on personal judgement ("subjectively chosen" [Bell et al., 2016]). Any cells with lower correlation R are disregarded. This poses a major challenge to the demand of robustness, because the choice of the threshold is up to the user. Also Bell et al. [2016] do not mention whether to use the same value in other study sites. The sensitivity analysis of this study reveals, that the accuracy of TWA is sensitive to the choice of the threshold θ_R. It further indicates that a strong relation exists between the length of the analysis window T and the value of θ_R. Based on the following hypotheses the estimation of θ_R is improved. Instead of adjusting θ_R with respect to available ground truth and/or personal judgement (experience) it is estimated with respect to the radar data set itself.

1. The overall (mean) correlation is related to the window length, in non-intertidal and intertidal areas: $\overline{R}_{intertidal}$=$f(T)$ and $\overline{R}_{non-intertidal}$=$f(T)$ (see Fig. 5.24). Below a certain window length non-intertidal (invalid) and intertidal (valid) areas are no longer distinguishable with respect to their overall (mean) correlation. This marks one (statistical) lower limit of window lengths.

2. The threshold θ_R thus also depends on the window length. To achieve the same/best accuracy it has to be adjusted with respect to the length of the analysis window: θ_R=$f(T)$.

3. The overall (mean) correlation of the intertidal (valid) area is related to the overall (mean) correlation of the non-intertidal (invalid) area (subtidal/sea or land): $\overline{R}_{intertidal}$=$f(\overline{R}_{non-intertidal})$. This was found empirically, but is expected to be founded in statistics. $R_{non-intertidal}$ can either be R_{sea} or R_{land}.

4. Findings indicate that the relation found for θ_R is not site-specific.

Due to lack in time this set of hypotheses is not investigated further. For this study therefore a rule of thumb is extracted instead, yet when neccessary θ_R is adjusted according to personal judgement:

$$\theta_R = \overline{R}_{non-intertidal} + 2\,\sigma_{R_{non-intertidal}} \text{ for } T \geq 8.3 \text{ days} \tag{4.3}$$

[5] It was found that from very short (5.2 days) to long (14.5 days) window lengths this minimum value ranged from 7 to 8. A value of 8 was therefore chosen as required minimum. See Sec. 5.3.4.

[6] Sec. 5.3.4 shows that any filtering above this value only yields unreliable results for the bathymetry.

$R_{non-intertidal}$ is a set of correlation values defined by a user-set window fully located offshore (never any transitions present, nor breaker zone). It is also possible to use land instead. The window should be large enough to yield a reliable estimate for $\overline{R}_{non-intertidal}$ and $\sigma_{R_{non-intertidal}}$. The factor for standard deviation is empirical and may not be valid for other study sites. The minimum analysis window length originates from the formulation of θ_{trans} and overrules the required minimum found in the sensitivity analysis of the window length. Both threshold formulations (Eq. 4.3 and Eq. 4.2) combined yield the rule of thumb:

$$\text{for } T \geq 8.3 \text{ days} \begin{cases} \theta_R = \overline{R}_{non-intertidal} + 2\,\sigma_{R_{non-intertidal}} \\ \theta_{trans} = 0.97\,T \end{cases} \tag{4.4}$$

It is not tested, whether this rule of thumb is site- and/or data-specific.

Fourth and last addition made to quality check, all cells that are left with no neighbour after filtering are removed. This is done not only for purpose of making the output look less messy. Any valid cell is most likely surrounded by other valid cells, whereas invalid cells share in overall a similar (low) correlation value or (low) number of transitions with their neighbouring cells. Any cells that remain single after filtering are thus most likely invalid cells that were just a little above the set thresholds and thus remained. This procedure may pose an issue for very strong filtering, thus values above reasonable for θ_R and θ_{trans}. In that case basically most of the cells will be filtered already and the filtered bathymetry is probably useless anyway, no matter if single cells are removed on top or not. Despite removing cells no effect on statistical measures, like rmse and bias, are detected. This is probably because only very few cells are without neighbours, which implies that this procedure predominantly works for the sake of layout.

4.4. Notes on Mathematical and Numerical Implementation

Mathematical formulation of TWA is based on the descriptions in Bell et al. [2016]. Note that only the correlation coefficient $R(z)$ is presented in the form of an equation, the rest is text-based. TWA itself is implemented in a MATLAB function. TWA is part of the toolbox RDB (Radar Derived Bathymetry). RDB toolbox is part of this work and contains a set of MATLAB functions for processing radar data into bathymetries, as well as useful pre- (e.g. average radar sequences, prepare data for required format) and post-processing functions (e.g. export to other formats, visualisation), see A.1 for an overview.

The gradients in the radar record are calculated as the difference between two successive points divided by their difference in time:

$$\bar{I}' = \frac{\Delta \bar{I}}{\Delta t} = \frac{\bar{I}_{i+1} - \bar{I}_i}{t_{i+1} - t_i} \tag{4.5}$$

The corresponding time stamp for the gradient is then:

$$\frac{t_{i+1} - t_i}{2} + t_i \tag{4.6}$$

The same peakfinding algorithm [Yoder, 2016] as mentioned in Bell et al. [2016] is used to find peaks in the absolute values of the gradient. It is not known if the peakfinding algorithm got tweaked and it is used with its default set of parameters. The timestamps of the peaks give the transition pattern. The next step is to create transition patterns from the water level record. First the water level record is interpolated to the same temporal grid like the radar record. A z grid is created, that resembles the resolution of the outcome. Unlike the procedure for the radar record, transitions are determined differently. For each z individually it is checked for each point in time of the water level record whether a cell would be dry or wet:

```
wet_or_dry(t) = ζ(t)≥z
```

Again for each z individually the times when a shift from dry to wet or vice versa takes place are marked:

```
wet_or_dry_i+1 - wet_or_dry_i is not 0 » transition at i+1/2
```

For each z now a transition pattern is available. This set of patterns is compared against the radar pattern by means of a Pearson correlation coefficient (MATLAB function corrcoef).

4.5. Limitations and Error Sources

Limitations and error sources directly linked to the principles used in TWA are discussed in this section. For limitations and error sources related to the study area see Sec. 5.2 or related to the study objective see Chap. 7. This section starts off with considerations about scales resolved in TWA as compared to camera-based approaches (e.g. shoreline detection in the spatial and not temporal domain). Furthermore an example is given why it is not unrestrictedly beneficial to use TWA with radar images recorded more frequently than 30 min. Shortcomings of the peakfinder algorithm are presented as well as examples for violating the main notion of TWA.

4.5.1. Assessment of Scales in Relation to Camera-based Approaches

With TWA shoreline detection (more precisely bathymetry retrieval) is shifted from the spatial to the temporal domain, for the benefit of robustness. Temporal resolution for shoreline detection in the spatial domain is governed by the quality of images (for camera-based methods that would be reduced by fog, rain and night) and amount of work needed to extract shoreline information. Additionally the spatial resolution may be low due to ambiguity. Blossier et al. [2016] for instance had to limit their analysis to the high water line. Temporal resolution in the case of TWA is governed by the method itself. The choice of analysis window determines which scales can be resolved. Those are most likely longer time scales (in the order of couple of days) than in the case of camera-based observations for instance (in the order of one tidal cycle). But spatial resolution is not determined by the method itself, as is the case for camera-based methods (see ambiguity). Instead the radar's resolution determines the smallest features representable. The largest temporal scale that can be resolved is probably in the order of a month, yet it is characterized as an average product. Limitations of TWA with respect to scales thus should be seen at both ends of the scale. It cannot resolve fast motion that takes place on timescales of a day. And neither can it resolve slow motion taking place on the scales of month. The spatial resolution may be improved in the near range, if polar coordinates instead of cartesian would be used (numerically more challenging to implement).

4.5.2. Limits of Temporal Resolution

Fig. A.6 shows that the tidal wave on the west side of Sylt takes about 20 min for a distance of roughly 13 km. The radar diameter is about 6 km, which corresponds to roughly 10 min for the tidal crest to travel from the most southern to the most northern part of the radar range. Under the assumption of a homogeneous water level in the complete radar range this may cause problems for the algorithm, if the radar sampling is faster than that. Given the 10 min averaging, maximum sampling is every 10 min. For a chosen water level at a certain time instant this implies that the most southern point has experienced this same water level about 5 min earlier and the most northern point is going to experience it in about 5 min. It is then possible that the detected wet-dry transitions in the water level record are allocated to an time stamp earlier or later. Note that those are rule of thumb calculations. No analysis has been conducted due to lack of data, if this actually causes significant decrease in accuracy. Also for this study even with the maximum sampling it is unlikely to become a major issue. Yet for study areas with radar radius larger than 3 km as is the case for Bell et al. [2016] this may actually be important. Effects of the neglected phase shift probably manifest as range dependencies of parameters or output of TWA.[7] Albeit range dependencies most likely originate from radar physics.

4.5.3. Shortcomings of Peakfinder Function

The Matlab function peakfinder used to find the steepest gradients did not get tweaked (defaults used). Detected peaks are found in relation to the rest of the time series. Therefore the number of transitions detected in the radar record only weakly correlates with the respectively found bed level (which is not expected). Especially when looking at the number of transitions in the water level record used for the best match this becomes clear.[8]

[7] This is not generally the case, but refers to the coincidence that the tidal wave almost travels straight through the radar range's center, due to the orientation of the coast.

[8] Transitions in the water level record are not detected with Matlab function peakfinder.

4.5.4. Knowledge Gap in Radar Physics

The assumption of the main notion of TWA, that steepest gradients mark the transitions is challenged by the radar physics. First of all it is not defined at what point a patch of sea floor actually is 'dry' or 'wet'. It is therefore also not clear at what point the transition takes place. See also top left in Fig. 4.3 (red crosses mark transitions detected in radar record). Transitions are not always at about the same intensity level. It appears that during flooding ($\bar{I}$ increasing) transitions are detected at higher intensity levels than during drying ($\bar{I}$ decreasing). Probably the processes of flooding and drying are fundamentally different, due to – amongst others – tidal asymmetry (current velocities), flow direction (modulating sea surface waves), sediment properties (pores), to mention just a few.

4.5.5. Issue of '2nd Shoreline' Artefact

The point made in the previous section – defining flooding and drying – may not be important for the performance of TWA, because it is a systematic error. Rather more severe is the cross-shore migration of the breaker zone in the frequency of the tide. It violates the main notion of TWA, namely that rapid changes in time in backscatter intensity are **exclusively** due to transitions from wet to dry and vice versa. The (cross-shore) position of the breaker zone depends on the depth. It therefore moves with the tide. For a fixed position the breaker zone moves past with a frequency related to the tidal period. Breaking events in a radar cell cause increased returns as compared to a cell with non breaking. This causes strong gradients (i.e. rapid changes) in the time series of backscatter intensities of the cell. In TWA this causes a transition pattern, that yields high cross-correlation coefficients, too. The passing breaker zone is thus mistaken as a wet-dry transition. In RDB this appears as an artefact and looks like a '2nd shoreline': a consistent patch of bed levels that is sloping towards offshore (see for example Fig. 4.6 and Fig. 6.1). Due to high correlation values and a sufficient number of transitions it cannot be filtered with the proposed quality check. For this study the '2nd shoreline' is masked out manually. Ruessink et al. [2002] describe a method (for a different purpose though) to identify the location of the breaker zone from radar images. This could be used to automate the masking. Nevertheless there is probably a way to remove the effect based on the method's technique, which should be preferred over the time-consuming task of manually or automated masking.

4.6. Summary

The radar data of this study is provided by a GEM radar operating at 9.41 GHz (X-band) with VV polarization. Radial resolution is 7.5 m (pulse length 50 ns, repetition at 2000 Hz), with 2 s per rotation, rotating for about 10 min every 30 min or 1 hr. The method used in this study to derive intertidal bathymetry from radar images is based on the Temporal Waterline Approach (TWA) by Bell et al. [2016]. TWA requires two inputs:

1. **10 min averages of backscatter intensity:** time series, for each radar cell, denoted by $\bar{I}$
2. **water levels:** time series, single location, tide and wind set-up

Bed levels are retrieved cell-wise by means of a normalized cross-correlation between (temporal) wetting-drying (i.e. transition) patterns in radar and water level data. In this study the quality check as originally described for TWA by Bell et al. [2016] is improved. Two thresholds are used, that filter too low cross-correlation (θ_R) and too low number of transitions (θ_{trans}) used for estimation of the cross-correlation coefficient. The choice for the first threshold θ_R got semi-automated, based on the radar data at hand. The latter threshold θ_{trans} is introduced within the scope of this study. Based on results from sensitivity analysis of TWA (Sec. 5.3) both thresholds are combined into a rule of thumb in order to semi-automate the quality check, see Eq. 4.4. There is indication, that the rule of thumb is not site-specific, yet it was not proven within this study. The performance of the adjusted TWA is mainly limited by its main notion:

> Rapid changes in time in mean backscatter intensity denote transitions from wet to dry and vice versa.

Cross-shore migration of the breaker zone causes rapid changes in the radar signal, too. This appears as a '2nd shoreline' in the radar-derived bathymetry (RDB) with high correlation values and is not filtered by the proposed quality check. In the scope of this study it got removed by hand.

5

Validation and Discussion of Radar-derived Bathymetry

This chapter is divided in three parts. A survey was conducted in May 2018 to collect ground truth for this study. Sec. 5.1 gives a detailed description of the campaign. Also results are presented and discussed. The ground truth serves as reference for validation (Sec. 5.2). Shown and discussed are absolute errors for two radar-derived bathymetries (RDBs). The ground truth is also used as reference for sensitivity analysis (Sec. 5.3). Investigatesd are the effect of four parameters of the Temporal Waterline Approach (TWA) on accuracy and coverage of RDB.

5.1. Ground Truth Collection

Ground truth was recorded on May 15 to 17, 2018 with a group of four. Measurements were taken around low water to capture as much as possible of the intertidal area. A stretch of almost 2 km beach south of the radar got covered. The decision whether to go north or south was made based on the conditions found on the first day of the survey. The southern part looked more interesting in terms of gradients, extent of ridges, runnels and channels. Two devices were in use to maximise the covered area. The first device is a nautical GPS system called Aquarius mounted to a wheelbarrow with Real Time Kinematic (RTK) support from a reference station using a second Aquarius as receiver. The second device consists of a drone mounted to a sledge with a mobile reference station providing RTK support. Both setups had been tested beforehand on pavement and grass at HZG. Since both setups are experimental they are described in more detail. Their properties are summarized in Tab. 5.1. The setup related to the wheelbarrow further is referenced as 'wheelbarrow', the other as 'sledge'.

In this section also the survey plan is introduced. Some attention is given to the processing of the raw data, because it took some time (understanding sledge output and dead ends in finding automated criteria mainly). In the concluding part of this section the final map (ground truth) is presented in context

	wheelbarrow	sledge
device	Thales Ashtech Aquarius Receiver	DJI Matrice M210 RTK
GNSS	only GPS	GPS and GLONASS
RTK	Thales Ashtech Aquarius Receiver	DJI D-RTK
horizontal precision	<4 cm	<1 cm
vertical precision	<6 cm	<1 cm
sampling frequency	2 Hz, 5 Hz	10 Hz

Table 5.1: properties of wheelbarrow and sledge used for ground truth collection **precision:** values represent standard deviation within one stationary measurement as presented in Tab. A.6

of the environmental conditions. Error sources and respective accuracies are indicated.

5.1.1. Wheelbarrow Setup

For the wheelbarrow setup technical support was provided by Marius Cysewski (hydrographer), part of the Radar Hydrography group at HZG. The receiver is more than 15 years old and uses Global Positioning System (GPS) operated by United States. GPS signals recorded with the moving device are corrected with GPS signals from a fixed device (reference station) to increase accuracies (RTK based). The reference station was checked with a fixed and known point close to Bunker Hill operated by the local authorities. The device is quite heavy, because it is meant to be built-in to a vessel. Radar Hydrography nevertheless has been using this device in the field. In previous surveys it was carried in a bag with two antennas mounted to a pole (one for receiving the position, one for receiving correction information from the reference station) to collect single points for calibration of other devices. Because this time a large area had to be covered a new setup was chosen, that enables faster tracking. Left sketch in Fig. 5.1 shows the general setup. The antenna receiving GPS position is mounted in front. The pole is as short as possible to reduce the error made by its inclination. On the other hand shading by wheelbarrow, the person pushing it or the box to hold receiver, logging device, cables and additionals has to be avoided to ensure a continuous signal. An optimum was found for about 70 cm above ground. The second antenna receives the signal from the reference station. The reference station is set up on the roof of the container on Bunker Hill, with the same receiver like in the wheelbarrow. The device in the wheelbarrow corrects the signal and writes output to a text file with 2 or 5 Hz (highest freguency possible for this device). It was difficult to find the optimum antenna configuration to receive the reference signal, because the quality of the received signal depends on the distance to the reference station as well as the respective lengths of the sending and receiving antennas. Two antenna lengths have been tested for Ultra High Frequency (UHF), here 457.410 MHz. Recordings were then performed with antenna lengths of $\lambda/2$ at wheelbarrow and reference station alike. Output was recorded in GGA strings: May 15 and 16 on a smartphone and May 17 on a Windows laptop. Despite testing beforehand the smartphone had issues in recording, which resulted in corrupted GGA strings. In some tracks (files) corruption was too severe. They had to be discarded. In some of the less severe corrupted files corrupted lines were removed manually. Tracks recorded with the laptop were all fine. For each new track the distance between antenna and floor had to be measured. Hand-written protocols were used to keep track of this and any other events.

5.1.2. Sledge Setup

The drone is a M210 RTK model from DJI's Matrice series[1]. A reference station is available, called D-RTK Ground System[2]. DJI [2017] specifies its accuracy as of 1 cm horizontally and 2 cm vertically. This setup is cheaper than state-of-the-art GNSS mapping systems with RTK. For this reason it was tested, if data collected with the drone could supplement the wheelbarrow data. The drone is fixed to a wooden sledge with 90° rotation. Thus both antennas are in line with the sledge pulling direction. They receive GPS as well as GLONASS information [DJI, 2018]. In the lower right of Fig. 5.1 the setup is sketched. Drone and reference station are both consumer products. Access to their collected data is given, but their output is not documented, which yields about 900 columns of data each sampled at 10 Hz. Judged by headers, data type, values and experience from Michael Streßer and Jochen Horstmann (Radar Hydrography group at HZG) columns with the relevant information were singled out and processed. No automated criteria could be found within the range of the selected columns to remove invalid data points. Most likely needed additional information is available in other columns. To find those is a time-consuming task and not relevant for this study. Instead each track has been checked individually. In case uncertainties about consistency of a track were too high, the full track got discarded. Part of the data set has been recorded simultaneously with the wheelbarrow data, which are two stationary measurements and one track. Those were used to check and correct the processing.

5.1.3. Survey Plan

This section provides a description of the planning process. The actual survey deviated slightly, which is indicated in the respective parts of the following sections.

[1] https://www.dji.com/de/matrice-200-series/info
[2] https://www.dji.com/de/d-rtk/info

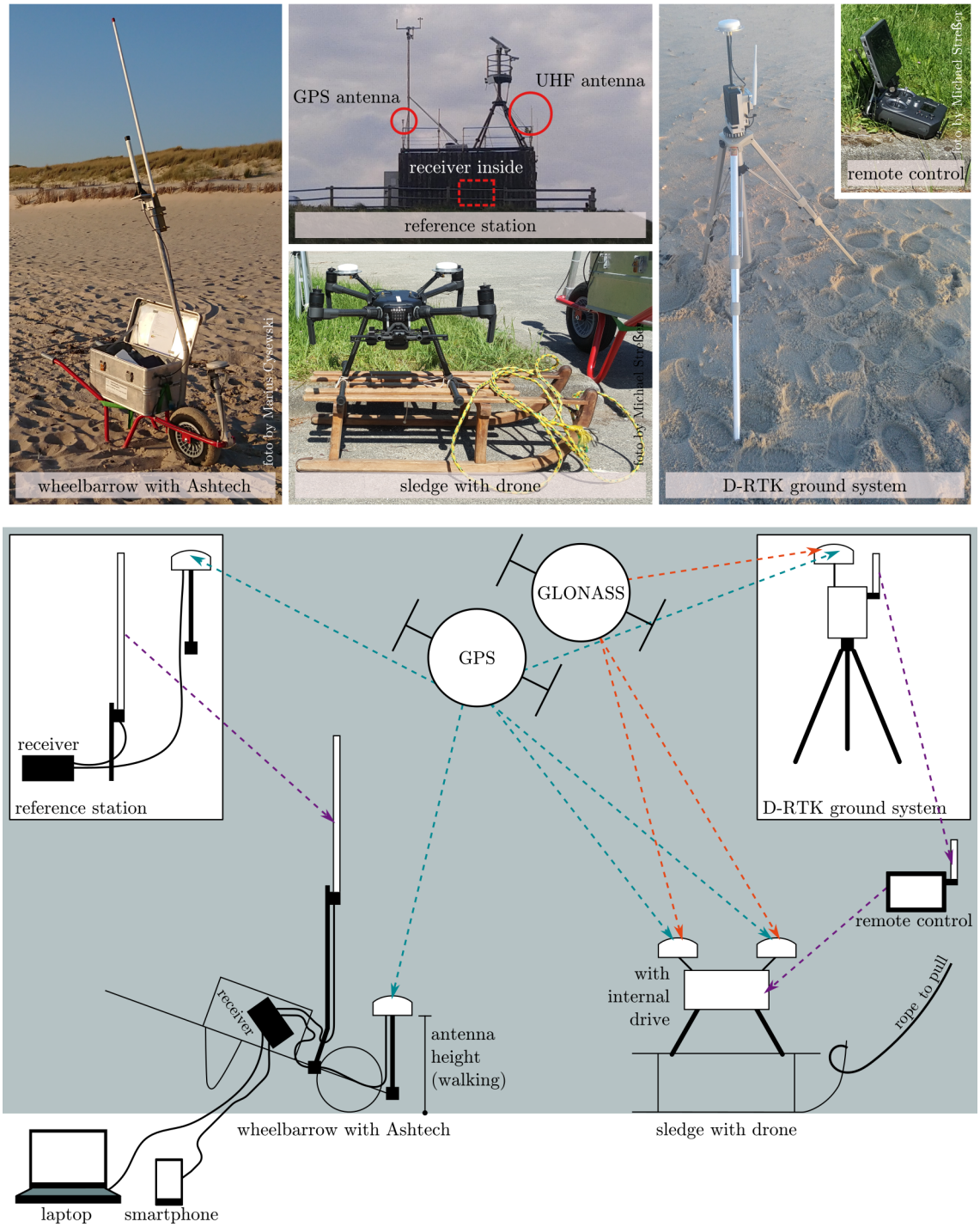

Figure 5.1: sketch of wheelbarrow and sledge setup **top:** fotos of elements presented in the sketch below **bottom:** setup of wheelbarrow (left) and sledge (right) GNSS system with respective RTK support **captured:** May 15 to 17, 2018 (survey) and May 8 to 9, 2018 (preceding tests)

The aim of the survey was to cover as much as possible of the intertidal area, in vertical as well as horizontal dimensions. The chosen devices are decisive for what can be measured, especially since it is not possible to go into the water. Three questions were major to the planning process:

1. survey period: when and how long
2. coordination and layout of walking paths
3. how to prove sufficient accuracy of sledge (drone) data

Low water below MLW is beneficial for this study's purpose. At Bunker Hill this usually is the case for easterly to southern winds and/or spring tide. The survey should also take place during a period of approximately stationary conditions, which implies mild wind (and wave) conditions[3]. The latter was expectedly the case, since the survey had to take place during early summer. Planning also included considerations about availability of staff, logistics, walking speed and costs.

It was unclear, if it would be possible to walk in transects perpendicular to the shoreline. Therefore two plans were sketched. One with transects and one where the paths would follow the waterline during ebb. On arrival at Bunker Hill the transect version was chosen. Walking speed and radar grid resolution (cell size $7.5\,\mathrm{m} \times 7.5\,\mathrm{m}$) determined minimum and maximum distance between transects, which was set to be between one and two cells. Additionally the waterline of each ridge should be walked to mark the extent and shape of the ridge as well as of the runnels and channels.

The sledge had shown promising results in the testing phase at HZG (in comparison to the wheelbarrow accuracies in all three dimensions are in the same order of magnitude). Nevertheless, for each day of the survey period a stationary measurement was scheduled. A fixed point should be measured by the wheelbarrow as well as by the sledge (not simultaneously). Those points were used later to calibrate the sledge data to the wheelbarrow to account for uncertainties in the sledge processing. Furthermore one track should be walked simultaneously, for which the wheelbarrow should follow the sledge as precisely as possible. For the remainder of the survey both devices should walk individually in order to maximise the area covered.

5.1.4. Raw Data Processing

The recorded data sets contain horizontal and vertical coordinates, timestamps and indicators for validity of each datapoint. A set of Matlab functions was implemented alongside the post-processing to read, cut, filter, visualise and convert the raw data.

The wheelbarrow tracks are a set of lines, each containing one GGA[4] string. They got checked for corrupted lines by hand. Either the file was discarded or corrupted lines got removed (depending on the severity of corruption). Each track then was filtered according to the GPS Quality Indicator (QI=4 is kept) and the number of satellites used (Sat$\geq$4 is kept). Additionally start and end of track were cut off by hand to remove lifting and settling the wheelbarrow. For few tracks also a criterion for Horizontal Dilusion of Precision was applied (HDOP$\leq$7 or smaller is kept). More detailed information about the output itself is available in the user manual of the Aquarius receiver, specifically p. 148 for an overview [Thales, 2002]. Processing protocols are available, in which single steps are recorded to go from raw to processed data.

Tracks recorded with the sledge are available as Comma Separated Values (CSV). Tracks without RTK positioning were discarded. Documentation on content and format of the CSV files is lacking. Despite efforts no automated criteria could be found to identify invalid points. Therefore each track was inspected individually and invalid parts cut out manually. According to header, data type, values and experience a set of columns from the approximately 900 columns available were selected for further processing. To calibrate sledge data to wheelbarrow data stationary measurements were employed. Stationary measurements are available for May 15 and 16. Because none is available on May 17 any sledge data of that day got discarded, since it could not be proven that the data is accurate. Offsets in all three dimensions are calculated between sledge and wheelbarrow data and applied to correct the sledge data (for details of offset estimation see Sec. A.5). The antenna height of the sledge is included in the vertical offset.

[3] This is a requirement for TWA. Storms in the North Sea usually do not last more than a couple of days, thus stationarity for more than that can only be achieved based on calm conditions.

[4] A GGA string is a NMEA sentence, that provides fix data in a certain format, see for instance `http://www.gpsinformation.org/dale/nmea.htm` or p. 148 in Thales [2002].

used columns:

```
rtkdata:Lon_P  rtkdata:Lat_P  rtkdata:Hmsl_P
GPS:dateTimeStamp  offsetTime[a]
```

[a] GPS:dateTimeStamp does not provide milliseconds, instead they are estimated from offsetTime (sampling took place at 10 Hz).

Detailed information about processing steps can be found in the Matlab functions and the respective processing protocols. Matlab functions are available to convert raw data to *.mat files and to cut, filter and visualize data sets (see A.1).

5.1.5. Results

Processed wheelbarrow and sledge data (Fig. 5.2) are merged into one data set (point cloud), which is referred to as 'ground truth' further on. In order to make ground truth comparable to RDB it is gridded to the radar grid using the median of all points within one radar cell[5].

Following figures depicting ground truth are split in two for the sake of layout, see ticks on y-axis. Shaded (grey) area indicates land. It resembles a shoreline extracted from ground truth at 0 m+MSL. Fig. 5.3 shows the merged point cloud. The following figure visualises how many datapoints lie within one cell (Fig. 5.4). Fig. 5.5 presents the gridded result, which is used as reference throughout the sensitivity analysis as well as validation. Some radar cells contain quite steep gradients. Spatial distribution of gradients is indicated by standard deviation per cell in Fig. 5.6. Large standard deviations indicate strong variations between datapoints within the same cell and therefore strong gradients. The gridding (i.e. the resolution of the radar grid) poses restriction on the accuracy of the final result in relation to the steep gradients observed. In short, if the standard deviation in one cell is in the order of say 0.5 m it is not possible (or at any point reasonable) to get a rmse of anything representing that cell's value in one or more orders of magnitude smaller.

In the process of gridding 198 660 datapoints are reduced to 2005 cells with a cellsize of 7.5 m $\times$ 7.5 m. Almost 2 km of beach and ridges in longshore direction and -1.3 to 3.9 m+MSL are covered by the survey (Fig. 5.3). Density of datapoints reduces in the most southern part, because in this part only wheelbarrow data is available (Fig. 5.2). The approach to combine two devices and take three days of measurements was successful in two respects. First, the survey covered 2 km of possible 6 km, which is sufficient for this study. Second and more important, density of datapoints improved. The increased density (sledge provides 73 % of datapoints) of datapoints proves beneficial, because it is not necessary to interpolate the results to get roughly continuous ground truth. This way no additional errors by interpolation are introduced.

The number of datapoints (Fig. 5.4) used to retrieve the median as the respective cell value is low in the most southern part, where only wheelbarrow data is available. The remaining part is covered quite well. In average about 100 datapoints were used for median calculation. The number of datapoints available is determined by the sampling frequency of the device and the walking speed. The sledge sampled twice as much as the wheelbarrow. Increasing walking speed causes density of datapoints to decrease and vice versa. Average speed was about 3 km/h, thus:

on average:

```
3 km/h → 9 s to walk across one radar cell of 7.5 m length
at  5 Hz: 45 datapoints sampled
at 10 Hz: 90 datapoints sampled
```

Walking up the beach slope took longer (density of datapoints increases) than walking down (density of datapoints decreases), as well as dry (loosely packed) sand was harder to push through, than wet (consolidated) sand. Additionally turns at the end of transects caused slowdown. On the ridges walking speed was predominantly influenced by the presence of ripples and steep gradients. Sometimes and in

[5] More than one re-gridding/interpolation option were considered. Amongst others, specifically the work of Plant et al. [2002] was consulted.

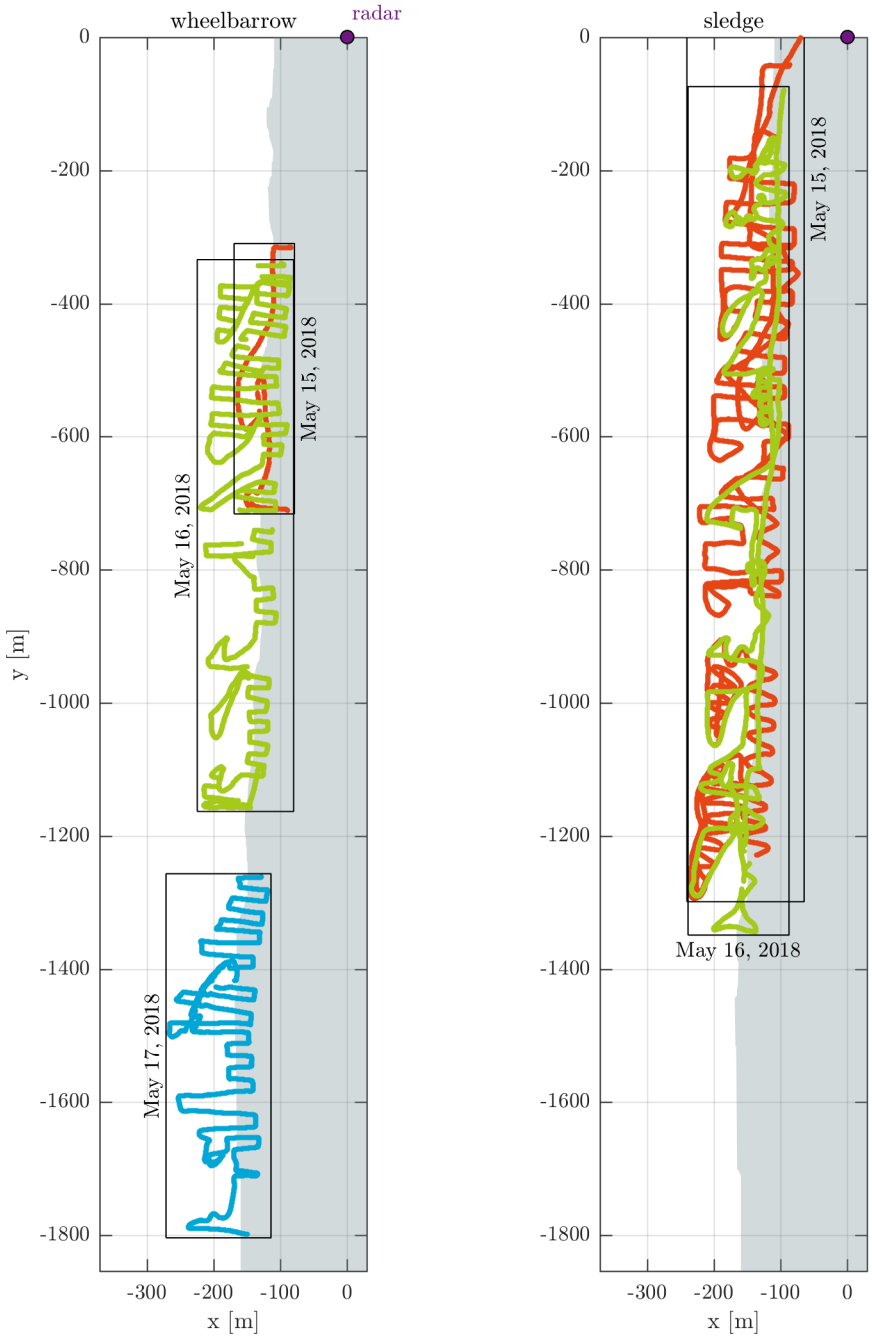

Figure 5.2: processed data sets constituting ground truth **shaded area:** indicates land, resembles shoreline extracted from ground truth at 0 m+MSL **source:** May 15 to 17, 2018, survey

some places ripples with wave lengths in the order of 50 cm and crest heights in the order of 5 cm were present that caused the wheelbarrow to jump, if walking too fast. In those parts the sledge performed better (faster walking speed possible). Yet, in turns and on steep gradients it had to be handled with more care to avoid tipping over and sideways sliding.

The gridded ground truth (Fig. 5.5) is not significantly different to the visualised datapoints. All ridges are represented well, as well as the runnel positions and gradients on the beach. Even strong gradients (as shown in right foto of Fig. 3.3) on the northward edges of the runnels are still present.

The standard deviation within one cell is large in regions of strong gradients. As expected this is the case for the beach slope and the northward edges of the runnels (Fig. 5.6). Standard deviations at the ridges are in the order of 0.1 m and smaller. Whereas on the beach and runnel edges they are rather above 0.1 m up to about 0.3 m (53 of 2005 cells have standard deviations larger than 0.3 m, up to 0.54 m). At y $\approx$ -1400 m information on the ridge is lacking, because quality was too low. Yet the runnel south of it got covered in sufficient quality. Its northward edge shows as a curved red line in the figure. The ungridded ground truth reveals, that the slope there was quite steep (similar to the right foto in Fig. 3.3) and had been walked once along its upper part and once along its lower part. It is unfortunate, that the data on the respective ridge is lacking, especially since the runnel was shallow enough to be walked through.

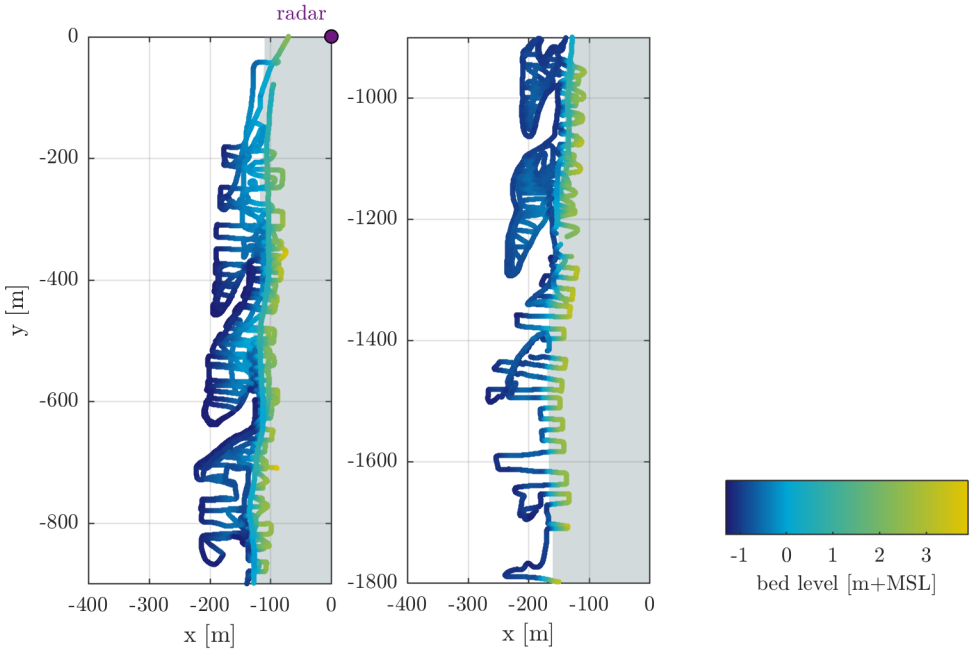

Figure 5.3: ground truth before gridding **colorbar:** in the color limits of gridded ground truth (see Fig. 5.5), 5 datapoints are above the maximum, 1492 are below, with a total of 198 660 datapoints **shaded area:** indicates land, resembles shoreline extracted from ground truth at 0 m+MSL **source:** May 15 to 17, 2018, survey

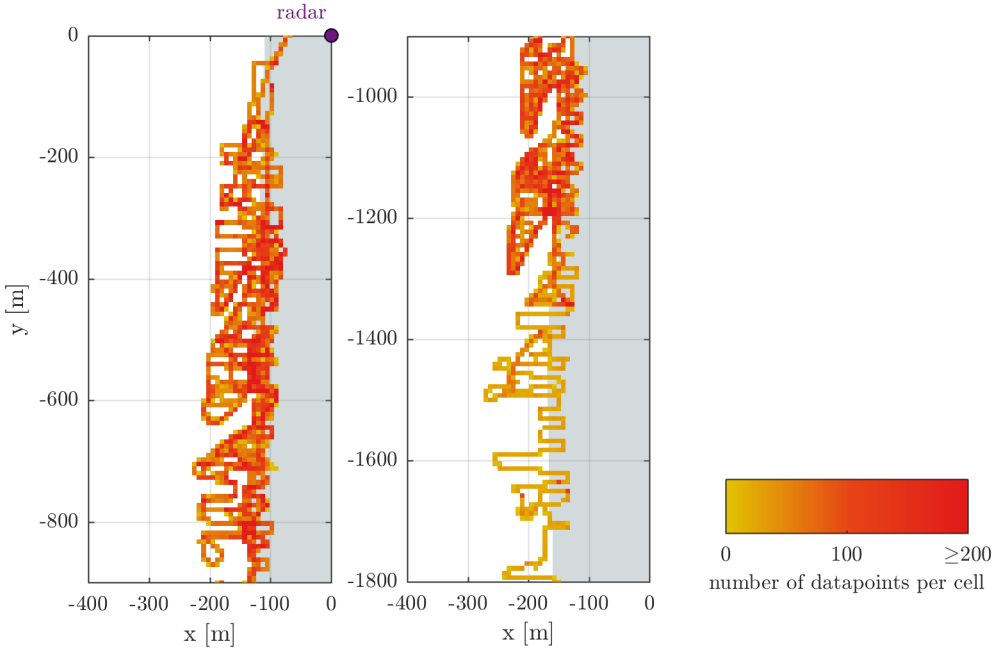

Figure 5.4: number of datapoints within one cell of gridded ground truth **colorbar:** upper limit is 94th percentile, maximum is 5942 **shaded area:** indicates land, resembles shoreline extracted from ground truth at 0 m+MSL **source:** May 15 to 17, 2018, survey

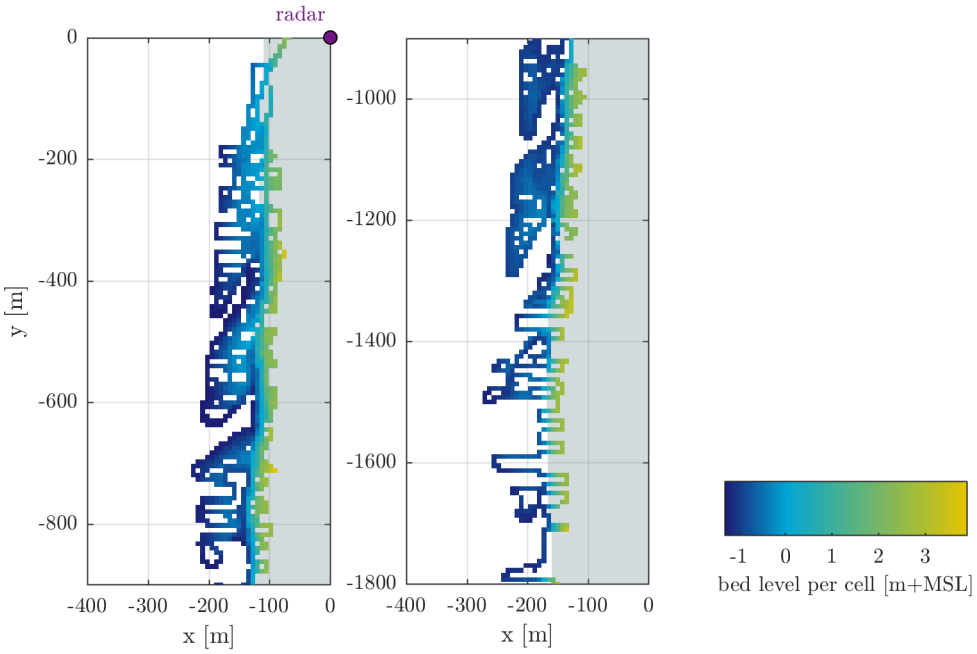

Figure 5.5: gridded ground truth **shaded area:** indicates land, resembles shoreline extracted from ground truth at 0 m+MSL **source:** May 15 to 17, 2018, survey

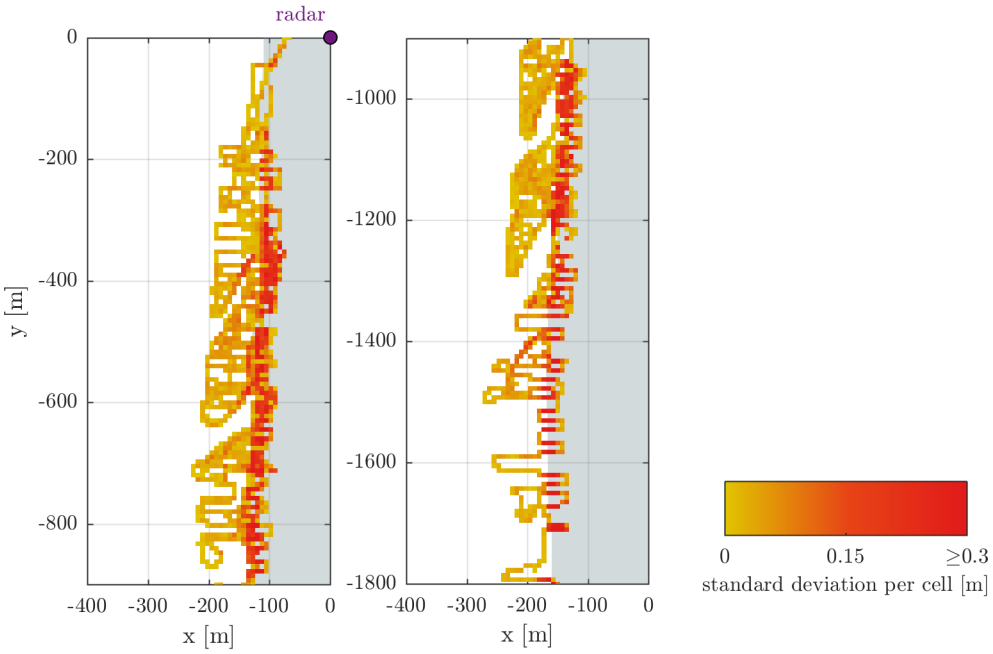

Figure 5.6: standard deviation of datapoints within one cell of gridded ground truth **colorbar:** upper limit is 97th percentile, maximum is 0.54 **shaded area:** indicates land, resembles shoreline extracted from ground truth at 0 m+MSL **source:** May 15 to 17, 2018, survey

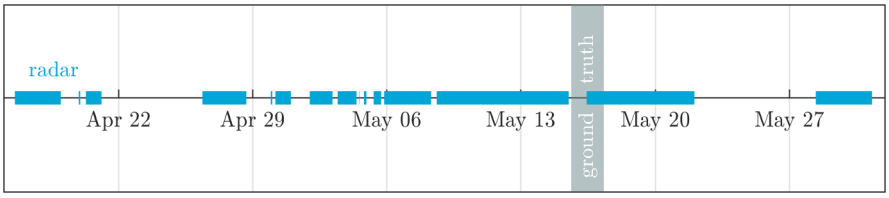

Figure 5.7: availability of radar data relevant with respect to ground truth survey **source:** ground truth from May 15 to 17, 2018, radar from April 16 to May 31, 2018

To complete the description of the survey the last figure in this section presents the availability of relevant radar data (Fig. 5.7). Only data is shown, that is considered good enough to be used. This predominantly means, that corner reflectors were available for georeferencing the radar images. About five days after the survey a gap of about one week is present, which is unfortunate for parts of the sensitivity analysis and validation. A gap of about one day is present during the survey. During this time a second radar was running, which caused interference patterns in the radar data. Those files got discarded, despite it is expected that the effect of this disruption is negligible.

5.1.6. Environmental Conditions

Information about environmental conditions (Fig. 5.8) is crucial for interpretation of results and therefore presented briefly. The performance of TWA is linked to the wave conditions (affecting the backscatter and therefore absolute intensities, which is input to the detection of transitions) and water levels (determines z range visible). Wave periods are most of the time quite short (wind sea), also during the survey. Wave heigths within a window of two weeks before and after the survey are also comparably low, except for about one day at the end of the survey. The period chosen for the survey reaches comparably low water levels, which is what was intended. About a week before (May 10) winds caused a strong wind setup, which may pose an issue for TWA. Wind speeds were temporarily higher during the survey from May 16 to 17. Due to the direction of the wind (from north to north-west) no significant wind setup occured. Nevertheless it was observed that the beach profile differed before and after increased wind. Steeper slopes on the beach after the wind increased, but no significant change in extent or location of ridges and runnels were observed. Ripple structures on top of the ridges were removed. Those changes are contributed to the impact of waves, which was also indicated by an upward shifted wash margin.

5.1.7. Error Sources and Accuracy

This last section lists sources for errors and their respective order of magnitude and direction. Tab. 5.1 already lists the accuracy of the receiving antennas. Tab. 5.2 adds error sources arising from surveying. It is sorted with decreasing relevance from top to bottom. A large error is not necessarily relevant, because it may only apply to certain regions or occur infrequently compared to other error sources. Additionally to Tab. 5.1 and Tab. 5.2 errors are also introduced by processing the measurements. This is not presented in more detail, but to mention just a few:

- manually cutting data sets
- lacking knowledge of what the sledge actually measured
- merging three days of surveying (which conflicts with bathymetric changes during survey)
- way of estimating and applying offsets
- gridding procedure

Indications of those errors are discussed briefly to present the quality of the ground truth gathered during the survey.

Vertical errors have to be judged differently than horizontal errors. Since the RDB is defined on cells of $7.5\,\mathrm{m} \times 7.5\,\mathrm{m}$ a horizontal error of couple of 10 cm is negligible. Furthermore errors in this order of magnitude only occur on the steep slopes of the beach and in turns. Those are only few datapoints compared to the full data set and the accuracy is therefore sufficient. In vertical direction the error has to be way smaller, because it is intended to resolve the vertical structure of the ridges. Those emerge about 50 cm above low water and therefore the error needs to be significantly lower than that. With

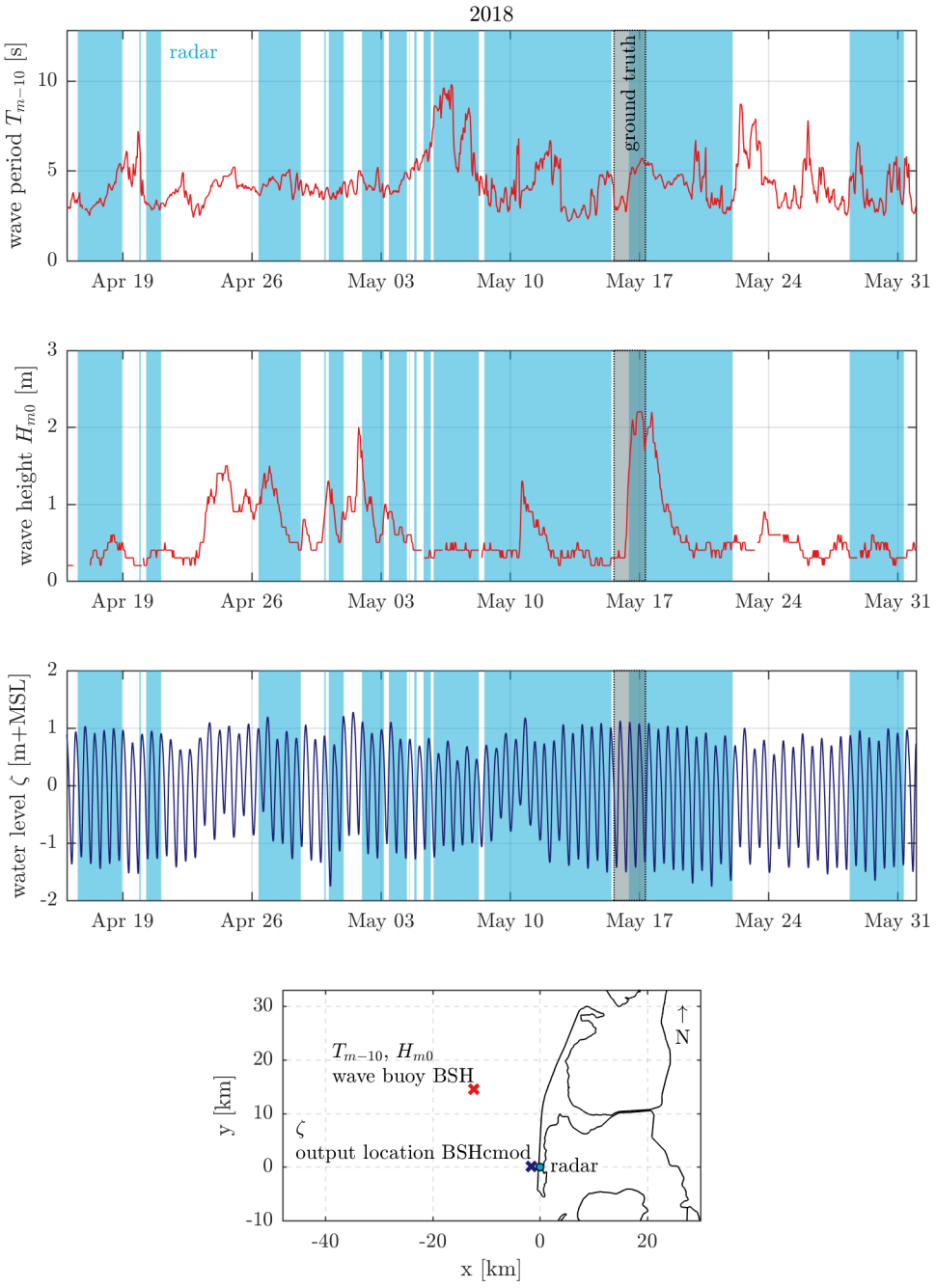

Figure 5.8: environmental conditions relevant with respect to ground truth survey **top three:** wave characteristics as hourly averages and water level every 15 min, shaded areas indicate availability of radar data (blue) and ground truth (grey) **bottom:** map of stations **data:** wave characteristics (at about 14 m depth) and water level from BSH, April 16 to May 31, 2018, map based on openstreetmap.org

Figure 5.9: impressions of error sources affecting quality of ground truth **captured:** May 15 to 17, 2018

respect to radar data sampling frequency, tidal range and period as well as available water level information, it should not be more than 10 cm. Some of the error sources may cancel out each other. Also most of the errors again occur on steep slopes and in turns. Combined with the precision of the positioning it is stated, that the wheelbarrow just suffices with probably an accuracy close to 10 cm, whereas the sledge is below 10 cm. For the full, ungridded data set the accuracy thus suffices. The gridded ground truth should show similar accuracy. No interpolation errors or similar are calculated to prove that, instead visual comparison between ungridded and gridded results was used. One important limitation arises from gridding. It has to be kept in mind, that cells of 7.5 m ×7.5 m size cannot capture small scale vertical variations, especially not on steep slopes. This possibly could be expressed in terms of accuracy. For this study its indication is, that the overall error that can be found during a validation cannot be lower than the error (standard deviation) made by gridding (merging couple of values into one). This accounts for the amount of information lost due to gridding. Because RDB uses the same grid a similar amount of information is not present. The error may sound large, but with respect to the spatial resolution this study is based on, it is sufficiently small.

A final remark on a more general matter related to different types of data sets. Whether it is better to interpolate ground truth to the radar resolution or – vice versa – refine the radar grid to a resolution matching ground truth has caused quite some internal discussion. For this work it was decided to

use the median of all points within one radar cell. This means information available in ground truth was dropped to match the degree of information available in the radar data. Problems arising when attempting to compare two different kinds of data sets, mostly relate to difference in data type.[6] Differences in data type emerge from the way data got collected. Radar data on the one hand is a geographical field (most likely). Yet it is not agreed whether it is a discrete or continuous field (2D, any point in space has a value). On the other hand the ground truth is comprised of geographical features (set of points). Those two conclusions can be drawn by looking at the way data is gathered. Radar data for instance takes many steps before it turns into an image, starting from electromagnetic signal: transmitted, scattered, smeared, moved by antenna, received, converted from analogue to digital, converted from complex numbers to real, converted from polar coordinates to Cartesian, to name just a few. The question remains how to make a geographical field comparable to geographical features. Apart from gridding ground truth and by this turn the geographical features into a discrete field (by median, mean, or any other estimation), it would also be possible to apply something like a 'smearing' mask, that imitates radar physics for instance. Which is not as straightforward. Albeit, this discussion is far off topic, despite very interesting and relates more to interpolation errors and a more fundamental question on how to validate (i.e. compare) different types of data (information).

[6] For a discussion on geographical fields and features see for instance Huisman and By [2009].

source	magnitude [cm] (direction)	details
horizontal coordinates		
sideways sliding	0 - 20 (±)	Especially in turns it can be observed that the point measured is not above the center of the sledge.
eccentricity of wheelbarrow antenne	0 - 10 (±)	The GPS antenna was mounted such that it is vertical, when lifted (by Lea Lange). Still, on steep slopes this may not hold anymore.
vertical coordinate		
wheelbarrow wheel sinks into sand	1 - 5 (+)	For loosely packed (dry) sand the wheel sinks deeper, than for consolidated (wet) sand. Dry sand usually was found on the beach, wet sand on the ridges (due to the drying caused by ebb).
sledge sinks into sand	0 - 2 (+)	Variation in sinking depth is smaller than for wheelbarrow wheel.
sledge nods	0 - 4 (−)	Depending on the way the rope was attached to the walker as well as the walking speed the sledge nodded with each step due to acceleration.
steep slopes	0 - 3 (±)	On steep slopes antenna height varies. Up the slope it increases, if the walker does not lift the handles a bit higher to compensate. Down the slope handles have to be lowered, which is not always fully possible because the wheelbarrow's legs may touch the ground. Not an issue on ridges.
ripple structures on ridges	0 - 5 (−)	Ripple structures with wave lengths in the order of the diameter of the wheel cause the wheelbarrow to jump, if walking too fast. Not relevant, since walking speed was adjusted accordingly. Yet, when walking slowly the wheelbarrow followed the ripples. It's worth a discussion, if that introduces errors, but due to the gridding this effect should average out.
wind perpendicular to track	0 - 1 (±)	Due to the big box on the wheelbarrow significant forces arise from wind blowing prependicular to the track. This was only the case on May 16. Due to another reason those tracks were not used at all. The sledge was less prone and additionally would have fallen, but not been tilted by wind.

Table 5.2: error sources affecting quality of ground truth **magnitude:** not for all sources it could be (or was) measured, it is therefore an expected/estimated value **direction:** some of the errors are not symmetrically distributed around the true value **(+):** measured value is always below true value **(−):** measured value is always above true value **(±):** measured value can be below or above true value

5.2. Validation of Radar-derived Bathymetry

Validation is divided in two parts. First radar-derived bathymetry (RDB) is compared to ground truth in a value-by-value comparison. Accuracy is similar to the one observed by Bell et al. [2016]. This section finalizes with a discussion of the validation procedure, since the nature of the compared data sets is intrinsically different.

5.2.1. Absolute Errors

Bell et al. [2016] validated TWA and thereby presented the accuracy of the method itself by incorporating the full radar range, i.e. more than the intertidal area (summarized in last paragraph of Sec. 4.1). This section deals with the accuracy in the intertidal area. Rmse in intertidal area is improved by ≈15 cm compared to the method's rmse of ≈60 cm. For the validation part the intertidal area is given by the overlap of RDB and ground truth. Ground truth covers intertidal area and above, whereas RDB covers intertidal area and some additional (incorrectly detected) parts located in the subtidal area. Effects like the '2nd shoreline' (see Fig. 4.6 and Fig. 6.1) are therefore not considered. Which explains the improved accuracy for the intertidal area over the full radar range. Rmse is 43 cm with a bias of 12 cm. Fig. 5.10 shows a map with absolute errors. Rmse and bias given above are based on an analysis window of 14.5 days. Additionally absolute errors for a 8.3 days period are shown in the right map. Bell et al. [2016] show that errors increase with distance from the radar (range dependency), which is related to radar physics (e.g. power decay, footprint of radar cell). This dependency is not visible in this data set, because number of valid (detected) cells also decreases with range. Furthermore a dependency in cross-shore direction is visible, which is indicated by the fitted lines in the scatter plots. This is contributed to the neglection of the water surface curvature induced by wave set-down and set-up (see Sec. 5.3.2). Bars are slightly overestimated by TWA, whereas the beach is underestimated. Since this is rather systematic it may be considered as a bias rather than an error. The water level record used in TWA strongly affects the vertical location of the fit (see Sec. 5.3.2).

Fig. 5.6 presented standard deviations of ground truth points within one radar cell (7.5m × 7.5 m). This is an indicator for the morphological variability present within one radar cell, which in turn indicates the minimum error possible (i.e. errors lower than that are not reliable). Fig. 5.11 relates standard deviation of ground truth within one radar cell with the respective error. The standard deviation of height variation within one cell reaches up to 36 cm. With the given spatial resolution of the radar it is therefore not possible to achieve accuracies better than in that same order (compare also to order of magnitude of $\overline{R}_2$=42 cm, Tab. A.7). This implies that TWA as presented by Bell et al. [2016] already works well, despite the comparably large error with respect to LiDAR, echosoundings or GPS surveys (which all operate on spatial scales in the order of 1 m and smaller). Furthermore it is implied, that prior knowledge of the rough extent of the intertidal area or breaker zones, makes it possible to retrieve bed levels with an accuracy as good as can be expected given the spatial resolution. If accuracies should be increased even more, it is first of all necessary to choose a spatial resolution that better suits the steep gradients found on the beach. For the variability and extent of the bars 7.5 m is sufficient.

Fig. 5.10 shows errors for an analysis period of 8.3 days. According to Blossier et al. [2016] this scale captures about 92 % morphological variability (given a spatial resolution of 7.5 m) as compared to 87 % for 14.5 days (or roughly 45 % for the current monitoring scheme by LKN.SH). The rmse (bias) is 46 cm (9 cm). Rmse and bias are in the same order of magnitude as for 14.5 days. This does not indicate that the analysis window can be chosen at will, see the next section for a sensitivity study (Sec. 5.3). It shows that a choice has to be made between capturing more variability with lower accuracy or less variability with an improved accuracy. This choice should primarily depend on the study objective, but may also be limited by data availability. For investigation of storm events (high temporal variability) it is probably sensible to use shorter analysis periods to observe changes in morphological features rather than looking into cell values. However for tracking of nourishments for example accuracy of single cells is more important, as they may serve as basis for volume estimations. Given the temporal scales are larger than for a storm, it is sensible to use 14.5 days as recommended by Bell et al. [2016] and make use of the improved accuracy.

5.2.2. Restrictions of Validation Procedure

Validation of TWA is a challenge. First of all due to the averaged character of the resulting RDB. To do a like-for-like comparison an averaged ground truth would be required. A survey would have to cover

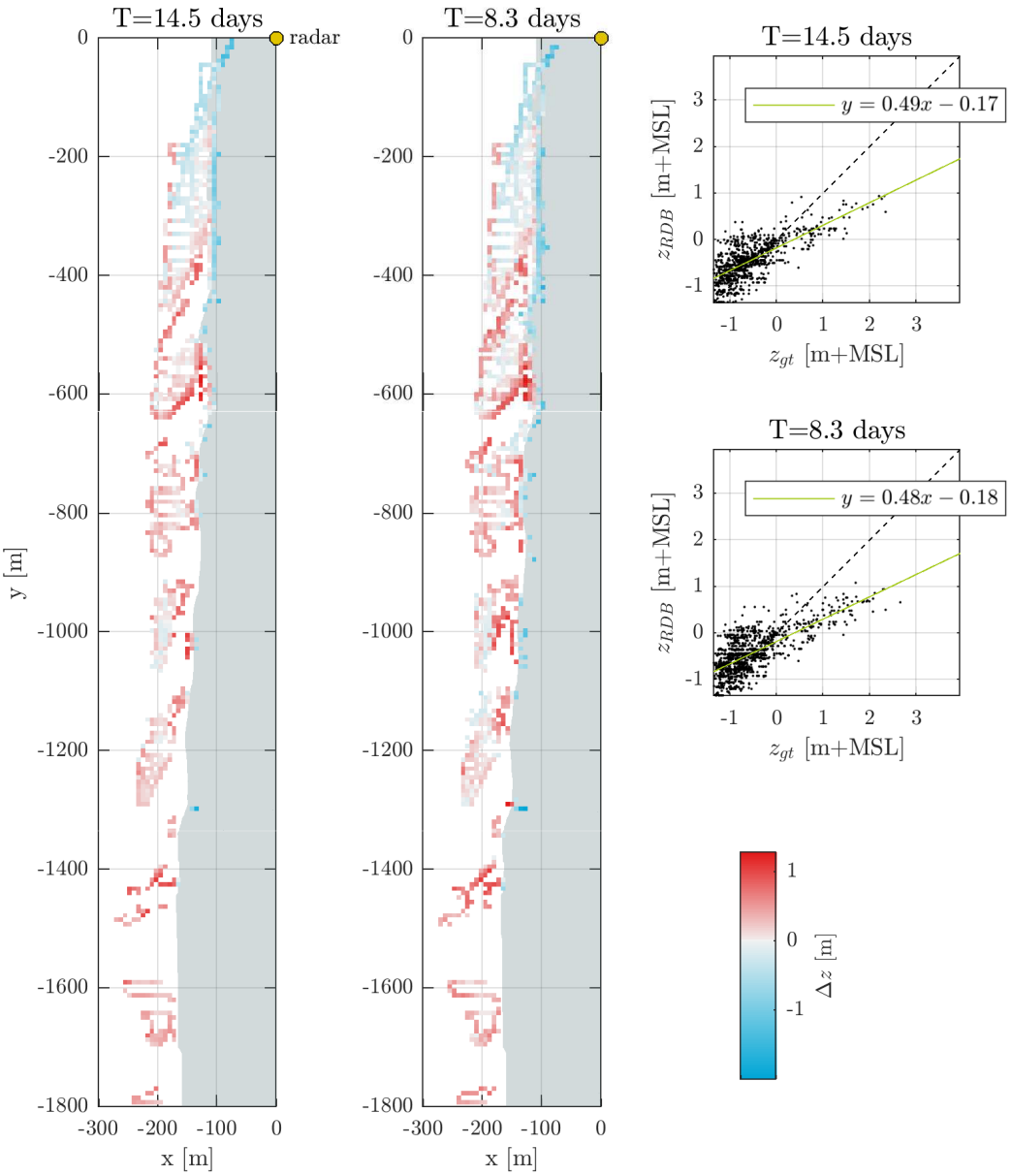

Figure 5.10: map and scatter of absolute errors between RDB and ground truth $\Delta z = z_{RDB} - z_{gt}$ **left map:** RDB covering 14.5 days (28 tidal cycles) **right map:** RDB covering 8.3 days (16 tidal cycles) **data:** left RDB (28 tidal cycles) from May 9 to 23, right RDB (16 tidal cycles) from May 12 to 20, both centered around May 16, 12:00, 2018, ground truth from May 15 to 17, 2018

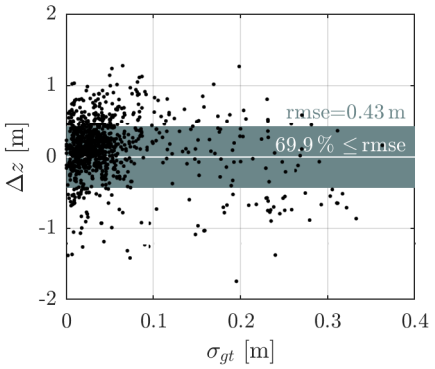

Figure 5.11: morphological variability captured within one radar cell, see Fig. 5.6 for map **x-axis:** standard deviation of ground truth within one radar cell **y-axis:** absolute error $\Delta z = z_{RDB} - z_{gt}$ **data:** ground truth from May 15 to 17, 2018

at least two weeks, with at least one measurement a day, better each tidal cycle. The results could then be averaged to yield something similar to RDB. It is expensive money- and time-wise to produce such an extensive data set. Instead one time instant is used in this study under the assumption of no significant bathymetric change in time within at least one week before and after the measurement. During the survey wind speeds increased as opposed to the mild winds before and after (see also Fig. 5.8). The beach profile appeared to be steeper after the strong winds, whereas the ridges looked similar, only ripple structures had vanished or changed. Therefore the assumption of an approximately stationary period for two weeks around the survey is challenged. Additionally to uncertainties about the formal similarity of ground truth and RDB, uncertainties also arise from the re-gridding procedure. Furthermore, GNSS surveys with RTK support are state of the art and their errors are reported, but given the experimental setup of the measuring devices (wheelbarrow and sledge alike) they are certainly altered. The wheelbarrow wheel for instance sank into the sand between 0 to 5 cm, given if the sand was wet or dry, densely or loosely packed (see Sec. 5.1.7), to mention just one. Those effects are expected to diminish through the re-gridding of the ground truth point cloud. The two-dimensional character increases the efforts of the actual comparison. Among others it requires a correct georeference for both data sets. Within the scope of this study only one data set of ground truth could be investigated to derive sensitivity and errors of TWA.

Finally there is a more fundamental challenge to validating RDB, or at that: remote sensing techniques as such. Opposed to established remote sensing techniques (like Acoustic Doppler Current Profiler) marine radar so far lacks exhaustive studies related to the backscatter mechanism and its processing performance in marine coastal environments. Some lab studies are available that investigate the effects of for example polarization and rain (e.g. Braun et al. [2002]), as well as experience from the years marine radar is in use in the Radar Hydrography group. With increasing knowledge about radar physics of X-band marine radar, also methods like TWA can be improved and their validity can be judged not only based on comparison to ground truth, but also on the physical mechanisms underlying the raw data. Comparison with ground truth alone for instance will not reveal, if the steepest gradient in mean backscatter intensity actually marks the transition from wet to dry (or merely the beginning of the drying or wetting).

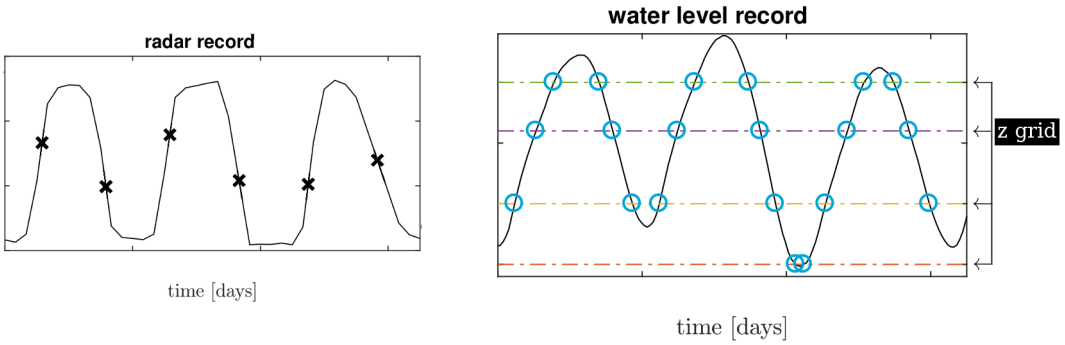

Figure 5.12: recap: role of z grid in TWA **data:** see Fig. 4.3

5.3. Sensitivity of Temporal Waterline Approach

This section provides a recommendation of how to choose parameters for Temporal Waterline Approach (TWA) specifically for the study area Bunker Hill. Sensitivities are described and parameters are chosen for the study area. Bathymetries are derived with varying sets of parameters and are compared to ground truth. For each parameter rmse, bias, correlation coefficient and standard deviation are calculated for the investigated parameter space. For the sake of readability those figures are placed in the appendix (A.4) and only decisive parts are presented in the scope of this section. The focus lies on the following parameters:

1. Resolution of Vertical Grid
2. Water Level Model
3. Analysis Window
4. Thresholds as Quality Measures

The sensitivity analysis starts off with the parameters used by Bell et al. [2016] to update them for Bunker Hill (Tab. 5.4). Results are summarized at the end of this chapter in Tab. 5.4.

5.3.1. Resolution of Vertical Grid

Bell et al. [2016] suggest to use a finer vertical resolution for study areas with smaller tidal range than in their case. The tidal range (TR) in Sylt is about 2 m for spring tides, opposed to more than 10 m in the original work. The aim of this section is to find an appropriate spacing dz for the z grid.

The z grid extracts information from the water level record about transitions from wet to dry and vice versa (see Fig. 5.12). The transitions in the radar record are found without the help of a z grid. In turn, the resolution of the RDB is determined by the resolution of the z grid (i.e. its equidistant spacing dz). Theoretically and by the way TWA is implemented numerically the accuracy of the final bathymetry increases with decreasing dz. Eventually it converges and further decreasing of dz does not improve the result further. The converging value of dz is not clearly defined. It is blurry due to restrictions like the equidistance of the z grid vs. the equitemporal grid of the water level record. Ideally dz relates to the change in water level ζ:

$$\frac{dz}{dt} \propto \frac{|\partial\zeta|}{\partial t} \tag{5.1}$$

For the given period of two weeks the water level change $\partial\zeta$[7] is distributed as presented in Fig. 5.13. More than 75 % of water level changes is below 25 cm. About 25 % of the changes are below 10 cm. Changes between 0 to 10 cm are almost equally distributed. It is therefore necessary to choose a spacing that is small enough to capture as much as possible of this small scale variations in water level. For a spacing of 2 cm about 5 % of the water level changes are undersampled. Further decreasing of dz does not improve the final result (variation in rmse and R diminishes, see also Fig. A.8).

[7] Water level change is calculated as difference of consecutive time steps: $\partial\zeta \approx \Delta\zeta = \zeta_{i+1} - \zeta_i$. Time between two consecutive steps is about 30 min.

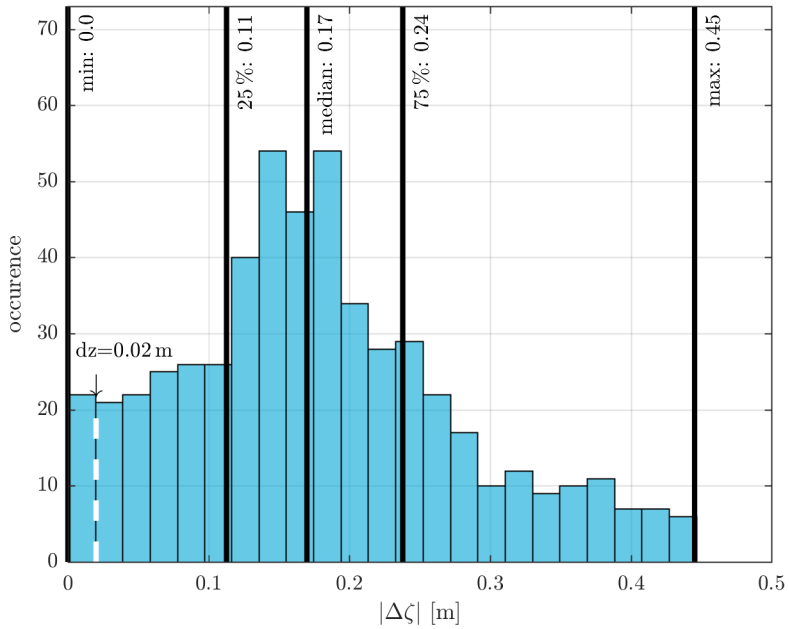

Figure 5.13: histogram of absolute water level changes **data:** water level record, May 9, 12:00 to 22, 2:00, 2018 (WLM-original)

	tide	meteo	run-up	wave set-up
	measured/modelled offshore		*here Stockdon et al. [2006, Eq. (19)]* / Eq. 2.3	
WLM-original	x	x		
WLM-updated	x	x	x	x

Table 5.3: contributions to water level models (WLM, Water Level Model)

The rmse between filtered RDB and ground truth is then 0.41 m and correlation is 0.72. For further processing a z grid resolution of 0.02 m is used.

5.3.2. Water Level Model

TWA uses water levels homogeneously in the full radar range. This is expected to cause significant underestimation[8] especially in the upper part of the intertidal area, because the cross-shore variation of water level is neglected. Furthermore the phase shift of the tidal wave in longshore direction is neglected, which is not of major concern here. The water level at the shore has major contributions from tide, wind and waves. The combination of tide and wind-induced setup is contained in the operational model from BSH (for data sources see Chap. 3). For estimation of wave set-up and run-up an empirical formula is used. Tested are two water level models (WLM), see Tab. 5.3. WLM-original resembles the one described by the original paper on TWA [Bell et al., 2016], whereas WLM-updated includes wave set-up and run-up. This is achieved in the same way as Blossier et al. [2016] describe it for their camera-based mapping of shorelines. Other formulations exist (e.g. Aarninkhof et al. [2003]), yet the video monitoring system Blossier et al. [2016] use is located on the same platform as the radar, thereby showing that it is valid to apply this water level model in this area.[9]

Although many assumptions underly WLM-updated and its various shapes in other publications used in the scope of shoreline detection, they prove to give satisfying results in at least some cases for camera-based techniques (see for instance Aarninkhof et al. [2003] with vertical errors up to 15 cm for

[8] or overestimation if the water level record is taken from the shoreline and not offshore
[9] They evaluated a range of MHW$\pm$0.2 m.

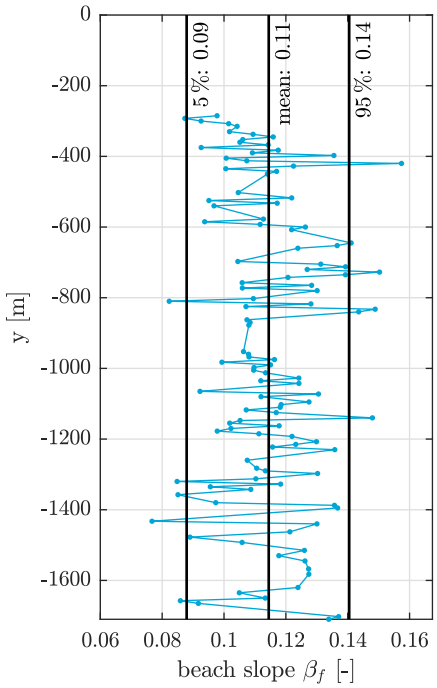

Figure 5.14: alongshore distribution of upper shoreface beach slope **data:** calculated from ground truth, May 15 to 17, 2018

85 % of their study area). In comparison to TWA none of them struggles with the concept of what can be perceived as the representative water level. Camera-based methods use at most 18 min of image sequences (e.g. Blossier et al. [2016]), which happens to be in the same order of magnitude as the time scales used to derive sea state statistics. Sea state statistics (as input to the water level models) and the camera data are defined for similar time scales. With respect to TWA at least couple of days need to be represented, which increases – amongst the other limitations of available run-up and set-up formulations – difficulty of defining a sensible water level model.

Both WLMs are applied homogeneously in the study area. This is based on the original approach by Bell et al. [2016], which use WLM-original homogeneously in the full area. Note that especially with the additional run-up and wave set-up in WLM-updated it might be necessary to resolve spatial variations. Slopes of the sandbars, the channels and the beach vary significantly and this could be captured in a spatially varying water level model. Improvements are expected to be marginal, especially as related to the effort to define appropriate slopes (of the yet unknown bathymetry) for the different features and the order of magnitude of average run-up and set-up.

The wave-induced setup on intermediate beaches is estimated as a 2 % exceedance value R_2. Stockdon et al. [2006] present an empirical formula for R_2 based on wave statistics and beach slope (Eq. 2.3). Hourly records of significant wave height H_s and period T_{m-01} from a buoy about 14 km offshore in about 14 m depth are chosen as input (time series: Fig. A.23). Blossier et al. [2016] successfully applied R_2 based on similar data sources in the same study area for a camera-based approach of extracting shorelines. Stockdon et al. [2006] define the beach slope β_f between the mean water level $\pm$ two times the standard deviation. This is not applicable at Sylt, because of sandbars and also lack of data in the lower lying parts (ground truth reaches down to -1.36 m+MSL, whereas $2\sigma(\zeta)$=1.57 m during the two weeks period for validation). Instead the upper shoreface beach slope β_f is calculated (as has been used by Blossier et al. [2016]) as the alongshore averaged slope of the line connecting the 0 m contour with its 2 m contour. This way the sandbars are excluded from the slope determination. Fig. 5.14 shows the longshore distribution of beach slopes. Mean slope of 0.11 is used for R_2 calculation (5th percentile is 0.09 and 95th percentile is 0.14, which is slightly milder than observed by Blossier et al. [2016], see also Sec. 3.1). Other β_f values were tested, too (see Fig. A.9 and Fig. A.10).

Opposing to the overall upper shoreface beach slope β_f Fig. 5.15 shows the cross-shore slope α.

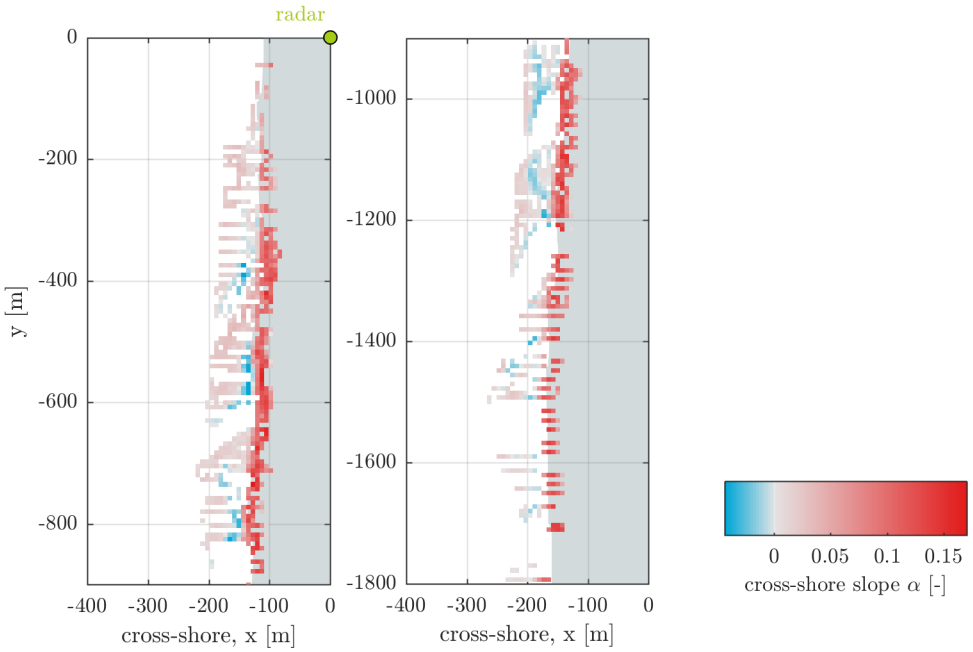

Figure 5.15: cross-shore slope of ground truth **data:** calculated from ground truth, May 15 to 17, 2018

It serves as separator between sandbars and beach. It is defined as the slope of a cell smoothed over three cells in cross-shore[10] direction. The slope of the beach ($\bar{\alpha}_{beach} \pm \sigma$=0.1±0.01) is steeper than of the sandbars ($|\bar{\alpha}_{sandbars}| \pm \sigma$=0.02±0.02). The offshore edge of the channels have negative slopes. A cross-shore slope α=0.07 yields a good criterion to distinguish beach and sandbars. Fig. 5.16 visualises the errors introduced by the choice of WLM. Time series of R_2 is added to the water level ζ before TWA performs the correlation analysis. The result is shown in the right figure. The x-axis represents ground truth via the cross-shore slope. Via the slope it is possible to distinguish between sandbars and beach. The y-axis shows the deviation between ground truth and the respective RDB. The purple bounds are based on the data presented in the left figure and put for reference. The number of points available for the sandbars is larger than available for the beach. Since the beach is quite steep it is usually only covered by roughly three radar cells (in cross-shore direction), whereas sandbars extend over significantly more radar cells. The rmse for WLM-original is 0.40 m. In case R_2 is applied (WLM-updated, right figure) ideally the point cloud would become more confined (lower rmse) and centered around zero (decreasing bias). Instead the overall rmse becomes worse as does the bias. Note that the application of R_2 is not equivalent to applying an offset, as can be seen by the changed shape of the point cloud. In more detail it is observed, that applying R_2 potentially increases accuracy for the beach, whereas it decreases accuracy for the sandbars. For four reasons it is decided to continue without applying R_2:

1. *focus:* sandbars contribute most to the final bathymetry, overall accuracy is thus predominantly determined by them. Application of R_2 is only beneficial for the beach, but not the sandbars (Fig. 5.16).

2. *data:* to determine R_2 additional data is needed, which poses problems, if not readily available and might introduce even more errors

3. *validity of formula:* the sandbars actually violate the underlying assumption of a plane beach. Furthermore R_2 is located at the shoreline. It cannot be applied homogeneously in cross-shore direction. It would be necessary to spatially resolve R_2. Even if TWA was implemented to spatially

[10] Cross-shore is approximated along the x-direction in this case, thus not perfectly perpendicular to the shoreline, which is not exactly north-south oriented, but inclined by about 3° (see Sec. 3).

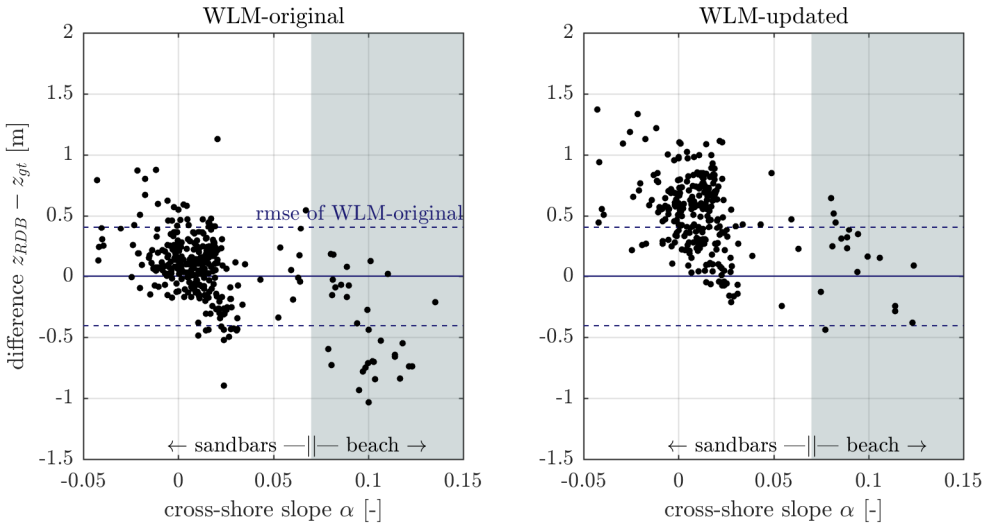

Figure 5.16: deviation of RDB from ground truth with relation to cross-shore slope **left:** WLM-original, R_2 not applied **right:** WLM-updated, R_2 applied **data:** ground truth from May 15 to 17, 2018 and RDB from May 9, 6:00 to 23, 18:00, 2018, filtered with θ_R=$\theta_{R,Bell}$=0.3, β_f=0.11

resolve water levels, the next problem would be how to define the decrease of R_2 in cross-shore direction.

4 *scales:* R_2 is in the same order of magnitude as the rmse (compare Tab. A.7), therefore no overall improvement can be expected by applying it, but probably the cross-shore dependency of rmse could be weakened.

The uncertainties introduced by more data sources and the formulation of R_2 counteract the gain in accuracy. Since no significant gains in accuracy can be expected it is opted to stay with as less data required as possible. This way TWA stays a method that does not require much input, yet yields robust results.

In case attempts are made to improve accuracy at costs of robustness, it is noted, that the accuracy depends on the spatial distribution of wave-induced setup and run-up. Two options are promising. Either, resolving the water level not only in time, but also in space, which potentially will increase the accuracy of the method. This could easily be achieved with an adapted numerical implementation, yet increased computational costs. Output from numerical models interpolated to the grid of the radar would serve as source, since the available monitoring network is not capable of producing a spatially resolved water level. Or, if no numerical model detailed enough is available it may be possible to extract an empirical formulation for the water surface's cross-shore curvature from the data itself, for example with a quadratic fit through the scatter (for a linear fit as example see Fig. 5.10). The shape of a quadratic fit may resemble very roughly the water surface's curvature and thus serve as basis for the cross-shore curvature of the water surface. Neither of the two options is tested in the scope of this study.

5.3.3. Analysis Window

Bell et al. [2016] choose the analysis window for TWA such that it incorporates the largest water level range. This will also be the range of bed levels 'visible' in RDB (Fig. 5.17). For the sake of simplicity they therefore recommend to use a two weeks window, thus one spring-neap tidal cycle (always contains largest possible astronomical tidal range). Despite the two weeks window approach it is still possible that TWA is not capable of resolving the lower lying parts, due to wind setup for example. It is therefore interesting to investigate how TWA performs for shorter and longer analysis windows. Bell et al. [2016] suppose that also shorter analysis windows are possible, which should have a trade-off based on statistical restrictions. Shorter analysis windows are desirable, because more variability is captured (e.g. five days required to monitor 95% variance of the shoreline [Blossier et al., 2016]). Longer analysis windows should show a trade-off as soon as the environmental conditions become non-stationary.

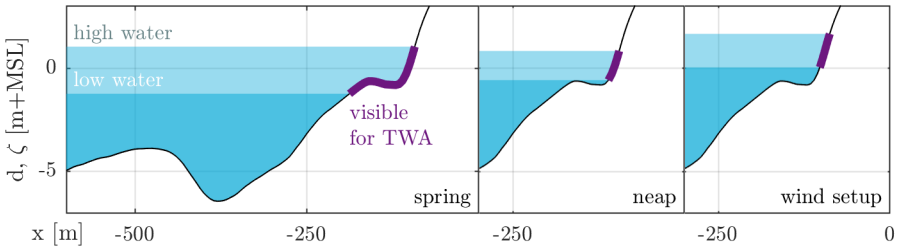

Figure 5.17: effect of different water level ranges on what is 'visible' to TWA **data:** profile from echosounding and GPS, Sept 2016, water levels extracted exemplarily from BSHcmod

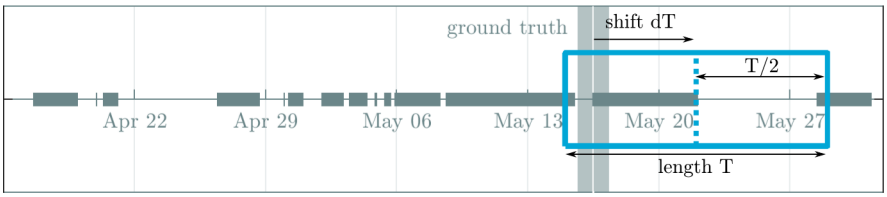

Figure 5.18: definition sketch of analysis window **shift:** defined positive to the right (forward in time), origin at May 16, 12:00, 2018 **background:** ground truth from May 15 to 17, 2018, radar from April 16 to May 31, 2018

It is expected that there is not one optimum window length, but a range. For shorter as well as longer analysis windows results become worse. Results from shorter windows will increase their degree of randomness and therefore be less reliable. Whereas for longer windows it becomes harder to tell what the result is representing. Given approximately stationary conditions during the period defined by the analysis window it is expected, that the RDB shows an average bathymetry of this period [Bell et al., 2016]. Two aspects of the analysis window are interesting:

1 length of analysis window → morphological variability captured

2 shifted center of analysis window → representative character of RDB

The analysis window is placed symmetrically in time around the time stamp a bathymetry shall be retrieved for. Fig. 5.18 provides a definition sketch. The possible range of window lengths as well as shifted centers is restricted by the availability of radar data as depicted in the background of Fig. 5.18. Before ground truth collection about three weeks of radar data are reasonable to use, because gaps are mostly less than a day long. One day of data is missing during ground truth collection, because the radar was under maintenance. Due to the large gap five days after ground truth collection it is not possible to investigate a potential maximum length for the analysis window. Instead the focus is on how short is still long enough. With respect to shifting the analysis window the data is not sufficiently good. It cannot be answered, if TWA produces an average bathymetry (which is resembled by $dT = 0$) or rather, how often and how strong RDBs deviate from this assumption and thus show the sensitivity of TWA towards dT. However, the data still reveals the effect of non-stationary conditions on RDB, because wind increased during ground truth collection.

Despite the lower bound that is presented below for window length T, this section proves that nevertheless the most important factor for sensitivity of TWA is the filtering applied (required minimum window length of 5.2 days will be increased to 8.3 days in the next section). Trends visible in Fig. 5.19 and Fig. 5.20 are governed by filtering, which appears to be dependent on the length of the analysis window.[11]

[11] Dependencies may also exist for other sensitivity parameters not considered in this study.

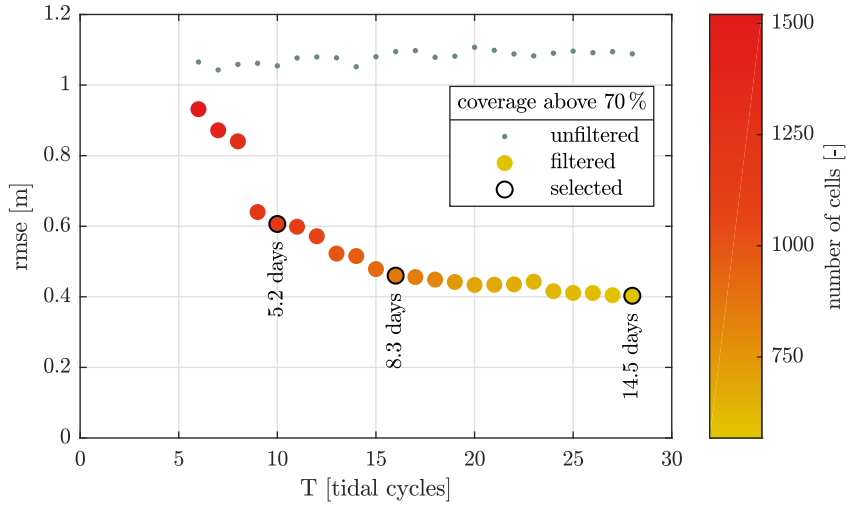

Figure 5.19: evolution of rmse with respect to length of analysis window **unfiltered:** based on about 2500 cells **coverage:** number of records over possible records (assuming one record each 30 min) in percent **data:** RDB derived in steps of one tidal cycle (12 hr and 25 min) centered around May 16, 12:00, 2018 with maximum period covered from May 9, 06:00 to May 23, 18:00, 2018, filtered with θ_R=$\theta_{R,Bell}$=0.3

```
filtering_thresholds = f(T)
```

In the remainder of this section the analyses on window length T and window shift dT are presented, but note that no clear sensitivities can be singled out.

1 length of analysis window T:

Fig. 5.19 shows the evolution of rmse with respect to length of analysis window. The rmse decreases with increasing length of the analysis window. It looks as if it approaches a minimum rmse of about 0.4 m. With respect to statistics this also holds for longer windows than indicated in Fig. 5.19. Yet, due to increasing likelihood of non-stationary environmental conditions with increasing window length it is expected that the rmse increases again for lengths larger than 15 days. Number of cells decreases with increasing window length, which is surprising at first thought. With longer windows the number of reliable cells should become larger. This is not the case, because the overall correlation level of a RDB decreases with increasing window lengths. Or differently put: for shorter window lengths it is required to increase θ_R to obtain the same RDB as for a longer window length. This dependency is further discussed in the next section (Sec. 5.3.4). Furthermore the decreasing coverage with increasing window length also contributes to an overall decrease in correlation level.

It is striking that the three points at the lower end of T are unexpectedly shifted upwards. This cannot be explained with wind, wave or water level conditions, neither with gaps in the radar data. It therefore must be related to statistics of the case or TWA. Because they are still following the overall trend – or put differently they appear to have a bias as compared to the other points – it cannot be the lower limit when the correlation analysis becomes unreliable. In that case the three points would show a certain degree of randomness which is not the case. Further discussion of this is provided in Sec. 5.3.4, because it is found that it relates to θ_{trans}. For further analysis of this section those three points at the lower limit of T are not considered.

The choice of window length strongly depends on the scope of the study, i.e. scales of the effects to be studied and data availability. For large data sets, for which it might be unhandy to manually check the water level conditions, it is useful to stay with the recommendation of Bell et al. [2016] and use 14 days (which in this study is set to 14.5 days or 28 tidal cycles). With intervals of 14.5 days about 85 % temporal variability can be resolved at Sylt [Blossier et al., 2016]. For studies focusing on faster scales it is possible to use shorter windows, yet at costs of accuracy as indicated by an increased rmse

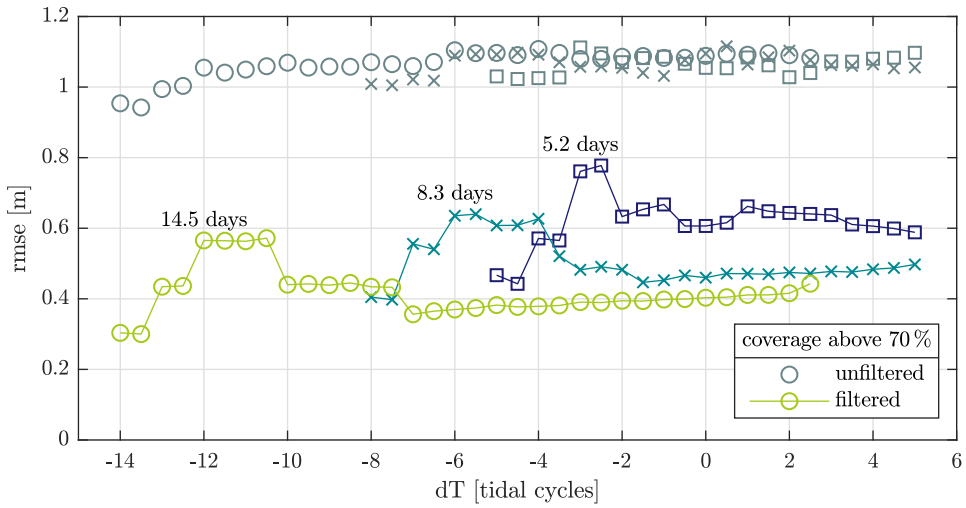

Figure 5.20: evolution of rmse with respect to shift of analysis window **unfiltered:** based on about 2500 cells **filtered:** annotations denote window length used for respective curve **coverage:** number of records over possible records (assuming one record each 30 min) in percent **data:** RDB derived in steps of half a tidal cycle (half of 12 hr and 25 min) centered around May 16, 12:00, 2018 with maximum period covered from May 1, 18:00 to May 26, 8:00, 2018, filtered with θ_R=$\theta_{R,Bell}$=0.3

(Fig. 5.19). Three different lengths are of interest for this study. First of all for the processing of a full year it is handy to use 14.5 days (full neap-spring cycle, rmse of 0.4 m). This is also the longest reasonable within this study, because for longer windows it cannot be proven how errors will evolve. The shortest is set to 5.2 days (rmse of 0.61 m). With this monitoring frequency 95 % variability of the shoreline can be traced [Blossier et al., 2016]. The rmse increases as compared to longer window lengths, but is still reasonable. 8.3 days are chosen as an inbetween value with a rmse of 0.46 m. Lengths shorter than this show a significant increase in rmse, which is approximately the same between 8.3 to 14.5 days.

2 shifted center of analysis window dT:

Since the representative character of RDB cannot be investigated due to lack of sufficient data, instead an interesting behaviour that was observed when shifting the window is presented. Fig. 5.20 presents the evolution of rmse over shift dT. To the left curves end, when the analysis window has no overlap with ground truth any more. To the right coverage decreases below 70 %. Shift is given as number of tidal cycles of the window's center from ground truth collection represented by May 16, 12:00, 2018 (middle of ground truth collection). Window lengths of 5.2, 8.3 and 14.5 days are used (10, 16 and 28 tidal cycles respectively, see also Fig. 5.19). All three curves exhibit a similar behaviour. The rmse stays roughly the same at first for increasing shift (foward and backward in time). Shifting further backwards in time rmse first increases, which is expected because the resemblance with ground truth should decrease. Yet rmse then decreases again, even lower as compared to no shift. This would be unexpected for a stationary case, because it would imply that the shifted RDB – that has no overlap with ground truth any more – fits better to the ground truth than the RDB centered around it. This may be due to violation of the stationarity assumption. Two changes in environmental conditions are present in the data record. First, a short period of large setup prior to the period of ground truth collection. Second, wind increased during second half of ground truth collection. Alternatively the peaks in Fig. 5.20 may also be based on the performance of the peakfinding algorithm, which during periods of overall similar backscatter intensity levels performs different than if a few days with high intensities (roughened surfaces and steeper waves due to high winds) are present in the record.

5.3.4. Thresholds as Quality Measures

Sensitivity analysis is quite important and the previous investigations mark major steps towards understanding how sensitive the method is to three of its main parameters. Nevertheless it boils down to the notion of the maximum correlation coefficient of a cell – or as it is thresholding in general – and it

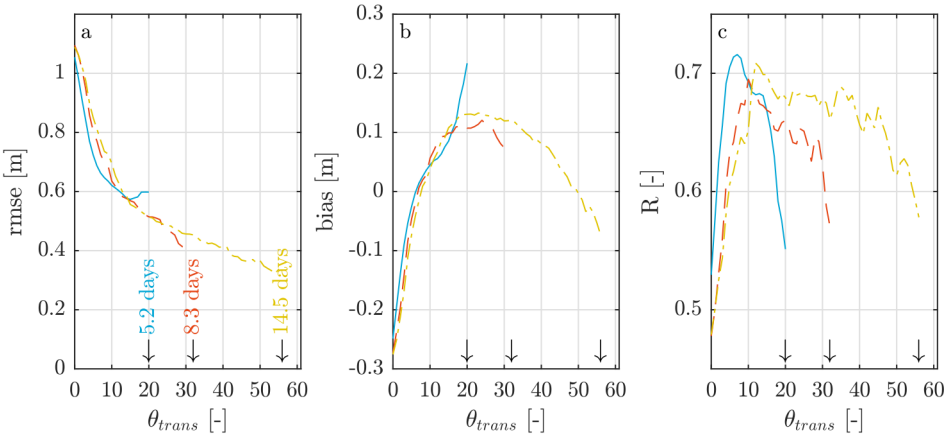

Figure 5.21: sensitivity of filtering by number of transitions. Largest threshold θ_{trans} applied equals the maximum number of transitions (physically) possible within the analysis window (given a semi-diurnal tide and two transitions per tide). **colors:** length of analysis window **arrows:** indicate maximum number of transitions possible, given a semi-diurnal tide and (theoretically) two transitions per tide **data:** RDB centered around May 16, 12:00, 2018 with maximum period covered from May 9, 6:00 to May 23, 18:00, 2018 (θ_R not applied) and statistical measures from comparison with ground truth, May 15 to 17, 2018

showed already throughout the investigation of the previous three parameters, that the choice of θ_{trans} and θ_R is the most crucial one. This section provides the analysis, which preceded the improvements to TWA presented in Sec. 4.3.

The correlation coefficient TWA is based on only is meaningful, if it is based on a reliable number of transitions. See for instance the case of the lowest level of a water level record: its pattern has only two transitions during the full analysis period. The risk, that it coincidentally yields a good match (high correlation) with the (radar) pattern observed from a cell on land or offshore is quite high. The result is that couple of cells on land and offshore get a high correlation, that cannot be filtered with θ_R without also filtering valid cells in the intertidal area. It is therefore sensible to use θ_{trans}. It is expected to show a lower limit (minimum number of transitions required) as well as an upper limit. The upper limit would be the number of transitions physically possible, thus depends on the tidal period and the analysis period T. In this study (semi-diurnal tide) the upper limit is 3.87 transitions per day (see Eq. 4.1), for 14.5 days this yields about 56 transitions at maximum. The lower limit is expected to be related to statistics rather than site-specific parameters. Fig. 5.21 shows the evolution of accuracy with respect to an increased filtering threshold for the number of transitions. Each curve represents a different analysis window length. Each curve is cut at its upper limit for θ_{trans} (indicated by arrows in Fig. 5.21). All of the three curves exhibit wiggling behaviour for θ_{trans} above this maximum (see Fig. A.17), which is related to a low number of cells remaining after filtering. Estimation of rmse and other statistical measures past those points becomes too unreliable. With increasing filtering rmse improves (Fig. 5.21 a). All three RDBs appear to be following the same (absolute) trend here. Only close to the maximum threshold they differ slightly (number of remaining cells too low). Bias (Fig. 5.21 b) improves up to a certain threshold (bias is approximately zero for θ_{trans}=7 for 5.2 and 8.3 days, and θ_{trans}=8 for 14.5 days). Above this threshold the bias is positive and increases up to the order of 10 cm. For the longest analysis window it then decreases again with increasing θ_{trans}. The behaviour reflected here relates to the fact, that number of transitions are not uniformly distributed over all bed levels (see boxplots in Fig. 5.22). Low and high areas potentially experience less transitions than areas located somewhere around mean water, because only very low/high water levels reach down/up there. Low values for θ_{trans} therefore predominantly remove cells at the lower/upper end of the full bed level range, as indicated by the two red lines to the left of Fig. 5.22. The red line to the right marks the physical maximum of transitions. The large negative bias (Fig. 5.21 b) for low values of θ_{trans} originates from a domination of incorrectly detected cells (no correlation filter applied). With increasing θ_{trans} (up to 7 or 8) this effect diminishes. As presented in the scatter plots in Fig. 5.10 certain bed levels are more prone to underestimation, some more to overestimation (inherent to TWA). Wrapped up, the beach is usually underestimated (negative bias) by TWA, whereas the lower lying parts are slightly

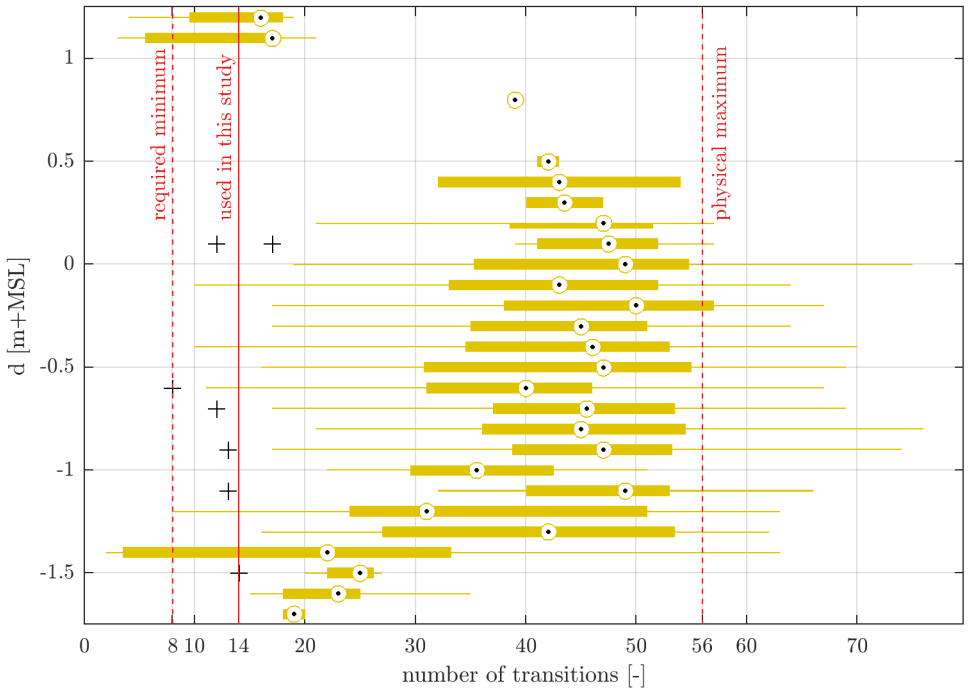

Figure 5.22: distribution of number of transitions over bed level classes in 14.5 days (boxplots) **vertical lines (from left to right):** statistically required minimum threshold (dashed), chosen threshold as presented in Sec. 4.3 (solid) and maximum of physically possible transitions in a pronounced semid-diurnal environment given a analysis window length of 28 tidal cycles (dashed) **data:** RDB from May 9, 6:00 to May 23, 18:00, 2018 (28 tidal cycles), filtered only with θ_R=$\theta_{R,Bell}$=0.3

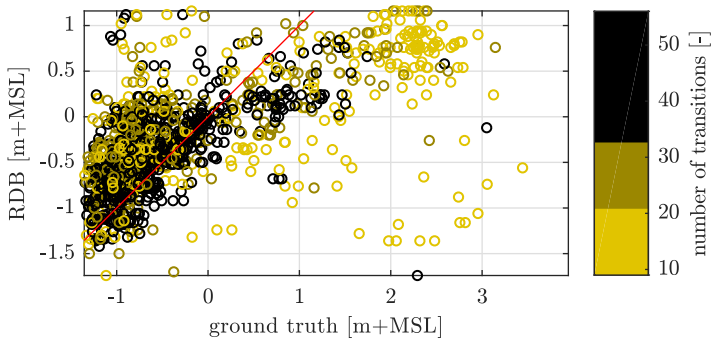

Figure 5.23: application of θ_{trans} leads to domination of lower lying areas **red line:** ideal fit (no bias), above has positive bias, below negative (see Sec. A.4 for definition) **colors (from bottom to top):** class limits mark frist zero-crossing in Fig. 5.21 (b), maximum bias, second zero-crossing and physical maximum of transitions. With increasing θ_{trans} only dark points remain. Initially (yellow to black) bias is negative due to domination of (yellow) datapoints to the very right. Intermediate filtering improves bias and eventually turns it positive, because lower lying parts dominate. **data:** RDB centered around May 16, 12:00, 2018 with maximum period covered from May 9, 6:00 to May 23, 18:00, 2018 and ground truth from May 15 to 17, 2018

overestimated (positive bias). With further increasing θ_{trans} the beach is filtered out faster (because fewer cells) than the lower lying parts. Therefore the bias becomes positive as it is now mainly based on cells in the lower lying areas. Opposing the other two (shorter) curves, the yellow curve for 14.5 days in Fig. 5.21 improves its bias and eventually reaches a negative bias again, albeit small. This can be explained by looking at Fig. 5.23. The scatter is colored by number of transitions. Black circles are what is left after a fairly high value for θ_{trans} is applied. Whereas all circles together represent what remains for a low threshold. It is clear that not only the outliers in the lower right corner are removed with increasing threshold, but most of the circles to the top right are removed, too. The lower lying parts in the lower left corner gain in dominance for increasing θ_{trans}.

Correlation (Fig. 5.21 c) peaks for all three curves for relatively low values of θ_{trans}. This supports the choice of a minimum threshold of at least eight transitions, which can be made slightly larger in relation to the window length (see Eq. 4.2).

The spot marked with 'noise (2)' in Fig. 4.6 (d) on p. 28 visualizes how the choice of θ_R influences the accuracy of RDB. Inappropriately chosen it does not remove all the noise and therefore disturbs the accuracy. Bell et al. [2016] find a value of $R \leq 0.3$ for non-intertidal areas, which is used to filter RDBs ($\theta_R = \theta_{R,Bell} = 0.3$). Fig. 5.24 shows that the overall correlation of intertidal and non-intertidal areas are dependent on the analysis window length T (see also Sec. 5.3.3). Overall correlation is denoted by the mean of all correlation values within a defined area. Additionally standard deviation within the defined area is calculated. Two areas are defined. Non-intertidal (i.e. invalid, because not visibile for TWA) area is selected from a region offshore (i.e. sea). Placed on land the defined area shows the same behaviour. Intertidal (i.e. valid, because visible for TWA) area is the area covered by groundtruth intersected with an intertidal range of bed levels. X-axis provides a reference to the number of averaged radar images (i.e. datapoints) used. To ease understanding the number of datapoints available are transformed to an (equivalent) window length T, assuming no gaps and records every 30 min. The dependence of overall correlation in intertidal areas on window length (i.e. number of datapoints) is obvious. This proves that also the choice of the threshold θ_R depends on the analysis window, thus $\theta_R = f(T)$. One implication is, that a short analysis window only then is non-beneficial if θ_R is chosen unaccordingly. Furthermore the overall correlations of intertidal and non-intertidal areas are correlated with each other, which serves as the basic idea for the rule of thumb in Eq. 4.3. Above window length of about three days both mean curves follow the same trend on different levels of R. Since the intertidal area is not yet known, it is not possible to retrieve the overall correlation of the intertidal area as a reference for a filtering threshold.

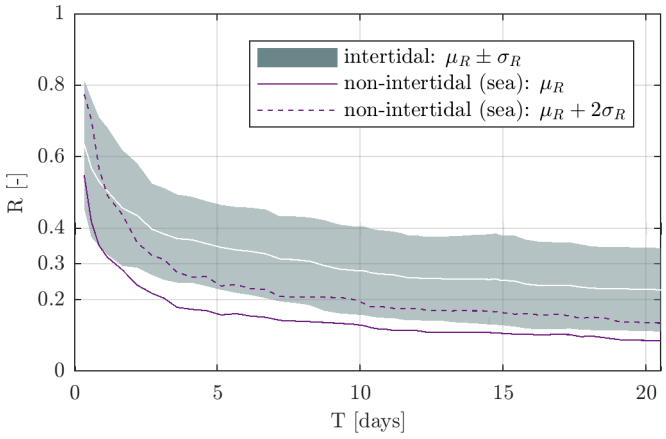

Figure 5.24: relation between overall correlation in non-intertidal and intertidal areas over window length T **x-axis:** here window length is the equivalent time if no gaps were present, thus number of averaged radar images times 30 min **data:** RDB derived in steps of one tidal cycle (12 hr and 25 min) centered around May 16, 12:00, 2018 with maximum period covered from May 9, 06:00 to May 23, 18:00, 2018, not filtered, but cut to intertidal and non-intertidal areas

Instead a reference area (of more than 100 cells) is defined, in a clearly non-intertidal area to retrieve the overall correlation of the solid, purple curve in Fig. 5.24. This value is combined with the standard deviation of itself, which results in the dashed, purple curve. It was found empirically, that adding two times the standard deviation works well for a rule of thumb to estimate θ_R.

Besides, Fig. 5.24 is a first indication that the rule of thumb (Eq. 4.3) is not site-specific, because the combination of 14 days with a threshold of $\theta_{R,Bell}$=0.3 as used by Bell et al. [2016] is also found there. Bell et al. [2016] used radar records between every 30 min to 1 hr, which results in an equivalent window length of 7 to 14 days in Fig. 5.24. The overall correlation μ_R of the intertidal area for 7 to 14 days is in the order of $\theta_{R,Bell}$. This is supported by experience made during sensitivity analysis. For analysis windows of 14.5 days (coverage usually below 80 %) $\theta_{R,Bell}$ worked well, but filtered a bit too much, whereas for shorter windows to many invalid cells remained and for longer windows too many valid cells were removed. Therefore it is reasonable that the chosen rule of thumb for θ_R (dashed, purple line in Fig. 5.24) is lower than $\theta_{R,Bell}$ in the range of 7 to 14 days, yet it still indicates, that this rule of thumb may also hold in other study sites and therefore is rather dominated by statistics than hydrodynamics or radar physics.

Fig. 5.25 shows rmse, bias and correlation over different θ_R for three different window lengths. Rmse (a) are first constant, i.e. $\theta_R \leq$0.1 does not make sense[12]. Rmse then improves by about 20 cm for increasing θ_R, which is as expected. However at a certain point filtering becomes too strict and too few cells remain to make up a reliable basis for statistical measures, neither does the RDB contain any useful bathymetric information any more (see also decrease in number of cells that remain after filtering in Fig. A.18). Tendency is the same for all three analysis windows. The longer the window the better the rmse. Or put differently: to achieve the same accuracy with different window lengths the filtering threshold has to be adjusted accordingly (the shorter the window the larger the threshold, indicated by the position of the arrows; see also Fig. 5.24). Bias (b) is in the order of 10 cm or below for all three cases. It reduces to zero for large θ_R, which is not of use, because barely any cells remain after filtering. Correlation between filtered RDB and ground truth (c) increases for all three window length with increasing θ_R, but only slightly. This indicates that the resemblance improves with increased filtering. For behaviour for even larger θ_R see Fig. A.20.

All three curves in Fig. 5.25 indicate that increased θ_R improves the overall resemblance of RDB with ground truth. Yet it becomes clear, that a compromise has to be made between a sensible (i.e. full coverage) bathymetry and its accuracy. The recommended rule of thumb in Eq. 4.4 for θ_{trans} and θ_R is such a compromise. Furthermore it is referred back to the previous section (e.g. Fig. 5.11), where the variability of Bunker Hill beach was related to the best achievable accuracy in the order of 40 cm for the steep beach.

[12] Probably this is the limit below which no correlation is present any more.

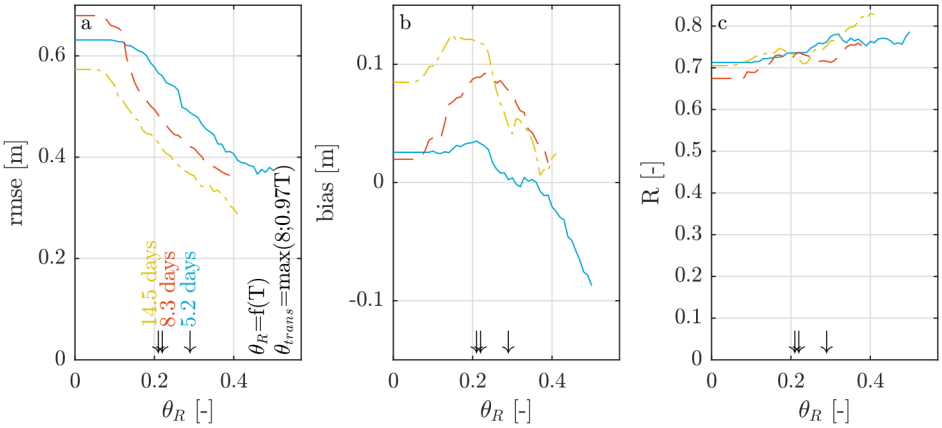

Figure 5.25: sensitivity of filtering by correlation. Largest threshold θ_R applied is the maximum correlation found in reference window for Eq. 4.4. To all three curves θ_{trans} of 8, 8 and 13 respectively is applied (acc. to Eq. 4.4). **colors:** length of analysis window **arrows:** indicate estimated θ_R according to Eq. 4.4 **data:** RDB centered around May 16, 12:00, 2018 with maximum period covered from May 9, 6:00 to May 23, 18:00, 2018 and statistical measures from comparison with ground truth, May 15 to 17, 2018

5.4. Summary

This chapter consists of three parts. Sec. 5.1 gives a detailed description of the ground truth collection. Sec. 5.2 presents errors measures in reference to ground truth. Sec. 5.3 investigates four parameters of the original Temporal Waterline Approach (TWA) with respect to their effect on radar-derived bathymetry (RDB), which led to improving the quality check in a rule of thumb (see Eq. 4.4).

	Bell et al. [2016]	**updated for Bunker Hill**		
	parameter	parameter	rmse	R
Bell et al. [2016]			≈0.60	-
Bunker Hill initially			0.41 m	0.70
resolution z grid	0.1 m	0.02 m	0.41 m	0.72
water level model	WLM-original	WLM-original	0.41 m	0.72
analysis window	14 days	14.5 days (≥8.3 days)	0.37 (0.46)	0.72 (0.67)
threshold θ_{trans}	0	θ_{trans}=13 (≥8) Eq. 4.2	0.36 (0.42)	0.76 (0.76)
threshold θ_R	0.3	θ_R=$f(T)$ Eq. 4.3	0.43 (0.47)	0.74 (0.71)

Table 5.4: set of parameters for TWA with results from sensitivity analysis

For ground truth collection two devices were used: a wheelbarrow (nautical GPS receiver) and a sledge (drone), both with RTK support. Accuracies of the receivers are below 6 cm (see Tab. 5.1). Three days of measurements from May 15 to 17, 2018, were merged. For two weeks before and after calm conditions prevailed, only at end of survey wind speeds were increased, with higher waves as result and some wind setup on the shore. A longshore stretch South of the radar of almost 2 km including beach and ridges was covered, from -1.3 up to 3.9 m+MSL (intertidal area and above). In addition to accuracies of the devices, errors of surveying add up to order of 10 cm for both devices and in horizontal as well as vertical direction (for details see Fig. 5.9 and Tab. 5.2). Results are gridded to match the radar grid of 7.5 m × 7.5 m cellsize. For gridding the median of all ground truth datapoints within one radar cell is calculated. Standard deviation of height values within one radar cell reaches up to 36 cm.

To validate applicability of TWA at Bunker Hill two RDBs with different analysis window length (14.5 and 8.3 days) are compared to ground truth. Rmse are 43 and 46 cm respectively, bias 12 and 9 cm.

Accuracy is in the same order of magnitude as spatial variation within one radar cell and the mean wave run-up. Range dependency of errors as observed by Bell et al. [2016] are not visible, but a cross-shore dependency, which roughly results in an underestimation of the beach and a slight overestimation of the bars, but overall the latter are matched well. The choice of the water level station strongly affects the degree of over- and underestimation (see also Sec. 5.3.2). Due to the way ground truth was collected this validation is restricted to the intertidal area. It shows that it is possible to improve the accuracy by about 15 cm if prior knowledge of the approximate extent of the intertidal area is considered. The validation procedure is challenged by the different nature of RDB (averaged) and ground truth (instantaneous).

The sensitivity analysis presented in Sec. 5.3 was conducted prior to the improvement of TWA, which was combined into a rule of thumb in Eq. 4.4. Four parameters of TWA are investigated [13]:

1. resolution of z grid: dz from 0.01 to 0.2 m
2. water level model: without and with wave induced effects
3. analysis window: T from 4 to 30 tidal cycles, dT from -14 to 5 tidal cycles
4. thresholds as quality measures: θ_{trans} from 0 to 56 transitions, θ_R from 0 to 1.0 (potentially)

Tab. 5.4 shows the results of the sensitivity analysis. Additionally rmse and correlation are listed for the updated values. Those are calculated between the filtered RDB and ground truth. Rows in the table are ordered chronologically. In the last row rmse and R are worse than in the step before. This is because sensitivity analysis is not optimizing accuracy alone, but aims at an optimum between full coverage of the intertidal area and sufficient accuracy. It is found that accuracy is not significantly improved by refining the resolution of the z grid. The equidistance of the z grid as opposed to the equitemporal grid of the water level record poses the main restriction here. A water level model including wave induced effects like set-up and run-up is tested based on an empirical formulation for a 2 % exceedance value R_2 by Stockdon et al. [2006], which is added to the water level record. RDBs are worse, if R_2 is included, because it neglects the water surface's (cross-shore) curvature. Improvements are only expected, if water levels are spatially resolved or an empirical correction is applied, which goes at costs of robustness of TWA. The investigation of window lengths T for analysis reveals, that the governing factor for TWA is the choice of thresholds in the quality check, namely they are (implicitly) dependent on the analysis window length. It is indicated that a range of 14.5 down to 8.3 days works well for TWA at Bunker Hill, and even down to 5.2 days may still work, if environmental conditions are pre-checked. Shifting the analysis window hints at the importance of the stationarity assumption, but did not reveal more due to lack of data. Two thresholds are investigated, which are combined into a rule of thumb (see Eq. 4.4). θ_{trans} is newly introduced and ensures that the cross-correlation coefficient is based on a sufficient number of transitions, i.e. at least 8 transitions. Maximum value is based on physical considerations of the number of possible transitions given a semi-diurnal tide with two transitions for each tidal cycle. This implies that the final range of z values is cut at the lower and upper end. θ_R is the threshold from the original publication by Bell et al. [2016]. Within this study it is found, that it depends on the overall correlation (in space) of the RDB and therefore is not well represented with a constant value. The overall correlation in turn depends on the window length T. Therefore if the window length is shortened θ_R should increase.

[13] complete investigation results are presented in A.4

6

Applications Foreshore Morphodynamics

Each radar-derive bathymetry (RDB) contains geographical data about bed levels in the intertidal area (maps). This data can be used either for classification (reducing amount of information) or to derive other quantities (adding information). Each RDB contains gaps outside the intertidal area (non-intertidal areas are not covered). Interpretation of RDBs is thus not straightforward for someone to whom the study area is unknown (for impressions of coastal zone at Bunker Hill see Fig. 3.3, p. 17). Fig. 6.1 therefore introduces a RDB for orientation, in which morphological features are identified and classified. Classification is done manually in a Geographic Information System (GIS) by interpreting values and gradients, as well as judging gaps from experience. Five classes are present. Sea and channels belong to the subtidal area, they are always wet. Whereas bars and wet beach make up the intertidal area. Areas that are never wet are for instance dry beach, dunes and the coast, thus land in general. For a collection of alternative terms for morphological features it is referred to Sec. 2.2.1.

The following section provides insight in the various applications possible with (time series of) RDBs. For an overview of applications from marine radar in general (e.g. current estimation, waves, etc.) see Sec. 1.1. Evolution of beach states is presented as an example. The chapter is concluded with a brief summary and indications on applicability of time series of RDBs.

6.1. Possibilities of Application in General

Applications in the coastal zone on the basis of RDBs are various. Possibilities include:

1. changes from winter to summer profile and back over one or more years (beach states)
2. effect of a storm event
3. evolution of nourishments
4. evolution of profiles
5. erosion and deposition
6. evolution of shoreline
7. migration of bars/rips
8. gradients (e.g. cross-shore gradients to find isolines)

Changes from winter to summer profile and back are observable without the help of hydrodynamic statistics[1] and sediment properties to calculate beach states in RDBs. The set of radar data of this

[1] Water level record being the only environmental parameter used in TWA.

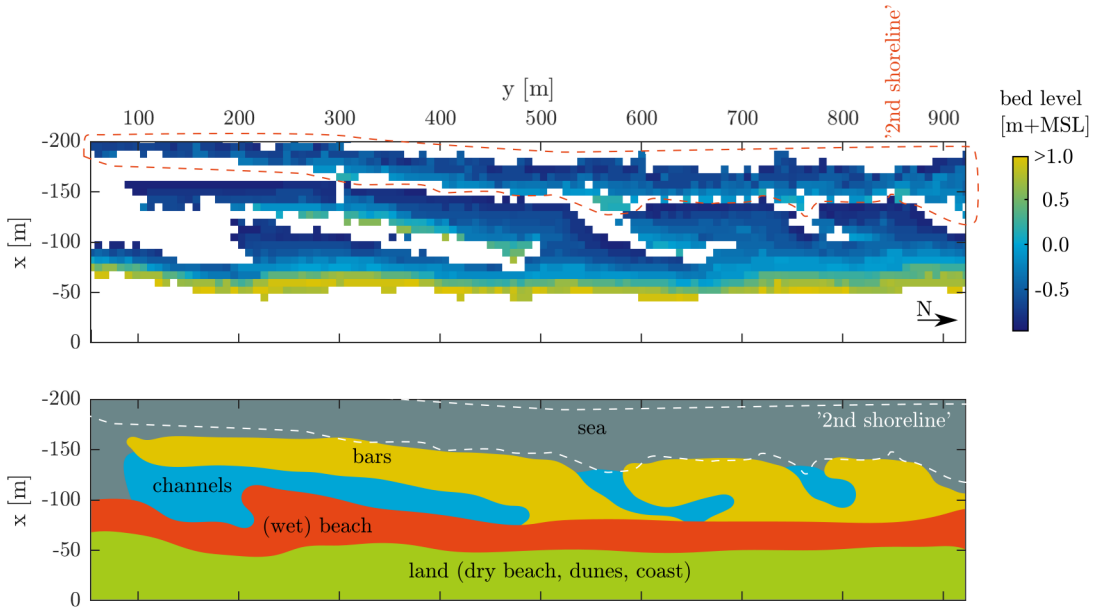

Figure 6.1: identification of morphological features in RDB **top:** radar-derived bathymetry **bottom:** identified morphological features. The sum of bars and wet beach makes up the intertidal area. **data:** RDB from Apr 20, 6:00 to May 4, 18:00, 2017 (28 tidal cycles), θ_{trans}=13 and θ_R=0.23 (acc. to Eq. 4.4), coverage is 94.1 %

study covers one year. About five years in total are available already for this study area (radar operation started in 2013). Within this five year data set more than one severe storm is captured. Its effect can be investigated by comparing pre and after storm conditions. For the time during the storm TWA is considered to be unreliable. Prominent events are for instance storm 'Xaver', that hit the German coast in the night from Dec 5 to 6, 2013 [Stockmann]. Or even several storms that occured in 2017 (BSH [2018] mentions four occasions in 2017 for storm surges). Sylt suffers from erosion, which is balanced by nourishments since 1984 [Ahrendt, 2001]. By analysing profile, shoreline or volume changes, or just visually, the evolution of beach nourishments can be tracked. From this information it can be learned how effective current strategies are. Despite the lack of bed level data below and above the intertidal area cross-shore profiles can easily be extracted from time series of RDBs. Amongst other profile evolution is therefore a sensible objective for studies, as well as estimation of reference profiles (e.g. equilibrium states defined by average of all profiles). If the longshore dimension is incorporated as well (full map), maps of differences between two time instants or one time instant and a reference map become of interest. Here the gaps cause similar problems as with the profiles. Especially if morphological features move outside the intertidal area (thus are not visible any more or only partly) the interpretation of such difference maps turns out challenging. In perspective of camera-based approaches, time series of RDBs are well capable of reproducing timelines or averages of shorelines as often presented in such studies. The extraction of more than one shoreline in a heterogeneous area like Bunker Hill beach often is too time-consuming for camera-based approaches (degree of automation is low if isolines are not closed, as for example for emerging ridges/bars or interruption from rips), which is why those studies often focus on a single shoreline (isoline) above MSL. With time series of RDBs it is easier to extract a set of isolines, because the process is reversed. Camera-based approaches first find a set of isolines and then interpolate those to constitute a full bathymetry, whereas radar-based approaches first find a bathymetry, from which isolines can be extracted with common geographical tools. By adding more isolines the analysis of shoreline evolution can thus be deepened. Migration speed and direction of bars (or rip channels) is prone to aliasing, if the sampling frequency does not match the rate of change. For Sylt beach profile measurements are available about once to four times a year (Gijsman et al. [2018] summarize monitoring characteristics on Sylt in their Table 1). Compared to other coastal areas this is well covered in terms of bathymetric survey. Especially since this data set extends back for more than 45 years. A time series of RDBs offers increased temporal and spatial coverage (at lower monetary costs), at costs of accuracy in height. This data can be judged visually

by tracking the distances and times a morphological feature travels to estimate its migration speed and direction. One advantage is that due to the high temporal resolution (with respect to morphodynamic scales at stake here) the result is more reliable, because risk of misinterpretation (e.g. a change in direction inbetween, stagnation, new feature formed) is reduced significantly. Apart from improving existing analysis methods, time series of RDBs have the potential to analyse new aspects. One quantity closely related to two-dimensional data sets is the slope. Simple techniques to extract slopes could be tested to look for correlations between gradients and isolines for instance. Isolines, i.e. contour of same level, are commonly used in order to describe shoreline evolution. Yet, in a study area with significant longshore variation (e.g. tidal range, wave angle, wave height) a single isoline may not characterize the shoreline accurately. Think for instance of the line a berm crest would yield in longshore direction. Due to longshore variations it is not of the same height everywhere. Such morphological features cannot be identified by isolines. For TWA it is not possible to see the berm (above intertidal area), yet similar reference lines (like a berm crest) must exist. The slope is expected to be a governing factor, as it is for the berm crest. Maybe a new type of reference line can be derived from long-term data sets of RDBs, comparable to lines of equal tidal range, but with a morphodynamic focus instead.

With time series of RDBs derived with TWA a wide range of applications in the coastal zone is possible. Especially application to questions relating to the foreshore (intertidal area) is in general promising. RDBs are capable of providing the same or more reliable/detailed morphological information as current state of the art tools (e.g. transition winter/summer profile, tracking of beach nourishments, shoreline evolution, migration of bars/rips). Interesting to note is, that all applications presented are based on the operation of a single radar station. RDBs capture better temporal variability than current methods (e.g. camera-based, LiDAR, echosoundings) and therefore allow more reliable calculation of morphological quantities (e.g. migration speeds). Furthermore for some applications, usage of RDBs increases quality of outcome because of improved temporal resolution (in comparison to current monitoring strategies) or larger coverage (in comparison to other remote techniques, e.g. cameras). Most important, time series of RDBs add insight into evolution of short time scales, i.e. scales in the order of two weeks, full year round, 24/7, combined with a robust, straightforward method to retrieve bed levels. This is an advantage over current monitoring strategies. Even over camera-based approaches (operate full year round, theoretically 24/7, but often suffer under low light conditions during night). So such time series of RDBs derived with TWA offer opportunities to test current hypotheses on coastal processes (e.g. transport, equilibria), to quantify coastal effects (e.g. nourishments, formation of bars) and eventually improve process understanding. RDB based analysis therefore takes a stake in the scientific push towards a holistic explanation on the complex system of the coastal zone.

6.2. Beach State Changes in 2017

For Jan 5 to Nov 2, 2017, RDBs are derived in steps of seven days. Each RDB covers 14.5 days. No radar records are available in December 2017. 45 RDBs are derived. For twelve RDBs coverage is too low according to Eq. 4.4's minimum requirement of at least 8.3 days. Another two RDBs are discarded, because the outcome with respect to strongly varying environmental conditions are considered unreliable. This leaves a total of 31 RDBs for a period of eleven months as indicated in Fig. 6.2 (almost three RDBs per month with default, automated parameters). Both filters are applied. Number of thresholds is calculated according to Eq. 4.4. For this application case $\theta_R = \theta_{R,Bell}$ is used. Analysis of beach states is reduced to a radius of 1.6 km, thus about 3.2 km beach. For comparability all RDBs are cut to the same range of z coordinates, thus only depth values in the range of -0.96 to 0.98 m+MSL are considered (for visualization: mean tidal range is almost 2 m, Chap. 3). Otherwise the appearance (disappearance) of cells over one time step cannot clearly be identified as bed level changes upward (downward).

Each RDB is assessed by eye and compared to schematics of beach states of Wright and Short [1984], their Fig. 2. Clearly two beach states are present in the time series, both are intermediate:

1 low tide terrace → Fig. 2.e. of Wright and Short [1984]

2 skewed transverse bar and rip → Fig. 2.d. of Wright and Short [1984]

Fig. 6.3 (top box) shows the results as timeline over 2017. In winter the beach shows a low tide terrace, characterized by long, shore parallel bars, separated from the beach by narrow runnels. Rip

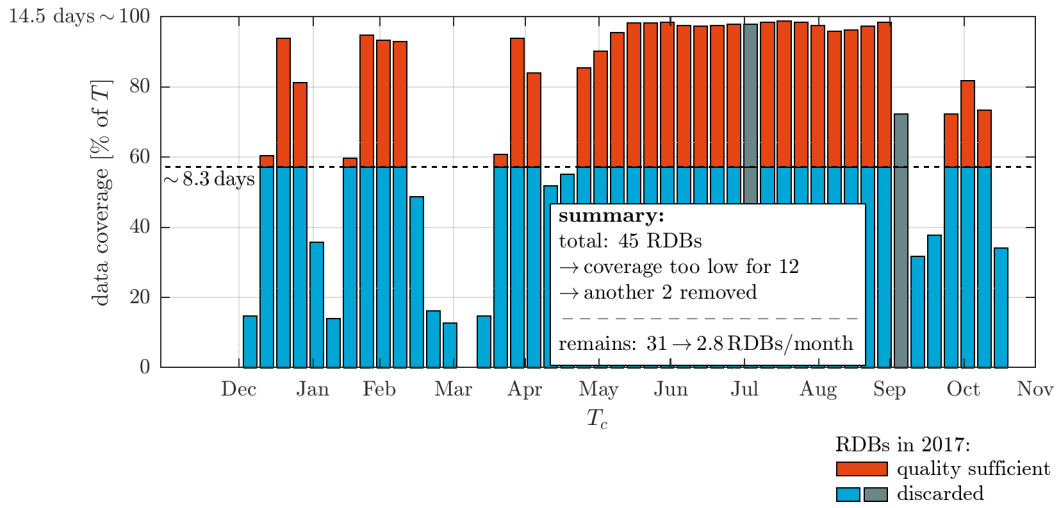

Figure 6.2: time series of RDBs available for 2017 **data coverage:** 100 % means that each hour a record is available for a period of about 14.5 days **grey:** manually removed after review of outcome with respect to environmental conditions **data:** RDBs from Jan 5 to Nov 2, 2017

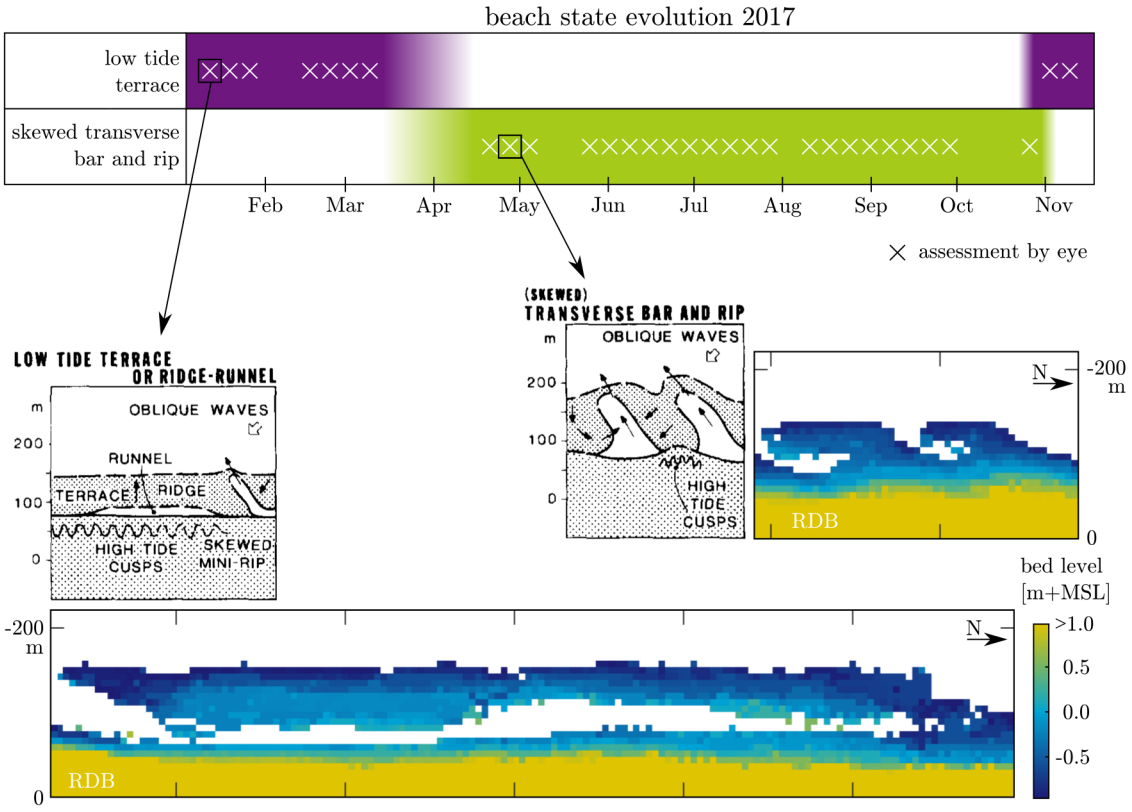

Figure 6.3: beach state evolution in 2017 assessed from time series of RDB. Assessed by eye in accordance to Wright and Short [1984], their Fig. 2. **upper part:** timeline of beach states **lower part:** one example for each beach state of assessment by eye to show resemblance. Schematics are show the reference beach state. Colored images are exemplary excerpts from the time series of RDBs, as indicated by the squared boxes in the timeline. **data:** schematics are extracted from Wright and Short [1984] and reduced in detail for the case at hand, RDBs range from Jan 5 to Nov 2, 2017, θ_{trans} acc. to Eq. 4.4, $\theta_R = \theta_{R,Bell}$=0.3

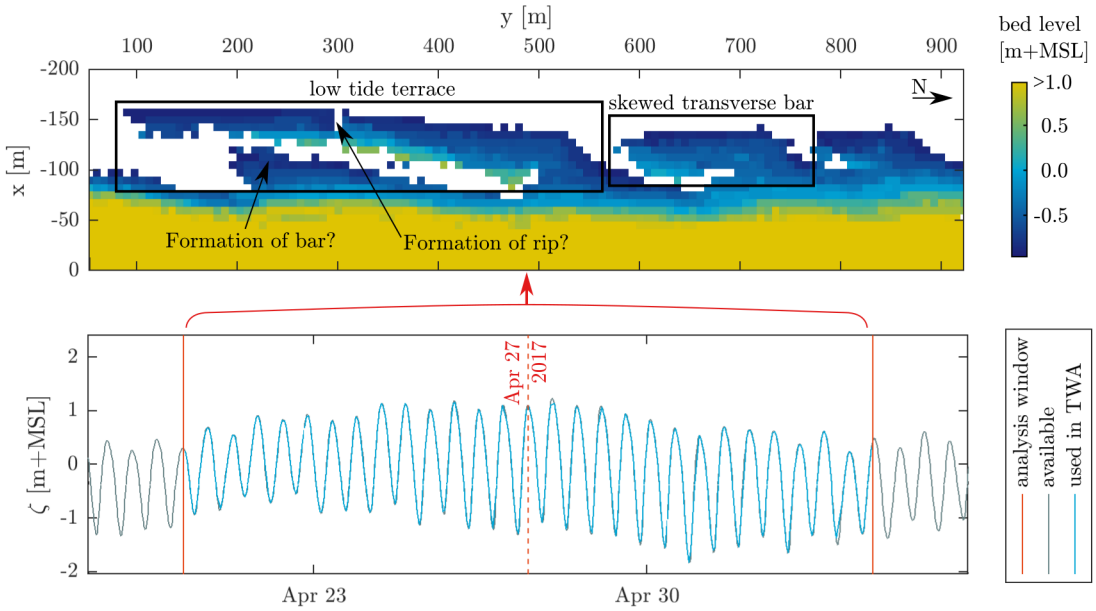

Figure 6.4: transition of two beach states does not happen simultaneously **top:** RDB depicting both beach states: low tide terrace and skewed transverse bar and rip **bottom:** water level record used in TWA to derive RDB **data:** RDB from Apr 20, 6:00 to May 4, 18:00, 2017 (28 tidal cycles), θ_{trans}=13 and θ_R=0.23 (acc. to Eq. 4.4), coverage is 94.1 %

channels occur between ridges. The shore parallel length of the ridge exceeds its width significantly. This is the main characteristic, that distinguishes the next beach state, during summer, from the low tide terrace. In April, rip channels become more frequent and the beach exhibits a skewed transverse bar and rip pattern, i.e. shore parallel length of bars becomes shorter and approximates its width. Additionally the dry beach (indicated in yellow with >1.0 m+MSL in Fig. 6.3) becomes wider, which indicates a steepening of the wet beach, because the bars do not move further offshore. Starting with November the beach state changes back to low tide terrace. The lower part of Fig. 6.3 gives one example for each beach state. Schematics are extracted and reduced in detail for the case at hand from Wright and Short [1984]. Colored images are excerpts from RDBs analysed in the scope of this application case (as indicated by the squared box in the timeline).

The transition between two beach states does not occur simultaneously on the full stretch of beach (see example in Fig. 6.4). Two skewed transverse bars are present, as well as a low tide terrace characteristic south of them. It cannot be observed how this transforms into a fully transverse bar and rip dominated state, because about a week later a nourishment is placed at this location. After the nourishment no obvious low tide terrace features are present any more.

For another time instant locally bed levels increase, where previously a narrow runnel was present (low tide terrace beach state). This may indicate a storm induced (wind was increased during that period) deposit of sediments, that for instance may initiate berm formation. Processes that lead to berm formation are explained by Bendixen et al. [2013]. See their section 'Introduction' for a review of other berm formation theories). But there is also another possibility to explain this sudden appearance of a 'heap of sand'. The 'heap' may also just be pooling water, that appears as high bed levels in RDB. This seems likely for two reasons. First of all is the shore parallel length of the 'heap' quite small. If it was storm induced it would be likely to observe a steepening beach over a significantly longer stretch of beach. Second, the evolution of this distinct spot in the weeks after the 'heap' appeared indicates, that a rip channel forms exactly in that spot and separates the low tide terrace that existed previously into two transverse bars. It appears, that first a pool of water developed behind the low tide terrace, in the runnel region. It than grows to a rip channel in probably a self-enforcing process. This serves as a good example to point back at the challenges of RDBs, that accompanies their potential for morphodynamics analyses.

6.3. Summary

A wide range of applications in the coastal zone based on (time series of) radar-derived bathymetries (RDBs) is possible, ranging from investigations of natural to anthropogenic events, on short to long time scales. Especially evolutions on short time scales (order of two weeks) are captured by the operational mode of a radar: all year round, 24/7. This may eventually lead to an improved understanding of the interactions in the complex system of the coastal zone.

A time series of 31 RDBs from Jan 5 to Nov 2, 2017, is used to present beach state evolution. About 3.2 km of beach are investigated based on schematics published by Wright and Short [1984]. The beach in front of Bunker Hill experiences a switch from a low tide terrace system to a skewed transverse bar and rip system in April. It switches back between October and November. The periodic change of characteristic morphological features is in accordance with theory of coastal processes. The data set indicates that the change does no happen simultaneously along the 3.2 km stretch. The detailed insight into the evolution could serve as a reference to theoretical models on beach states, that often are based on hydrodynamic and sedimentary characteristics of the study area.

7

Discussion of Study Objective

This chapter discusses the study objective, which is combined into two study questions as presented in the introduction of this work (Sec. 1.2). Key findings from all parts of the study serve as arguments for the discussion, even though the study questions themselves are pointing at the final stage of this study, the application.

What is the Added Value of Operating Shore-based X-band Marine Radar? Sec. 1.1 lists several quantities that marine radar is able to provide and are relevant for observation of the coastal zone. Output ranges from meteorological (e.g. wind), over hydrodynamic (e.g. waves) and morphodynamic (e.g. bathymetry) to biological (e.g. individual tracking) quantities. In general terms the added value of marine radar operation is the diversity of data sets captured within one device. The specific case of this study focuses on a highly dynamic environment located at the exposed side of the Wadden Sea island Sylt (German Bight). The complex system in front of the coast is a threat to humans and property during extreme events, e.g. storm surges, whereas during calm conditions it serves for recreation (tourism is one of the main economical drivers). Research therefore focuses on processes at stake to improve coastal protection strategies. But current monitoring schemes do not cover short time scales of weeks and shorter. At Sylt for example monitoring by local authorities is conducted roughly four times a year, which covers 45 % of the morphological variability [Blossier et al., 2016]. The Temporal Waterline Approach (TWA) supplements the radar data recorded at Bunker Hill and fills gaps in established monitoring schemes. Still, it cannot fully replace those schemes, because of limitations in height accuracy. Time series of radar-derived bathymetry (RDB) provide information about morphological evolution in the intertidal area. Work of engineers and scientists alike is potentially supported by this data sets. For example, with the help of RDB it should be possible to track beach nourishments on a weekly scale to evaluate their effect and efficiency. In research morphodynamic theories can be supported or improved that are founded on low temporal resolution data, for instance. As indicated by the findings of this study the added value of operating shore-based X-band marine radar at Bunker Hill is the capacity of capturing time scales in the order of one week combined with a robust method and low-cost operation of a radar station. Nevertheless, so far TWA is still under development and has only been applied to few study sites. It is therefore not yet proven, if this added value of operating a radar station is specific to Bunker Hill. But this study indicates, that TWA in combination with the semi-automated quality check presented in this study is not site-specific. For three reasons further studies should rather focus on applying TWA than improving it further.

First, the method itself is sufficiently accurate in relation to scales of variation present at Bunker Hill (e.g. wave run-up, cell size), despite substantial errors in RDB outside the intertidal area (introduced by cross-shore migration of breaker zone, see Sec. 4.5.5).

Second, the semi-automation of the quality check reduces influences of the researcher. Furthermore it is based on the radar data itself and it is likely that it is therefore not only applicable for the same radar at a different location, but also for a different radar. This was not tested within this study.

Third, further improvements (i.e. optimizing accuracy vs. full coverage of intertidal area) comes at costs of robustness. One example is the water level model. TWA uses a homogeneous water level, which is a simple and strong assumption. Accuracies are lowered due to this assumption by

probably 10 cm or more. Yet if the water level record was spatially resolved this would require a two-dimensional input of water levels, which in practice can be as difficult to get as a bathymetry every couple of weeks. Even if hydrodynamic output of an operational numerical model is available, are uncertainties introduced, because the bed level is not known. Within the scope of studies that require high level of detail or accuracy, it may be feasible to reduce TWA's robustness and for example base the method on a spatially resolved water level. Nevertheless this will most likely result in a site- and radar-specific version of TWA and will not be available for wide range applications in various study sites any more.

Those three reasons also point at shortcomings of TWA, which should be considered when turning to a new study site or another data set. Nevertheless further investigations should focus on three aspects of application, which will help to establish TWA as a robust and reliable tool to derive intertidal bathymetry in complex coastal systems:

1. more study sites, ideally with different hydrodynamic and/or morphodynamic conditions
2. more data sets at already tested study sites
3. more radar types

The original study site has a tidal range of 10 m, whereas Sylt only experiences 2 m. The set of hydrodynamic conditions in which intertidal bathymetry retrieval can be conducted should be broadened with respect to wave and current conditions for example, to prove that TWA is not site-specific. The same holds for the range of morphodynamic conditions. This study focussed on an intermediate beach. Other options are reflective and dissipative beaches or tidal flats. The latter could be investigated with the radar station South of the Wadden Sea island Norderney (German Bight), which started operating recently and shares the same specifications as the radar of this study.

From the wide range of potential applications of TWA output outlined in Sec. 6.1 only one example is presented in detail in this study. It should be tested in how far the potential is actually given in order to show the diversity not only of the radar device itself, but of time series of intertidal bathymetry as well. The focus on applications is rather important, because it may bridge the gap between theory and practice and thus value the scientific work. Although it has stopped by now a X-band radar station has been operating in the vicinity of the Sand Motor (Netherlands). Because the Sand Motor is covered with an extensive monitoring scheme, it is possible to not only work with the radar data to test applications, but also to conduct thorough comparison with other kinds of data sets to validate the results.

Last but not least, other radar devices should be used as well, if possible. The range of specifications in which TWA works well is probably narrow, yet this study has already shown that it is not necessary to use HH polarization for example (this study uses VV polarization) or 3.75 m squared cell size (this study uses 7.5 m squared). The radar station at the Sand Motor could serve as a potential case for this.

How Does the Distinct Channel-shoal Pattern of Sylt Develop in the Course of One Year? This distinct question is answered in detail in Chap. 6. With the help of the application case there it is proven, that time series of radar-derived intertidal bathymetry add information to existing theory. The specific question of beach evolution is tackled with the concept of beach states as presented in schematics by Wright and Short [1984]. The time series of RDB was processed automatically, namely without checking environmental conditions prior to the retrieval. Sufficient coverage within the analysis windows was ensured with a threshold. A quick review of the results revealed unreliable RDBs. From this time series of RDB it was straightforward to extract the beach states and find times when states change. Those beach state changes are related to changes in hydrodynamic forcing (here: wind sea or swell domination), which in turn alter the morphology (i.e. beach state). It proves that RDB is capable of reproducing theory of beach states without additional effort on fitting TWA to the application case. As discussed in the first study question, the application does not only show that it can reproduce the theory, but it also offers additional details on the processes underlying this theory. To mention just one, it is visible in the time series, that the change between two beach states does not happen simultaneously. At least one example was found that indicates how the transition is taking place, probably by splitting the long ridges of the winter season into shorter bars. At this stage it is only shown that application is straightforward and that potential for new insights is present, yet more detailed investigation of RDB

is needed, which links back to one of the main points presented in the previous section: focus on application rather than further improvements of the method. Especially since interpretation of RDB at the current stage of TWA still requires a skilled scientist or engineer to identify for example areas with pooling water. Pooling water appears as a 'heap' of sand in RDB and cannot be identified directly from a single RDB, but requires to look at the evolution to judge whether actually a deposition took place or if pooling water is mistaken as a surface.

With respect to the second study question focus on application is particularly promising, because not many methods are available that resolve the channel-shoal pattern at Bunker Hill with a high temporal resolution. Despite the decreased accuracy of RDBs in comparison to other mapping methods, it offers a temporal resolution that can resolve at least up to 80 % of shoreline variability (compare Blossier et al. [2016]). For certain study objectives this is prerequisite to ensure sensible results, yet with current methods effort and/or costs are high to achieve this level of temporal detail. Therefore RDB constitutes an additional tool in the repertoire of a coastal engineer or scientist.

8

Conclusions and Outlook

A modified version of the Temporal Waterline Approach by Bell et al. [2016] with an improved quality check is implemented and tested. The radar station (X-band) at Bunker Hill (Sylt) operated by Radar Hydrography group (Helmholtz-Zentrum Geesthacht) provides the data required for retrieval of intertidal bathymetry. A time series covering one year with approximately one radar-derived bathymetry (RDB) every two weeks is retrieved for a stretch of 3.2 km of intertidal area. The study consists of three main parts. First the original Temporal Waterline Approach (TWA) and its modifications are presented (Chap. 4). Those modifications are based on the results found in the second part, which deals with validation and a sensitivity study (Chap. 5). The third part indicates the wide range of potential applications for RDB and visualises this with an example of beach state evolution in the course of one year (Chap. 6).

The method implemented, modified, tested and applied in this study is the Temporal Waterline Approach (TWA). TWA is presented as a robust method for retrieval of averaged intertidal bathymetry from radar data by Bell et al. [2016]. Main input to TWA is mean backscatter intensity of a radar and water level information in one location. The radar data of this study is provided by a GEM radar operating at 9.41 GHz (X-band) with VV polarization at Bunker Hill, Sylt (Wadden Sea island in German Bight). Radial resolution is 7.5 m. New as compared to the original publication is a second threshold in the quality check, as well as the semi-automation of the first threshold. This modifications are combined into a rule of thumb for threshold estimation, which improves the robustness of the method. One substantial error is not solved in the scope of this study. The quality check is supposed to mark all grid cells as unreliable, that are outside the intertidal area. This does not work for the non-intertidal part offshore of the bars, where the breaker zone passes during a tidal cycle. For the application case these artefacts were removed manually.

A survey was conducted from may 15 to 17, 2018, to collect ground truth of the intertidal area. 2 km of ridges and beach are covered, between -1.3 up to 3.9 m+MSL (intertidal area and above). Two GNSS devices with RTK support were used in an experimental setup. Errors due to receivers and surveying conditions add up to approximately 10 cm in horizontal and vertical direction. Ground truth was processed on a grid matching the grid of the radar. In comparison to ground truth root mean square errors are in the order of 40 to 50 cm with bias in the order of 10 cm. Morphological variability (one standard deviation) within one radar cell as well as mean wave run-up are in the order of 40 cm. A range dependency of errors is not visible. But in cross-shore direction errors are systematic. Lower lying areas (e.g. bars) are slightly overestimated, whereas the beach is underestimated by TWA, due to the neglection of the spatially varying water level (radar range up to 3.26 km). Sensitivity analysis shows that TWA is most sensitive to the choice of the thresholds in the quality check. Sufficient accuracy and full coverage are opposing demands on TWA's output and are optimized within the sensitivity analysis. Furthermore resolution of vertical grid, inclusion of wave induced effects on the water level (homogeneously) and properties of the analysis window (length and position of center) are analysed.

RDB has the potential to serve as basis for a wide range of applications, including natural and anthropogenic events, as well as time scales of couple of days up to couple of weeks. Beach state evolution at Bunker Hill in the course of 2017 was chosen as application case to visualise not only that it is possible to reproduce theory, but that it may add new insights to it as well, e.g. how the transitions

between two beach states takes place. The data set contains roughly one RDB every two weeks for eleven month on a stretch of 3.2 km, including the switch from winter to summer profile and back.

This study, as also indicated by the original work, shows that the method is not fully developed for every day's use, yet. Main issues relate to the incorrect detection of the breaker zone as wet-dry transitions as well as pooling water. It is recommended to get acquainted with TWA and the study area prior to using RDB. Basic knowledge of radar physics is beneficial for understanding TWA. If TWA is applied to a new study site it should be judged upon (amongst others) the operational mode of the radar (X-band, VV- and HH-polarization are both fine), the frequency of recording (high enough to resolve tidal cycle, e.g. at least hourly records for semi-diurnal environments, but also not too often with respect to the tidal propagation), the radar record length (at least 8 min to ensure hydrodynamic representativeness) and the availability of water level records (either measured or modelled).

Shore-based X-band marine radar supplements existing monitoring schemes of the intertidal area by filling gaps in bathymetric survey. Morphological variability captured at Bunker Hill is potentially increased from 45 % (current monitoring scheme of local authorities) to 80 % with low costs and effort. Time series of RDB derived with TWA is capable of reproducing theory (e.g. beach state evolution), adding details to it (e.g. point in time when winter profile switches to summer and back again) and potentially improving the understanding of the underlying physics (e.g. how the transition between two beach states evolves). Shortcomings of the method itself are predominantly related to radar physics, the implementation of the method or ensure its robustness. This study has shown that RDB is sufficiently accurate, most likely not site-specific and most of the improvements would come at costs of the robustness. It is therefore concluded that further research should focus on application rather than improvements of TWA. Application cases should be selected whether they capture a new study site, contain more radar data at a tested study site or use another setup of the radar. This will support to establish intertidal bathymetry from shore-based marine radar as a robust and reliable tool for engineers and scientists working in coastal zones around the globe and may bridge the gap between theory and practice to improve coastal protection strategies.

Bibliography

D. I. N. 4049-3. Hydrologie - Teil 3: Begriffe zur quantitativen Hydrologie. Deutsche Norm DIN 4049-3: 1994-10, Normenausschuß Wasserwesen (Deutsches Institut für Normung e.V.), Oct. 1994.

S. G. J. Aarninkhof, I. L. Turner, T. D. T. Dronkers, M. Caljouw, and L. Nipius. A video-based technique for mapping intertidal beach bathymetry. *Coastal Engineering*, 49(2003):275–289, 2003.

K. Ahrendt. Expected effect of climate change on Sylt island: results from a multidisciplinary German project. *Climate Research*, 18:141–146, 2001. ISSN 0936-577X, 1616-1572. doi: 10.3354/cr018141. URL http://www.int-res.com/abstracts/cr/v18/n1-2/p141-146/.

L. Aragonés, J. I. Pagán, I. López, and J. C. Serra. Depth of closure: New calculation method based on sediment data. *International Journal of Sediment Research*, 33(2):198–207, June 2018. ISSN 10016279. doi: 10.1016/j.ijsrc.2017.12.001. URL https://linkinghub.elsevier.com/retrieve/pii/S1001627917300471.

AWL. Fachplan Küstenschutz Sylt: Fortschreibung. Technical Report AWL 1997, Amt für Land- und Wasserwirtschaft Husum, Aug. 1997.

J. A. Battjes. Surf similarity. In *Proceedings 14th Conference*, pages 466–480, New York, 1974.

P. S. Bell. Shallow water bathymetry derived from an analysis of X-band marine radar images of waves. *Coastal Engineering*, 37(3-4):513–527, Aug. 1999. ISSN 03783839. doi: 10.1016/S0378-3839(99)00041-1. URL http://linkinghub.elsevier.com/retrieve/pii/S0378383999000411.

P. S. Bell and J. C. Osler. Mapping bathymetry using X-band marine radar data recorded from a moving vessel. *Ocean Dynamics*, 61:2141–2156, 2011.

P. S. Bell, C. O. Bird, and A. J. Plater. A temporal waterline approach to mapping intertidal areas using X-band marine radar. *Coastal Engineering*, 107:84–101, 2016.

M. Bendixen, L. B. Clemmensen, and A. Kroon. Sandy berm and beach-ridge formation in relation to extreme sea-levels: A Danish example in a micro-tidal environment. *Marine Geology*, 344:53–64, Oct. 2013. ISSN 00253227. doi: 10.1016/j.margeo.2013.07.006. URL https://linkinghub.elsevier.com/retrieve/pii/S0025322713001473.

B. Blossier, K. R. Bryan, C. J. Daly, and C. Winter. Spatial and temporal scales of shoreline morphodynamics derived from video camera observations for the island of Sylt, German Wadden Sea. *Geo-Mar Lett*, 2016.

N. Braun, M. Gade, and P. A. Lange. The effect of artificial rain on wave spectra and multi-polarisation X band radar backscatter. *International Journal of Remote Sensing*, 23(20):4305–4323, Jan. 2002. ISSN 0143-1161, 1366-5901. doi: 10.1080/01431160110106032. URL https://www.tandfonline.com/doi/full/10.1080/01431160110106032.

BSH. Berichte zu Sturmfluten und extremen Wasserständen, 2018. URL http://www.bsh.de/webcode/1653010.

R. Carrasco, J. Horstmann, and J. Seemann. Significant Wave Height Measured by Coherent X-Band Radar. *IEEE Transactions on Geoscience and Remote Sensing*, 55(9):5355–5365, Sept. 2017. ISSN 0196-2892, 1558-0644. doi: 10.1109/TGRS.2017.2706067. URL http://ieeexplore.ieee.org/document/7982956/.

CEM. Coastal terminology and geologic environments (Part IV-1). In *Coastal Engineering Manual*, EM 1110-2-1100. U.S. Army Corps of Engineers, 2 edition, Apr. 2002a. URL https://app.knovel.com/web/view/pdf/show.v/rcid:kpCEM0000P/cid:kt003W70R2/viewerType:pdf//root_slug:iv-1-coastal-terminology-and-geologic-environments/url_slug:iv-1-coastal-terminology?cid=kt003W70R2&b-toc-cid=kpCEM0000P&b-toc-root-slug=&b-toc-url-slug=iv-1-coastal-terminology&b-toc-title=Coastal%20Engineering%20Manual.

CEM. Water wave mechanics (Part II-1). In *Coastal Engineering Manual*, EM 1110-2-1100. U.S. Army Corps of Engineers, 2 edition, Apr. 2002b. URL https://app.knovel.com/web/view/pdf/show.v/rcid:kpCEM0000P/cid:kt003W6FM3/url_slug:part-ii/root_slug:coastal-engineering-manual/viewerType:pdf/?jsp=/content/pdf/1326/01326_05a.pdf.

H. Dankert. Ocean wind fields retrieved from radar-image sequences. *Journal of Geophysical Research*, 108(C11), 2003. ISSN 0148-0227. doi: 10.1029/2003JC002056. URL http://doi.wiley.com/10.1029/2003JC002056.

J. L. Davies. *Geographical Variation in Coastal Development*. Number 4 in Geomorphology Texts. Longman, London (UK), 2nd edition, 1980. ISBN 0-582-49006-5.

R. A. Davis and M. O. Hayes. What is a wave-dominated coast? *Marine Geology*, 60(1984):313–329, 1984.

S. Dick, E. Kleine, S. H. Müller-Navarra, H. Klein, and H. Komo. The Operational Circulation Model of BSH (BSHcmod): Model description and validation. Technical Report 29/2001, BSH, 2001.

DJI. D-RTK User Manual, 2017.

DJI. Matrice 200 series - M210/M210 RTK User Manual v1.2, Feb. 2018.

J. Ehlers. *The Morphodynamics of the Wadden Sea*. A.A. Balkema, 1988.

J. Friedman. Development of an X-band Radar Depth Inversion Model at the Sand Motor. Master's thesis, Technische Universiteit Delft, Delft (NL), 2014. URL https://repository.tudelft.nl/islandora/object/uuid%3A2d4773bd-50e5-4507-ae64-1b7c333fb7c1?collection=education.

R. Gijsman, J. Visscher, and T. Schlurmann. A method to systematically classify design characteristics of sand nourishments. *COASTAL ENGINEERING*, page 12, 2018.

M. O. Hayes. Barrier Island Morphology as a Function of Tidal and Wave Regime. In *Barrier Islands*. Academic Press, 1979.

S. D. Hicks. Tide and Current Glossary. glossary, National Ocean Service (NOAA), Silver Spring, MD, Jan. 2000. URL https://www.co-ops.nos.noaa.gov/publications/glossary2.pdf.

R. Holman, N. Plant, and T. Holland. cBathy : A robust algorithm for estimating nearshore bathymetry. *Journal of Geophysical Research*, 118:2595–2609, 2013.

L. H. Holthuijsen. *Waves in Oceanic and Coastal Waters*. Cambridge University Press, Cambridge, 2007. doi:10.1017/CBO9780511618536.

J. Horstmann, J. C. N. Borge, J. Seemann, R. Carrasco, and B. Lund. Wind, Wave, and Current Retrieval Utilizing X-Band Marine Radars (Chapter 16). In *Coastal Ocean Observing Systems*, pages 281–304. Elsevier, 2015. ISBN 978-0-12-802022-7. doi: 10.1016/B978-0-12-802022-7.00016-X. URL https://linkinghub.elsevier.com/retrieve/pii/B978012802022700016X.

O. Huisman and R. A. d. By. *Principles of geographic information systems: an introductory textbook*. The International Institute for Geo-Information Science and Earth Observation (ITC), Enschede, 2009. ISBN 978-90-6164-269-5. URL http://itc.nl/library/papers_2009/general/PrinciplesGIS.pdf. OCLC: 847211143.

ITU-R. Nomenclature of the frequency and wavelengh bands used in telecommunications. Recommendation ITU-R V.431-8, ITU, Geneva, Aug. 2015. URL https://www.itu.int/dms_pubrec/itu-r/rec/v/R-REC-V.431-8-201508-I!!PDF-E.pdf.

A. T. Jessup, W. C. Keller, and W. K. Melville. Measurements of sea spikes in microwave backscatter at moderate incidence. *Journal of Geophysical Research*, 95(C6):9679, 1990. ISSN 0148-0227. doi: 10.1029/JC095iC06p09679. URL http://doi.wiley.com/10.1029/JC095iC06p09679.

N. C. Kraus, M. Larson, and R. A. Wise. Depth of Closure in Beach-Fill Design. technical note CETN II-40, Coastal And Hydraulics Laboratory (U.S. Army Engineer Waterways Experiment Station), Mar. 1998. URL https://apps.dtic.mil/dtic/tr/fulltext/u2/a578584.pdf.

E. P. Kvale. The origin of neap-spring tidal cycles. *Marine Geology*, 235(1-4):5–18, Dec. 2006. ISSN 00253227. doi: 10.1016/j.margeo.2006.10.001. URL http://linkinghub.elsevier.com/retrieve/pii/S0025322706002544.

P. H. Y. Lee, J. D. Barter, K. L. Beach, C. L. Hindman, B. M. Lake, H. Rungaldier, J. C. Shelton, A. B. Williams, R. Yee, and H. C. Yuen. X band microwave backscattering from ocean waves. *Journal of Geophysical Research*, 100(C2):2591, 1995. ISSN 0148-0227. doi: 10.1029/94JC02741. URL http://doi.wiley.com/10.1029/94JC02741.

LKN.SH. Küstenschutz auf Sylt - Sandaufspülungen 2017. Technical report, Landesbetrieb für Küstenschutz, Nationalpark und Meeresschutz Schleswig-Holstein, 2017.

LKN.SH. Küstenschutz auf Sylt - Sandaufspülungen 2018. Technical report, Landesbetrieb für Küstenschutz, Nationalpark und Meeresschutz Schleswig-Holstein, 2018.

D. R. Lyzenga, A. L. Maffett, and R. A. Shuchman. The Contribution of Wedge Scattering to the Radar Cross Section of the Ocean Surface. *IEEE Transactions on Geoscience and Remote Sensing*, GE-21(4):502–505, Oct. 1983. ISSN 0196-2892. doi: 10.1109/TGRS.1983.350513. URL http://ieeexplore.ieee.org/document/4157446/.

D. L. McCann and P. S. Bell. Observations and tracking of killer whales (*Orcinus orca*) with shore-based X-band marine radar at a marine energy test site. *Marine Mammal Science*, 33(3):904–912, July 2017. ISSN 08240469. doi: 10.1111/mms.12395. URL http://doi.wiley.com/10.1111/mms.12395.

H. D. Niemeyer. Die ursächliche Deutung von Transportphänomenen als Gestaltungsgrundlage fur Strandauffüllungen. *Die Küste*, 54(1992):53–92, 1992.

J. Nieto Borge, G. R. RodrÍguez, K. Hessner, and P. I. González. Inversion of Marine Radar Images for Surface Wave Analysis. *Journal of Atmospheric and Oceanic Technology*, 21(8):1291–1300, Aug. 2004. ISSN 0739-0572, 1520-0426. doi: 10.1175/1520-0426(2004)021<1291:IOMRIF>2.0.CO;2. URL http://journals.ametsoc.org/doi/abs/10.1175/1520-0426%282004%29021%3C1291%3AIOMRIF%3E2.0.CO%3B2.

J. C. Nieto Borge, K. Reichert, and J. Dittmer. Use of nautical radar as a wave monitoring instrument. *Coastal Engineering*, 37(3-4):331–342, Aug. 1999. ISSN 03783839. doi: 10.1016/S0378-3839(99)00032-0. URL http://linkinghub.elsevier.com/retrieve/pii/S0378383999000320.

A. C. Ortiz and A. D. Ashton. Exploring shoreface dynamics and a mechanistic explanation for a morphodynamic depth of closure: Morphodynamic Depth of Closure. *Journal of Geophysical Research: Earth Surface*, 121(2):442–464, Feb. 2016. ISSN 21699003. doi: 10.1002/2015JF003699. URL http://doi.wiley.com/10.1002/2015JF003699.

R. Palacios. deg2utm (version 1.0), 2006a. URL https://de.mathworks.com/matlabcentral/fileexchange/10915-deg2utm.

R. Palacios. utm2deg (version 1.0), 2006b. URL https://de.mathworks.com/matlabcentral/fileexchange/10914-utm2deg.

N. G. Plant, K. Holland, and J. A. Puleo. Analysis of the scale of errors in nearshore bathymetric data. *Marine Geology*, 191(1-2):71–86, Nov. 2002. ISSN 00253227. doi: 10.1016/S0025-3227(02)00497-8. URL http://linkinghub.elsevier.com/retrieve/pii/S0025322702004978.

N. G. Plant, S. G. J. Aarninkhof, I. L. Turner, and K. S. Kingston. The Performance of Shoreline Detection Models Applied to Video Imagery. *Journal of Coastal Research*, 23(3):658–670, May 2007. ISSN 0749-0208, 1551-5036. doi: 10.2112/1551-5036(2007)23[658:TPOSDM]2.0.CO;2. URL http://www.bioone.org/doi/abs/10.2112/1551-5036%282007%2923%5B658%3ATPOSDM%5D2.0.CO%3B2.

W. J. Plant and G. Farquharson. Wave shadowing and modulation of microwave backscatter from the ocean: WAVE SHADOWING AND MODULATION. *Journal of Geophysical Research: Oceans*, 117 (C8):n/a–n/a, Aug. 2012. ISSN 01480227. doi: 10.1029/2012JC007912. URL http://doi.wiley.com/10.1029/2012JC007912.

B. Ruessink, P. Bell, I. van Enckevort, and S. Aarninkhof. Nearshore bar crest location quantified from time-averaged X-band radar images. *Coastal Engineering*, 45(1):19–32, Mar. 2002. ISSN 03783839. doi: 10.1016/S0378-3839(01)00042-4. URL http://linkinghub.elsevier.com/retrieve/pii/S0378383901000424.

C. M. Senet, J. Seemann, S. Flampouris, and F. Ziemer. Determination of bathymetric and current maps by the method DiSC based on the analysis of nautical X-Band radar image sequences of the sea surface. *IEEE Trans Geosci Remote Sens*, 46(8):2267–2279, 2008. URL https://ieeexplore.ieee.org/document/4558037.

M. J. Stive, S. G. Aarninkhof, L. Hamm, H. Hanson, M. Larson, K. M. Wijnberg, R. J. Nicholls, and M. Capobianco. Variability of shore and shoreline evolution. *Coastal Engineering*, 47(2):211–235, Dec. 2002. ISSN 03783839. doi: 10.1016/S0378-3839(02)00126-6. URL http://linkinghub.elsevier.com/retrieve/pii/S0378383902001266.

H. F. Stockdon, R. A. Holman, P. A. Howd, and A. H. Sallenger. Empirical parameterization of setup, swash, and runup. *Coastal Engineering*, 53(7):573–588, May 2006. ISSN 03783839. doi: 10.1016/j.coastaleng.2005.12.005. URL http://linkinghub.elsevier.com/retrieve/pii/S0378383906000044.

K. Stockmann. Die Nordseesturmfluten vom 5. und 6.12.2013. Technical Report bm1101, BSH. URL https://www.bsh.de/DE/THEMEN/Wasserstand_und_Gezeiten/Sturmfluten/_Anlagen/Downloads/Nordsee_Sturmflut_20131206.pdf;jsessionid=BEE989CC723643F29F13276F9ECCC98B.live21303?__blob=publicationFile&v=3.

M. Streßer. *Erfassung der Dynamik des Wellenbrechens mit einem dopplerisierten Mikrowellenradar*. Diplomarbeit, Leibniz Universität Hannover, Hannover (DE), 2014.

I. Svendsen. Mass flux and undertow in a surf zone. *Coastal Engineering*, 8(4):347–365, Nov. 1984. ISSN 03783839. doi: 10.1016/0378-3839(84)90030-9. URL http://linkinghub.elsevier.com/retrieve/pii/0378383984900309.

Thales. *Aquarius2 & Aquarius Series: User Manual*. Thales Navigation, France, digital edition, 2002. URL http://sup.xenya.si/sup/info/magellan(thalesnavigation)/reference_manuals/Aquarius/English/P0101434RevBEng.pdf.

D. Trizna and D. Carlson. Studies of dual polarized low grazing angle radar sea scatter in nearshore regions. *IEEE Transactions on Geoscience and Remote Sensing*, 34(3):747–757, May 1996. ISSN 01962892. doi: 10.1109/36.499754. URL http://ieeexplore.ieee.org/document/499754/.

D. J. Wallace, J. B. Anderson, and R. A. Fernández. Transgressive Ravinement versus Depth of Closure: A Geological Perspective from the Upper Texas Coast. *Journal of Coastal Research*, 26:1057–1067, Nov. 2010. ISSN 0749-0208, 1551-5036. doi: 10.2112/JCOASTRES-D-10-00034.1. URL http://www.bioone.org/doi/abs/10.2112/JCOASTRES-D-10-00034.1.

L. D. Wright and A. D. Short. Morphodynamic Variability of Surf Zones and Beaches: A Synthesis. *Marine Geology*, 56:93–118, 1984.

N. Yoder. peakfinder (version 2.0.2), 2016. URL `https://de.mathworks.com/matlabcentral/fileexchange/25500`.

M. Zeiler, P. Milbradt, A. Plüß, and J. Valerius. Modelling Large Scale Sediment Transport in the German Bight (North Sea). *Die Küste*, 81(2014):369–392, 2014.

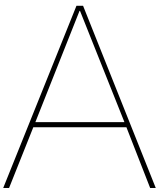

Appendix

A.1. RDB Toolbox (MATLAB)

MATLAB functions written and used for wheelbarrow processing:

```
ashtechlog2mat(logpath,antennaheight)[a]
ashtechraw2mat(rawpath,antennaheight)[b]
cutAshtech(matpath,idc)
filterAshtech(matpath,filterQI,filterSat,filterHDOP)
checkAshtech(matpath,filterQIflag)
```

[a] recordings from smartphone
[b] recordings from Windows laptop

MATLAB functions written and used for sledge processing:

```
djicsv2mat(csvpath)
cutDji(matpath,idc)
filterDji(matpath,datafields,values,operators)
checkDji(matpath)
```

A.2. Supplementary Material: Study Area at Bunker Hill, Sylt

This section provides supplementary information that serves as basis for the classification and description of the study area in Sec. 3.

A.2.1. Beach State

Fig. A.1 shows the schematics of possible beach states found at Bunker Hill (Fig. 2. a. and e. from Wright and Short [1984]). The intertidal area is characterized by a skewed transverse bar and rip setup throughout most of the year. Further offshore there is an additional bar, that can be seen in LiDAR and echosoundings as well as by the presence of a second (outer) breaker zone. This submerged bar is present continuously as indicated by LKN.SH (see also Fig. A.2).

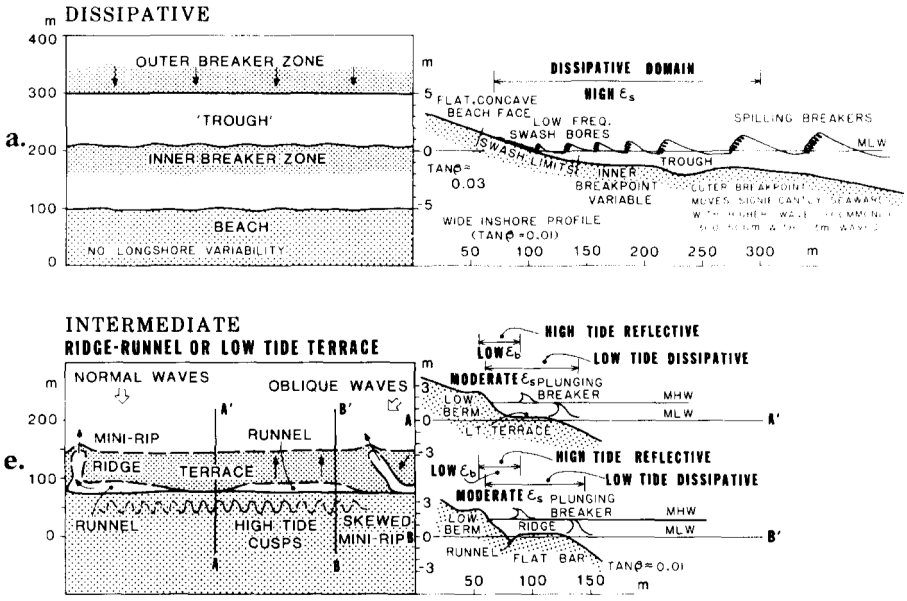

Figure A.1: schematics of beach states ”dissipative” and ”intermediate: ridge-runnel” **source:** Fig. 2. a. and e. from Wright and Short [1984]: ”Plan and profile configurations of the six major beach states”

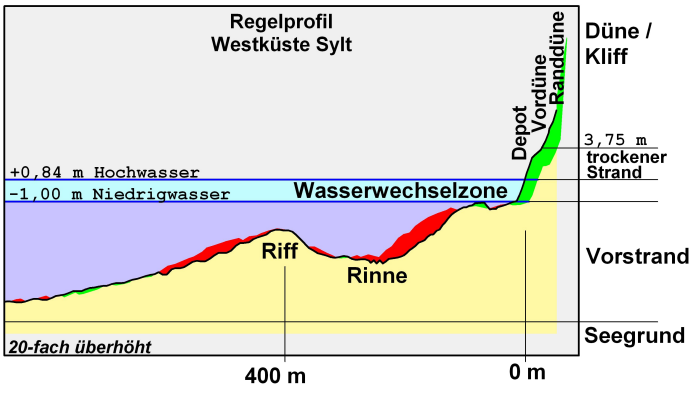

Figure A.2: beach profile at Sylt with location of submerged bar (”Riff”: bar, ”Rinne”: trough) **x-axis:** the radar is mounted approximatly at -100 m **source:** `www.schleswig-holstein.de/DE`

Classification of the wave regime on Sylt is based on measurements in 2017 at Westerland buoy. The tidal regime is judged by the tidal range of three tidal gauges located at Hörnum, Westerland and

List. Wave characteristics provided by BSH, water levels by LKN.SH and WSA Tönning. See Fig. A.3 for time series of peak period, wave height and water level in the course of 2017. Only data tagged with the best quality (according to automated quality control) is used. Additionally extreme outliers are removed, that are above the 99.5th percentile (data of 2 days in one year). By this approach wave heights in the order of the water depth are removed. Those are physically speaking unlikely to impossible. Problems probably arise because the wave height is defined based on spectral moments. Tab. A.1 shows the summary statistics of wave period, height and direction. Fig. A.4 relates direction of the wave to occurence of wave height and peak period. Most of the waves are coming from west-south-west to north-west (clockwise). Swell predominantly arrives from west-north-west to west-north. The swell originates from storms in the North Atlantic Ocean, from where they enter the North Sea. Sea states with shorter wave periods come from west-south-west to north-west direction. The fetch in those directions is still long enough (>500 km) to cause high waves, yet it is not large enough to generate swell.

	min	5th	mean (median)	95th	max	st. dev.	
H_s [m]	0.10	0.30	1.08 (0.90)	2.40	4.00	0.67	**medium wave energy**
T_p [s]	1.7	2.9	6.6 (5.9)	12.5	18.2	2.9	**predominantly wind sea**
θ [°]	2.00	118.9	264.2 (278.0)	317.0	358.0	60.28	**mainly westerly waves**

Table A.1: summary statistics of wave characteristics **5th and 95th:** respective percentiles **direction:** defined as coming from with nautical convention (north is 0°, clockwise)

TABLE 4. Coastal Types - Medium Wave Energy (H = 60-150 cm)

Class	*Tidal Range*	*Example*
Microtidal	*0-1 m*	*Gulf of St. Lawrence*
Low-mesotidal	*1-2 m*	*New Jersey*
High-mesotidal	*2-3.5 m*	*Plum Island, Mass.*
Low-macrotidal	*3.5-5 m*	*German Bight*
Macrotidal	*5 m*	*Bristol Bay, Alaska*

Table A.2: classes of tidal regime **source:** Table 4. from Hayes [1979]: "Coastal Types - Medium Wave Energy (H=60-150 cm)"

Standort	HHThw	HThw	MThw	NNthw	HHtnw	MTnw	NTnw	NNtnw
	[cm PN] PN=-500 cm+MSL							
List / Sylt	905 24.11.1981 seit 07.04.1898	815 08.01.2005 2004/2013	**588** 2004/2013	338 07.12.1959 seit 07.04.1898	760 24.11.1981 seit 07.04.1898	**409** 2004/2013	250 23.03.2013 2004/2013	146 07.12.1959 seit 07.04.1898
Hörnum / Sylt	905 24.11.1981 seit 01.01.1914	818 31.01.2013 2004/2013	**603** 2004/2013	369 07.12.1959 seit 01.01.1914	730 26.01.1990 seit 01.01.1914	**398** 2004/2013	238 24.12.2002 2004/2013	136 15.03.1964 seit 01.01.1914
Westerland pile: 2006 to 2015	MNTnw = 299 cm, MTnw = 405 cm, MHTnw = 599 cm, MNThw = 473 cm, MThw = 588 cm, MHThw = 768 cm						PN=-501 cm+MSL	

Table A.3: statistics of tidal gauges List, Westerland and Hörnum **HHThw**=HHW (extreme/highest high water) **MNTnw**=MLLW **MTnw**=MLW **MThw**=MHW **MHThw**=MHHW **NNTnw**=LLW (extreme/lowest low water) – equalities found from comparing DIN 4049-3 [Oct 1994] and Hicks [2000] **source:** extracted relevant rows from table on `wsa-toenning.wsv.de` and `www.umweltdaten.landsh.de/pegel`

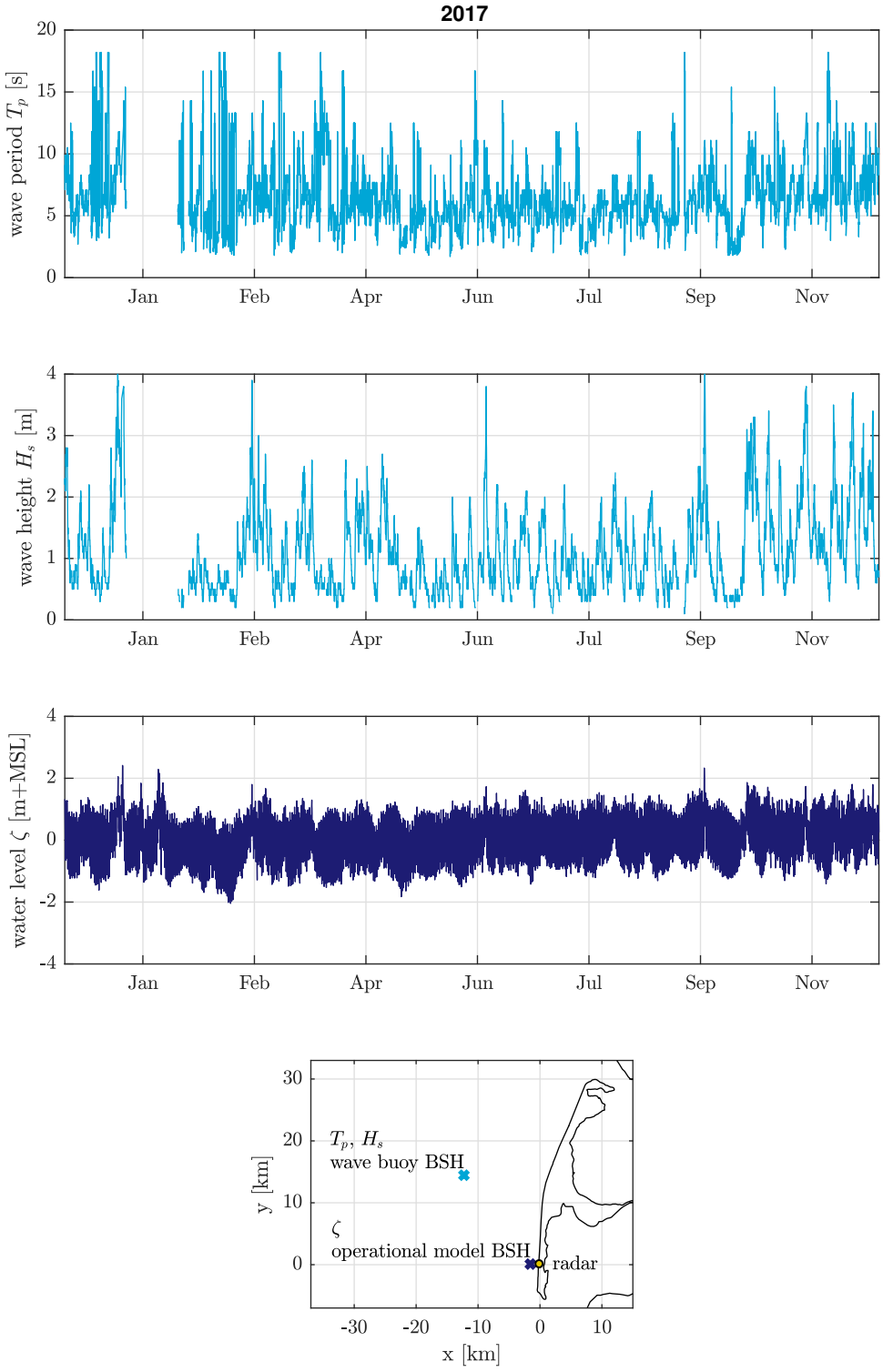

Figure A.3: wave characteristics and water level used for classification of Sylt **top three:** wave characteristics as hourly averages and water level every 15 min **bottom:** map of stations **data:** wave characteristics (at about 14 m depth) and water level from BSH, December 1, 2016 to November 30, 2017, map based on openstreetmap.org

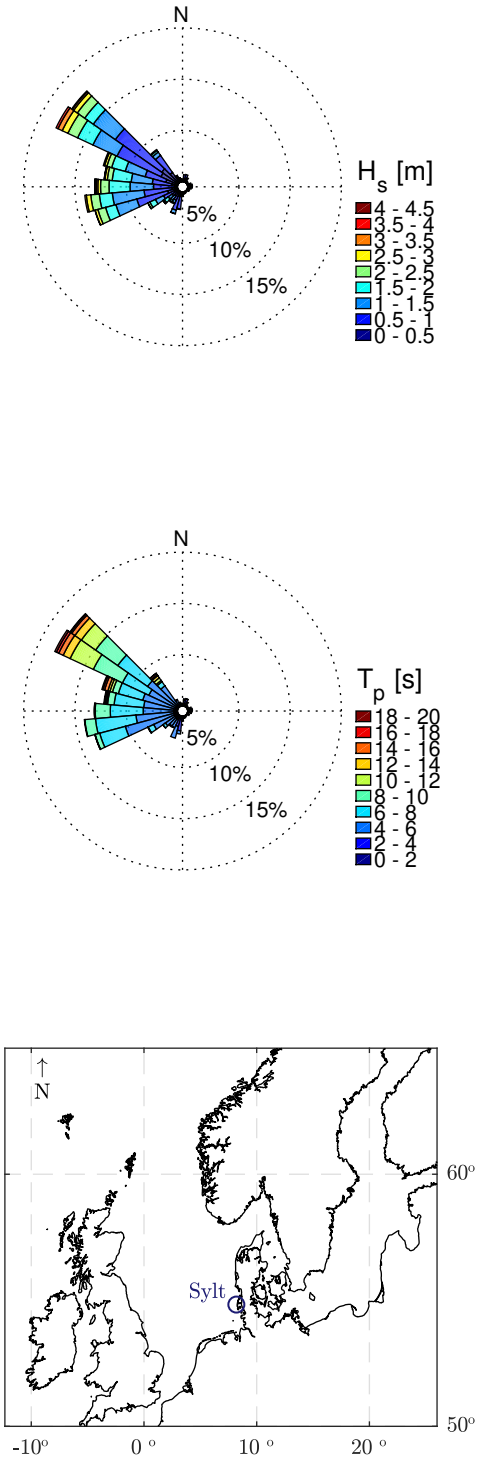

Figure A.4: directionality of sea state in 2017 **top and middle:** $H_s = 4\,m$ is the 99.5th percentile, direction defined as "coming from" (created with MATLAB function wind_rose.m by M MA) **bottom:** map of North Sea **data:** wave characteristics (at about 14 m depth) from BSH buoy in front of Westerland (see Fig. A.3), December 1, 2016 to Novemver 30, 2017, map based on openstreetmap.org

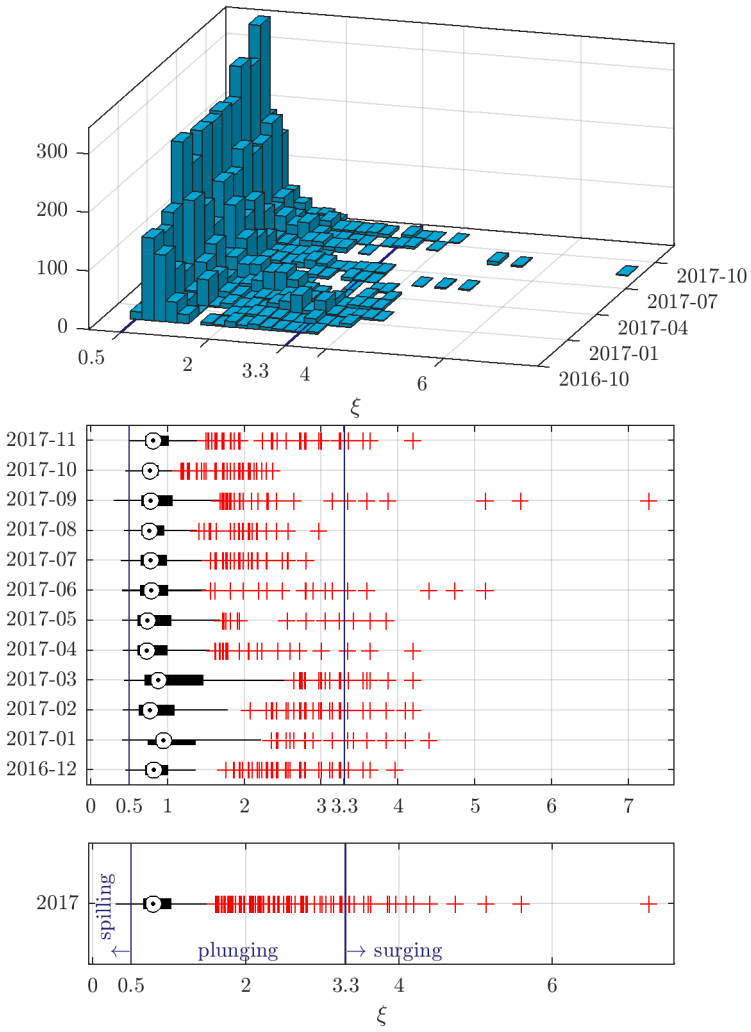

Figure A.5: surf similarity parameter in 2017. Due to changing format in data output one year period of 2017 extends from Dec 1, 2016 to Nov 30, 2017. **x-axis:** ξ after Eq. 2.1, limits of breaker type from Battjes [1974] **data:** wave characteristics (at about 14 m depth) from BSH buoy in front of Westerland (see Fig. A.3), December 1, 2016 to Novemver 30, 2017 (deep water, using linear wave theory), beach slope β_f=0.11 from ground truth May 15 to 17, 2018

WGS84		UTM (EPSG:5555)		BH-CRS		ground level
Lon	Lat	x [m]	y [m]	x [m]	y [m]	z [m+MSL]
radio mast Loran-C Rantum, 193 m high:						
8°17'37.0"	**54°48'29"**	454598.27	6073661.09	687.78	1972.85	3
radio mast Loran-C Rantum, 193 m high, adjusted:						
8.29365340°	54.80830744°	454601.27	6073689.09	**690.78**	**2000.85**	3
corner reflector 1, about 1.20 m high:						
8.28238223°	54.79477432°	**453861.44**	**6072190.58**	-49.05	502.34	2.42
corner reflector 2, about 1.20 m high:						
8.28228588°	54.79880483°	**453859.84**	**6072639.13**	-50.66	950.89	2.34

Table A.4: georeferencing points **bold:** original coordinates, transformed to the other CRS' respectively **source:** radio mast coordinates from structurae.net/structures/loran-c-transmitter, corner reflector data from ground truth collection (Sec. 5.1)

A.2.2. Georeferencing

Positions of two corner reflectors were measured during the survey from May 15 to 17, 2018. The wheelbarrow was placed as close as possible to the corner reflector (within a radius of $\leq$0.5 m). The two data sets were originally recorded in Longitude and Latitude. Those were transformed to UTM before averaging to yield the position of the two corner reflectors. The positions are relevant for georeferencing the radar images.

A.2.3. Coordinate Transformations

coordinate transformations:

```
Lon-Lat ↔ UTM[a]:    deg2utm(…) and utm2deg(…) [b]
    UTM ↔ BH-CRS: utm2bh(…) and bh2utm(…)
```

[a] EPSG:5555
[b] Palacios [2006a,b]

A.3. Supplementary Material: Data Sources

A.3.1. Source for Water Level Record

There is no tidal gauge in front of Bunker Hill. Therefore a decision has to be made whether to use measurements from tidal gauges Hörnum or Westerland shifted by an average phase shift to match Bunker Hill's conditions or use model output. To make sure the modelled output from the operational model of BSH (BSHcmod, described in Dick et al. [2001]) is plausible it is compared to Westerland (Fig. A.6 and Fig. A.7). Hörnum is disregarded because it is influenced by reflection and less representative for Bunker Hill than Westerland. The tidal range observed in the operational model is slightly

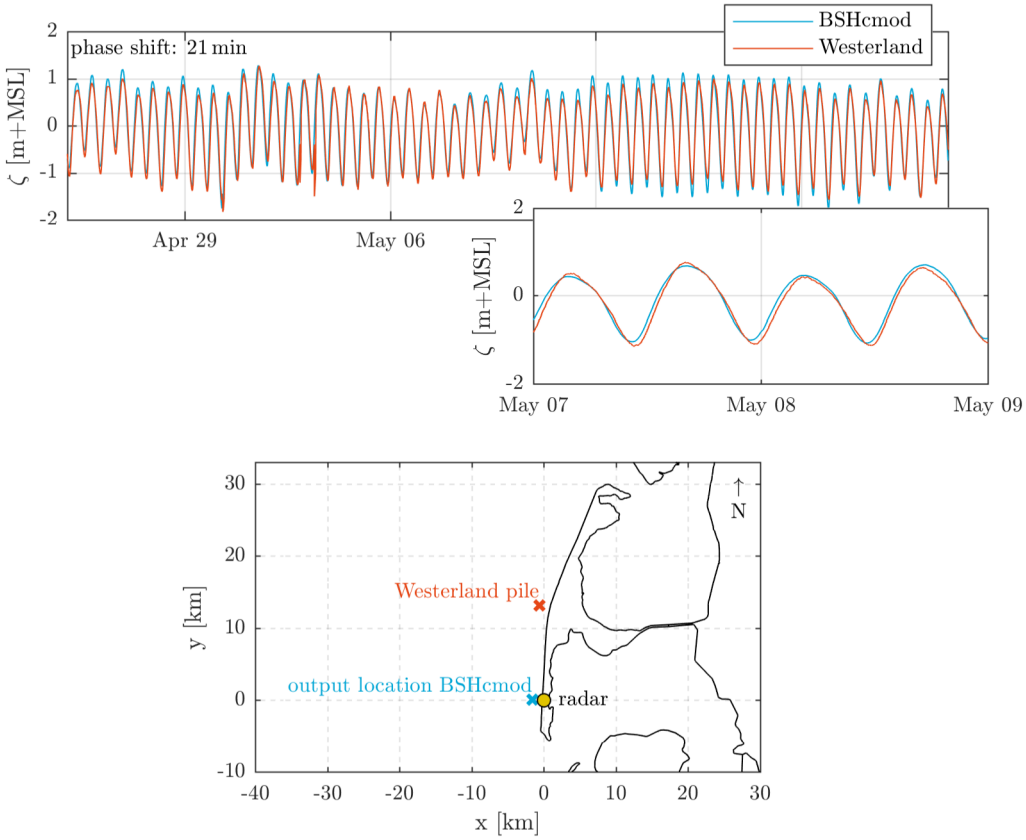

Figure A.6: phase shift between tidal records at Westerland pile and from operational model of BSH **top:** (average) phase shift is found by means of cross-correlation between the two records **bottom:** location of Westerland pile and the output location of the model **data:** Apr 25 to May 25, 2018, map based on openstreetmap.org

larger than at Westerland. Westerland pile and the output location of the operational model from BSH are approximately 1 km away from the shore. Standard deviation of high water and low water for the west coast of Sylt are below 20 cm [Dick et al., 2001]. Deviations in Fig. A.6 might thus relate to errors in the model, but also to other factors like the tilt of the shoreline at Westerland or the depths. Differences in the water level in the order of 10 cm are expected to have no significant effect on the outcome of the method. The correct phase of the signal is deemed more important.

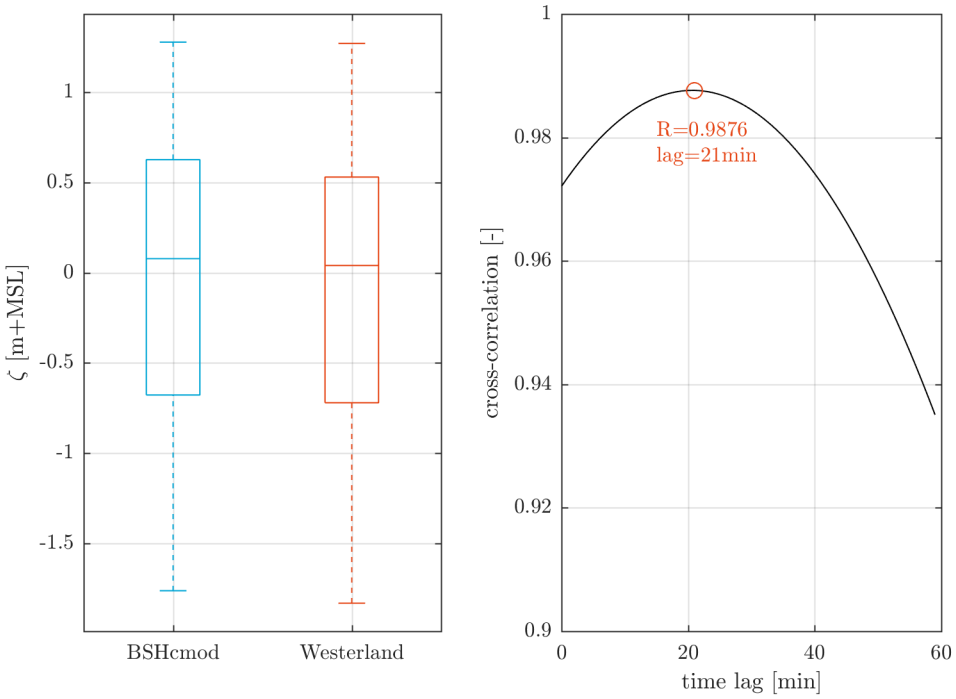

Figure A.7: distribution of ζ at and time lage between Westerland pile and BSHcmod **left:** box-plots for both locations **right:** cross-correlation to find average phase shift **data:** Apr 25 to May 25, 2017

A.4. Supplementary Material: Sensitivity Analysis

On the following pages figures are presented that show details about the sensitivity analysis. For each case a figure consisting of six subfigures is presented. The error measures presented are based on the difference between RDB and ground truth:

```
difference = RDB - ground truth
```

Two data sets are presented each time:

1. unfiltered: no quality measures are applied to the RDB
2. filtered: all cells of RDB with a R<0.3 are removed

Additionally all cells, that are not covered by a respective cell in the ground truth data set, also are removed, no matter the magnitude of R_{max}.

Each figure starts with the top left plot. Values of parameters, i.e resolution of z grid (dz), water level model (β_f), analysis window (T, dT) and thresholds (θ_{trans}, θ_R), are depicted on the x-axis for all plots. For each value of a parameter the range of bed levels will be different. This is related to the water level record used respectively. In order to make results comparable between different parameter values the z range of the bed levels is cut to the mutual range ('equal range'). Additionally figures are presented with the original z range ('varying z range'). The effect is negligible, yet both cases are presented.

Next is the top right plot. It shows the number of cells underlying the estimation of error measures, i.e. rmse, bias, correlation coefficient and standard deviation. In small grey dots the number of cells without filtering is shown. In blue circles the number of cells left after filtering is shown. A solid green circle denotes the choice that is made for further processing. For varying z range the grey dots show all the exact same number, whereas for equal z range they might differ slightly.

The same color code as for the number of cells is used in the remaining plots. The rmse, bias, correlation coefficient and standard deviation are all four defined on the difference defined above.

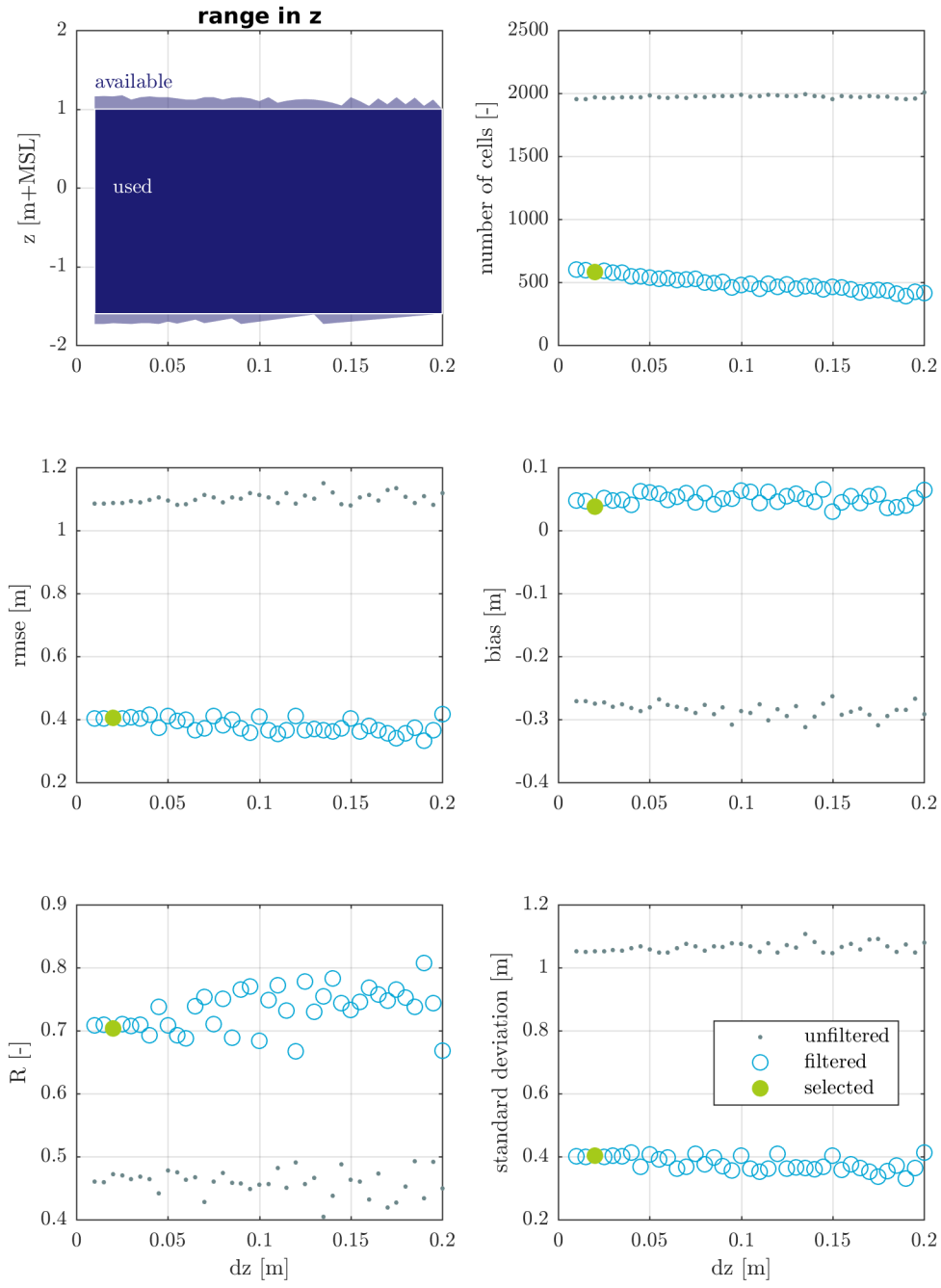

Figure A.8: error measures for varying resolution of z grid **top left:** all RDBs are cut to the same z grid in order to ensure comparability **notes:** with the given setup it is not possible to see the trend of increasing accuracy for decreasing dz, yet it shows that for decreasing dz a stable error is reached for dz=0.03 m. Because it suits better any needs of our decimal numeral system dz=0.02 m is chosen. This figure supports the choice made in Sec. 5.3.1. **data:** RDB derived for May 9, 12:00 to May 22, 2:00, 2018

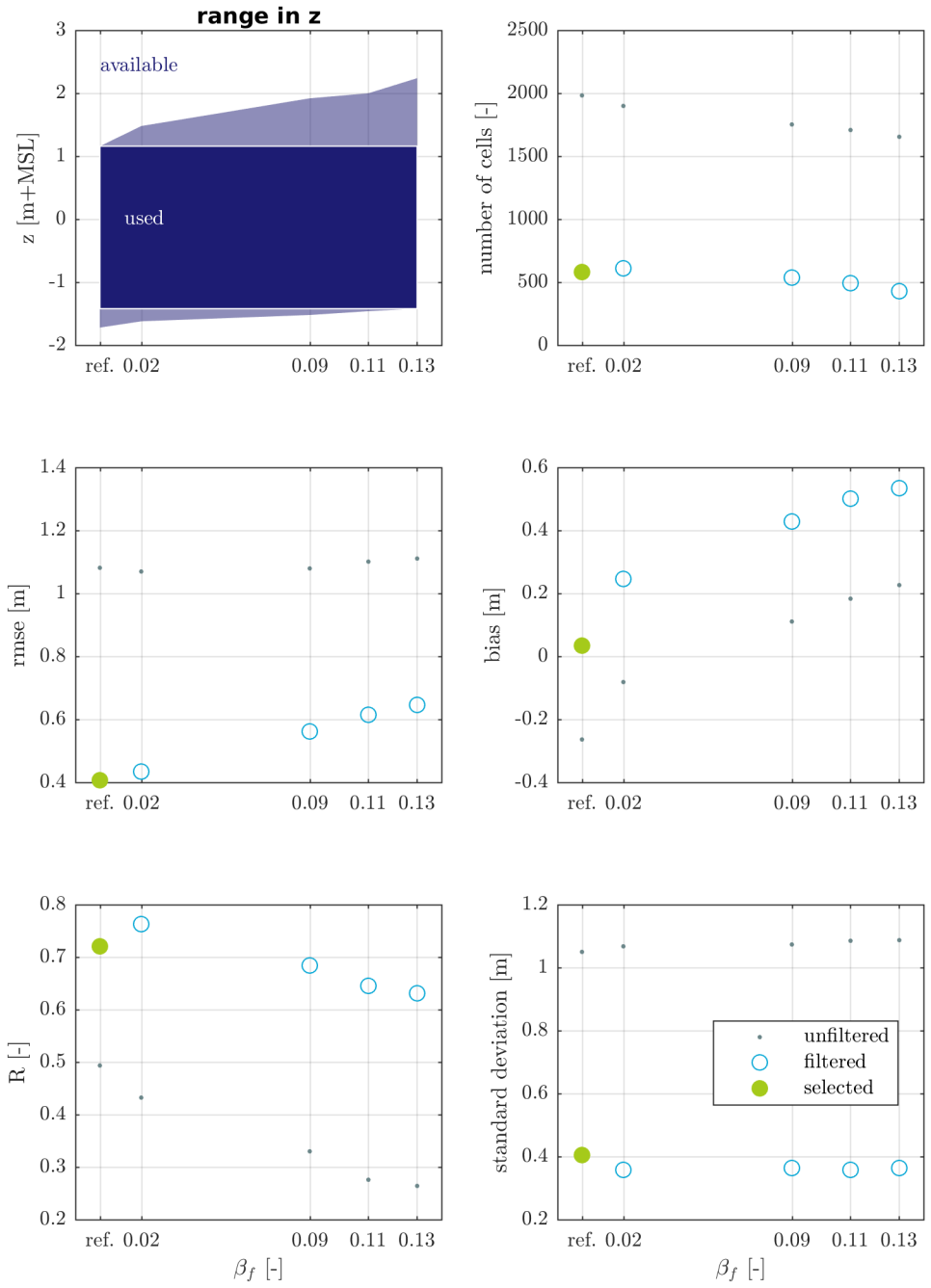

Figure A.9: error measures for different water level models - equal z range **top left:** all RDBs are cut to the same z grid in order to ensure comparability **x-axis:** 'ref.' marks the reference case, thus WLM-original (no R_2 applied) **notes:** accuracy decreases with steepening slope. Only initially for quite a mild slope that resembles the ridges (not the beach) an overall improvement in correlation can be seen. This figure supports the choice made in Sec. 5.3.2. **data:** RDB derived for May 9, 12:00 to May 22, 2:00, 2018

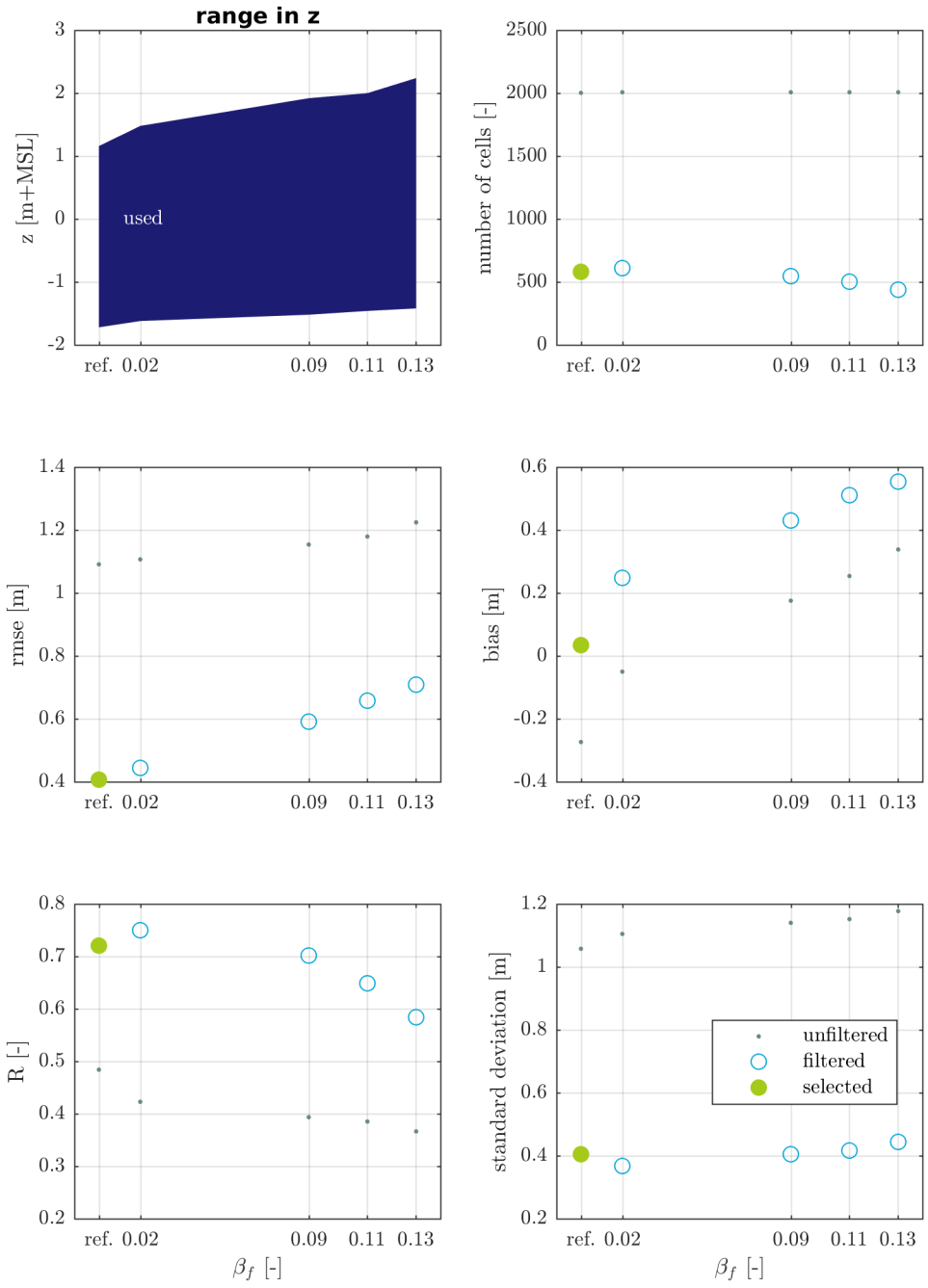

Figure A.10: error measures for different water level models - varying z range **top left:** in this case no z values are cut-off. Therefore also cells with high altutide due to the increase in water level by R_2 are part of the analysis. **notes:** There is only little deviation with respect to Fig. A.9. This figure supports the choice made in Sec. 5.3.2. **data:** RDB derived for May 9, 12:00 to May 22, 2:00, 2018

As an example and also because it appears quite important for the threshold sensitivity in Sec. 5.3.4 the following Fig. A.11 is explained in more detail. The window length are based on steps of a tidal cycle, which is slightly more than half a day. For the sake of readability specific points in Fig. A.11 are referenced with full and half days. No window length is chosen, because the choice has to be made based on the studies purpose.

All graphs apart from correlation coefficient are kind of smooth, whereas the correlation coefficient fluctuates much. In all graphs a jump is observed between 4 to 4.5 days, except for the number of cells. The jump therefore is not cause by a drop in number of cells. Environmental conditions do not reveal any significant (abrupt) changes that could explain that drop, too. Water level is quite homogeneous and no other gaps than the one during ground truth is present for window lengths up to 4.5 days. Wave heights have been increased for part of the period of 4.5 days, yet there is no obvious correlation with the significant jump. The mean radar images themselves do not show any striking changes, that could explain the jump. Therefore the jump probably relates to statistics. See Sec. 5.3.4 how the statistics (i.e. randomness) is dependent on the length of the window.

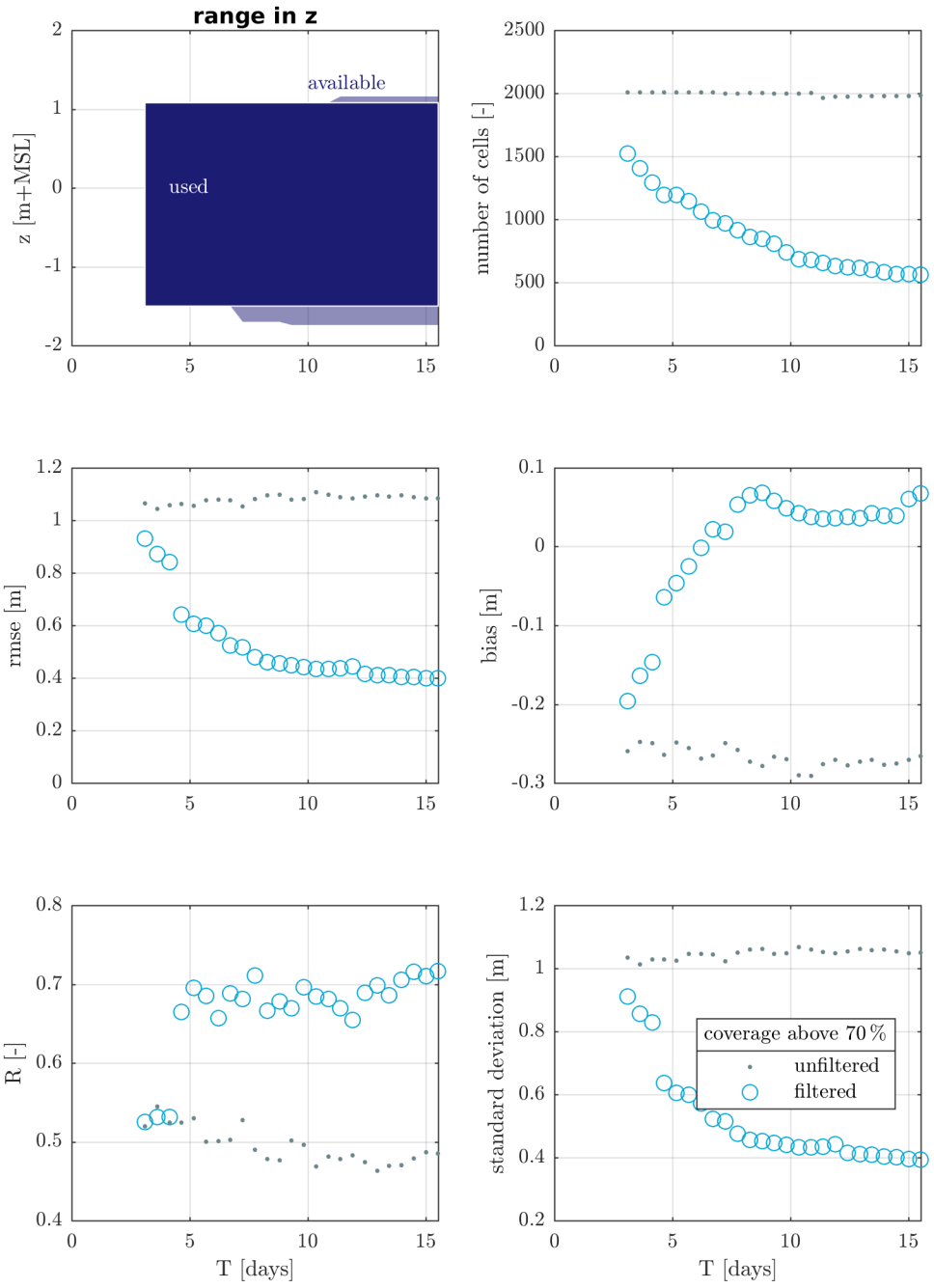

Figure A.11: error measures for different analysis windows - equal z range **top left:** all RDBs are cut to the same z grid in order to ensure comparability. This figure supports the choice made in Sec. 5.3.3. **coverage:** number of records over possible records (assuming one record each 30 min) in percent **data:** RDB derived in steps of one tidal cycle (12 hr and 25 min) centered around May 16, 12:00, 2018 with maximum period covered from May 6, 4:30 to May 26, 20:30

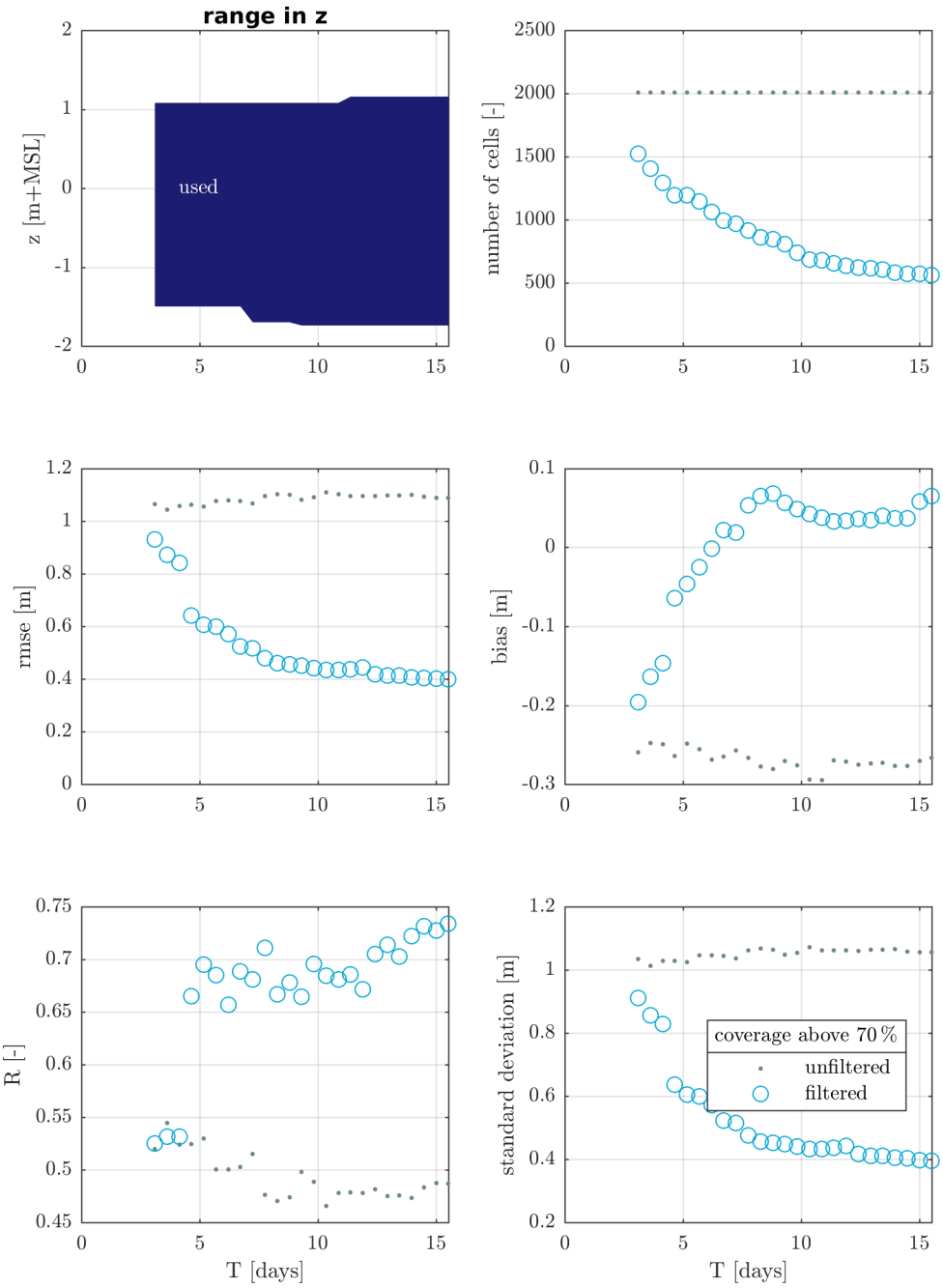

Figure A.12: error measures for different analysis windows - varying z range **top left:** in this case no z values are cut-off. It makes no difference in comparison to an equal z range as can be seen by the almost unchanged number of cells in the top right frame (as compared to Fig. A.11) **notes:** No other additional information as compared to Fig. A.11 other than that the choice of z range is not important in this case. This figure supports the choice made in Sec. 5.3.3. **coverage:** number of records over possible records (assuming one record each 30 min) in percent **data:** RDB derived in steps of one tidal cycle (12 hr and 25 min) centered around May 16, 12:00, 2018 with maximum period covered from May 6, 4:30 to May 26, 20:30

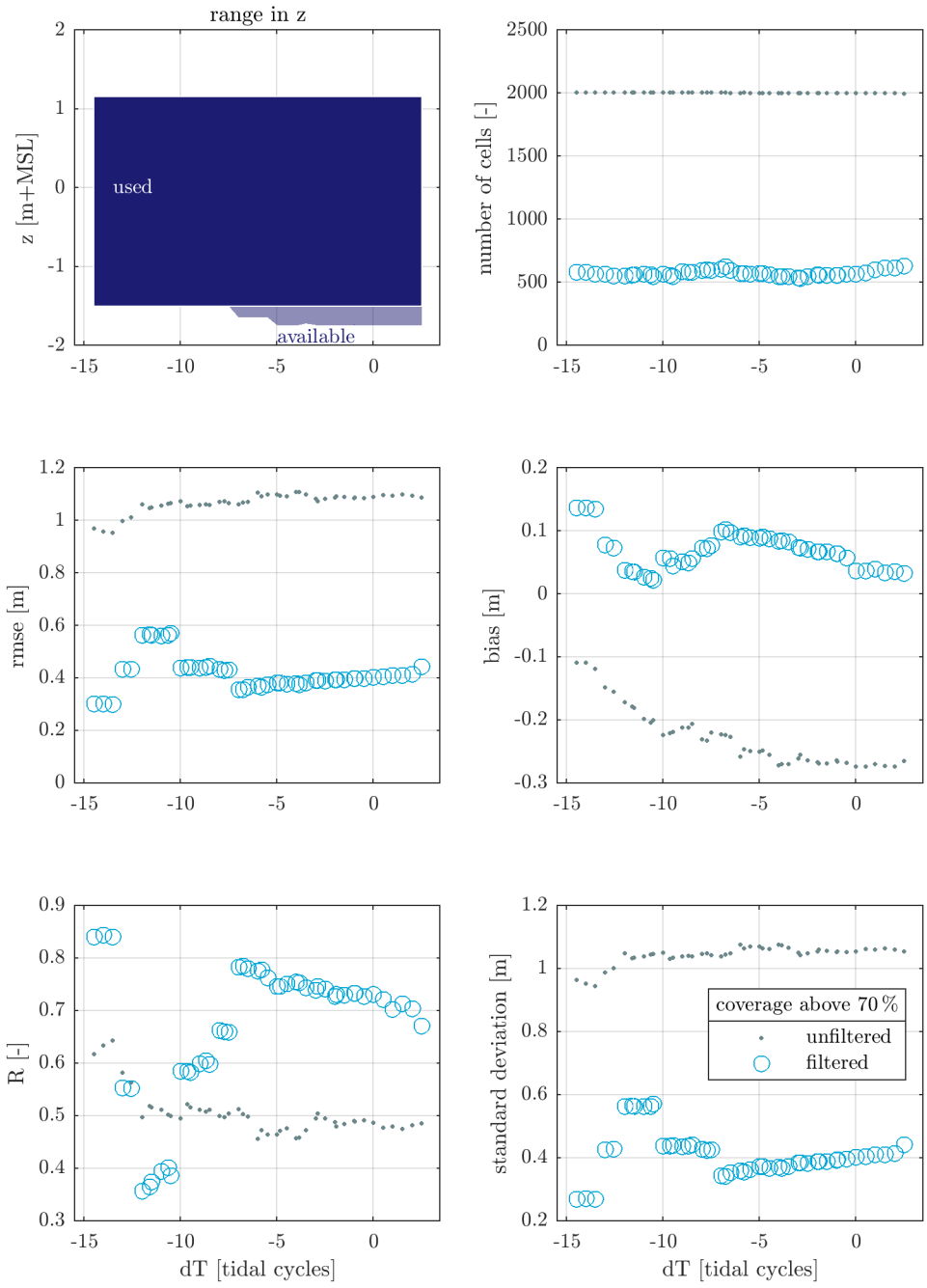

Figure A.13: error measures for shifted analysis window (28 tidal cycles long) - equal z range **top left:** all RDBs are cut to the same z grid in order to ensure comparability. This figure supports the choice made in Sec. 5.3.3. **coverage:** number of records over possible records (assuming one record each 30 min) in percent **data:** RDB derived in steps of half a tidal cycle (half of 12 hr and 25 min) centered around May 16, 12:00, 2018 with maximum period covered from May 6, 4:30 to May 26, 20:30

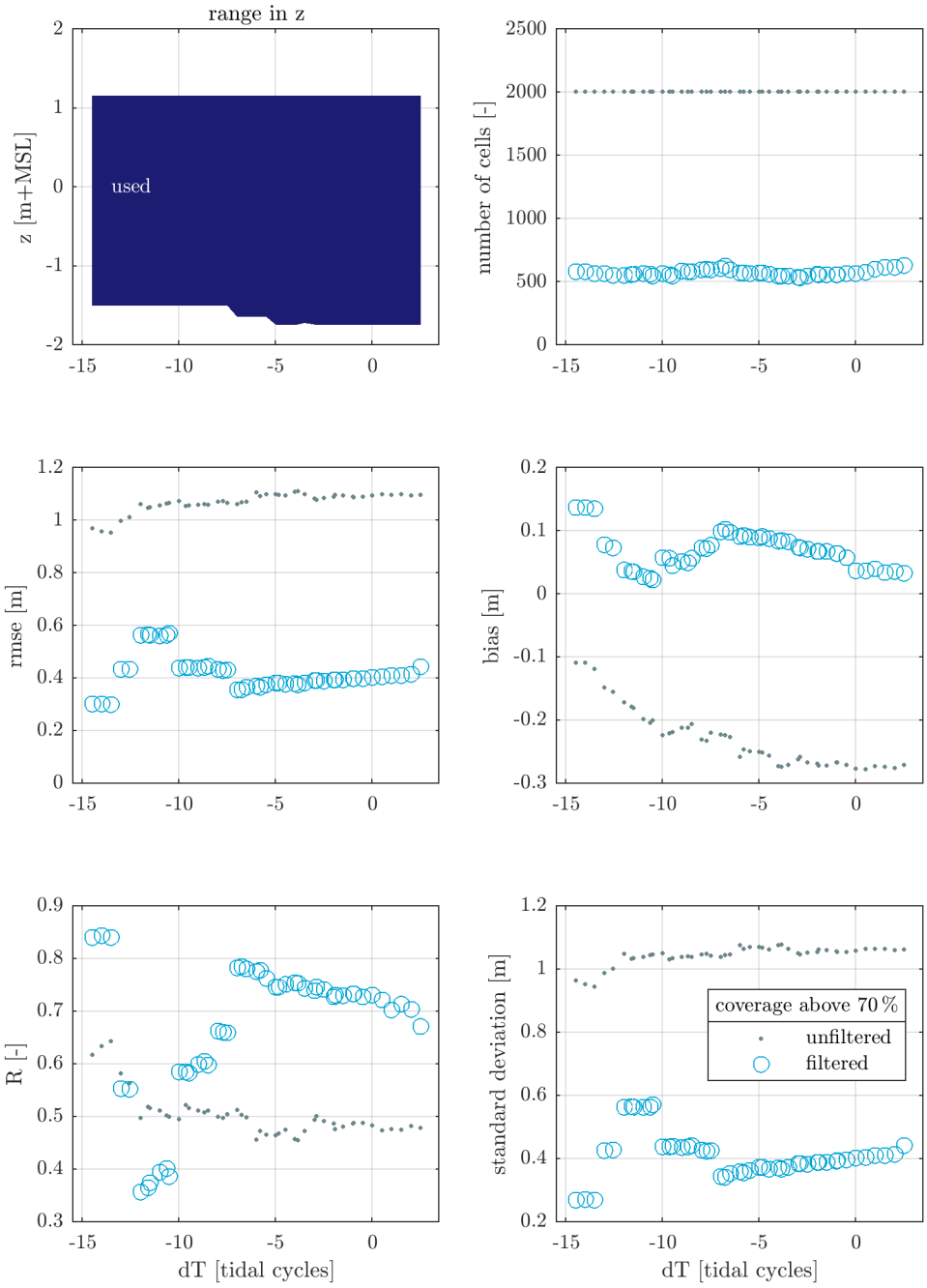

Figure A.14: error measures for different analysis window (28 tidal cycles long) - varying z range **top left:** in this case no z values are cut-off. It makes no difference in comparison to an equal z range as can be seen by the almost unchanged number of cells in the top right frame (as compared to Fig. A.13) **notes:** No other additional information as compared to Fig. A.11 other than that the choice of z range is not important in this case. This figure supports the choice made in Sec. 5.3.3. **coverage:** number of records over possible records (assuming one record each 30 min) in percent **data:** RDB derived in steps of half a tidal cycle (half of 12 hr and 25 min) centered around May 16, 12:00, 2018 with maximum period covered from May 6, 4:30 to May 26, 20:30

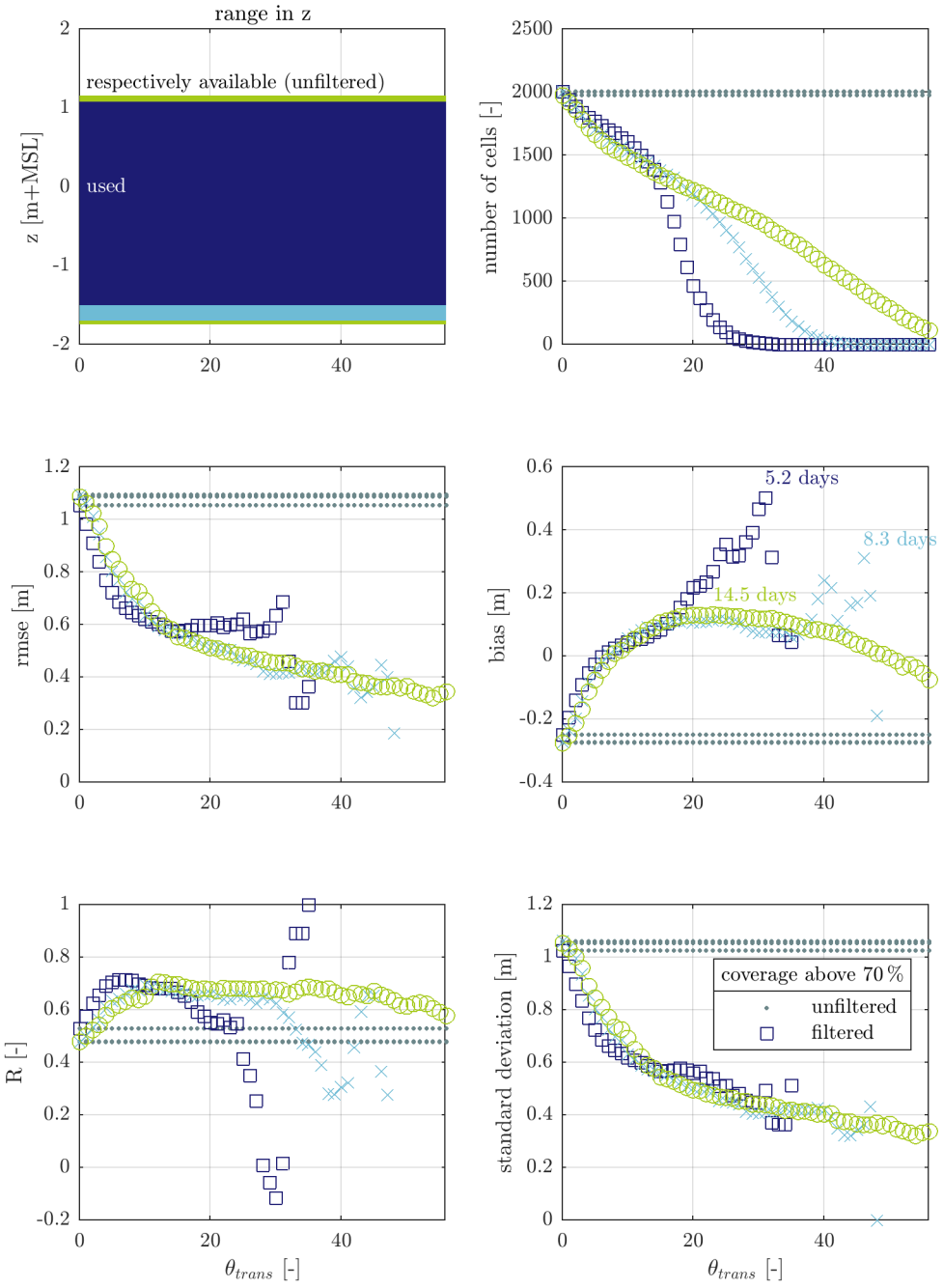

Figure A.15: error measures for increasing θ_{trans} - equal z range **top left:** all RDBs are cut to the same z grid in order to ensure comparability **top right:** depending on the window length there is a maximum number of potential transitions, which is twice per tidal cycle. Therefore the three curves approach zero for about twice their lengths in tidal cycles. **coverage:** number of records over possible records (assuming one record each 30 min) in percent **data:** RDB presented in three different window length: 28, 16 and 10 tidal cycles (about 14.5, 8.3 and 5.2 days) around May 16, 12:00, 2018 with maximum period covered from May 9, 6:30 to May 22, 1:30

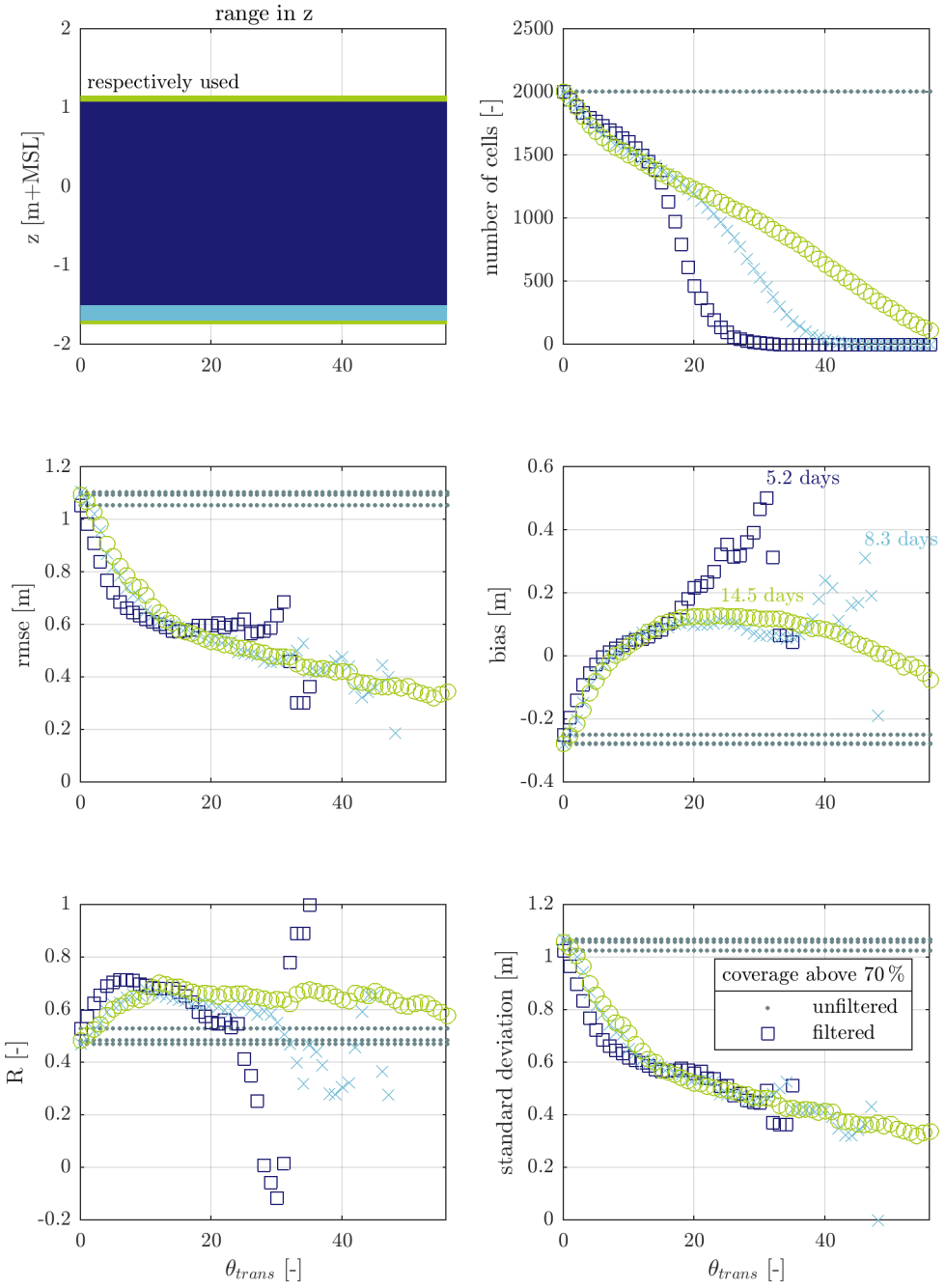

Figure A.16: error measures for increasing θ_{trans} - varying z range **top left:** in this case no z values are cut-off. It makes no difference in comparison to an equal z range as can be seen by the almost unchanged number of cells in the top right frame (as compared to Fig. A.15) **coverage:** number of records over possible records (assuming one record each 30 min) in percent **data:** RDB presented in three different window length: 28, 16 and 10 tidal cycles (about 14.5, 8.3 and 5.2 days) around May 16, 12:00, 2018 with maximum period covered from May 9, 6:30 to May 22, 1:30

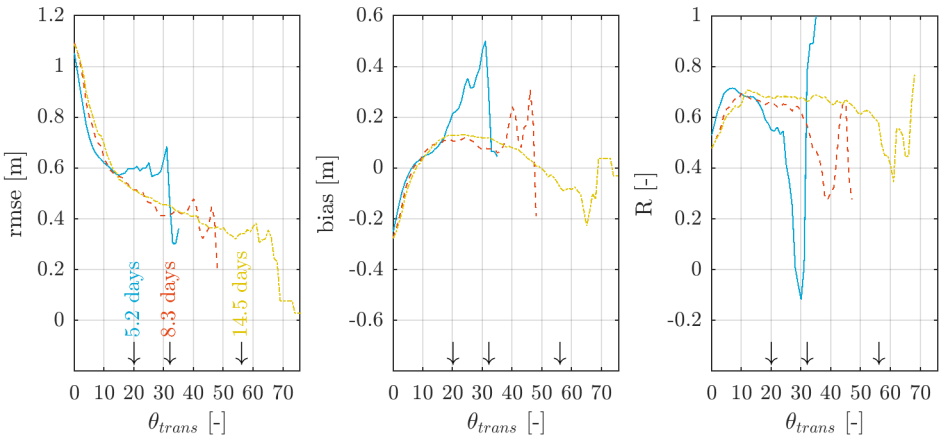

Figure A.17: sensitivity of filtering by number of transitions without cutting at possible maximum number of transitions. Lines end where filtering removes all cells. **colors:** length of analysis window **arrows:** indicate maximum number of transitions possible, given a semi-diurnal tide and (theoretically) two transitions per tide **data:** RDB centered around May 16, 12:00, 2018 with maximum period covered from May 9, 6:00 to May 23, 18:00, 2018

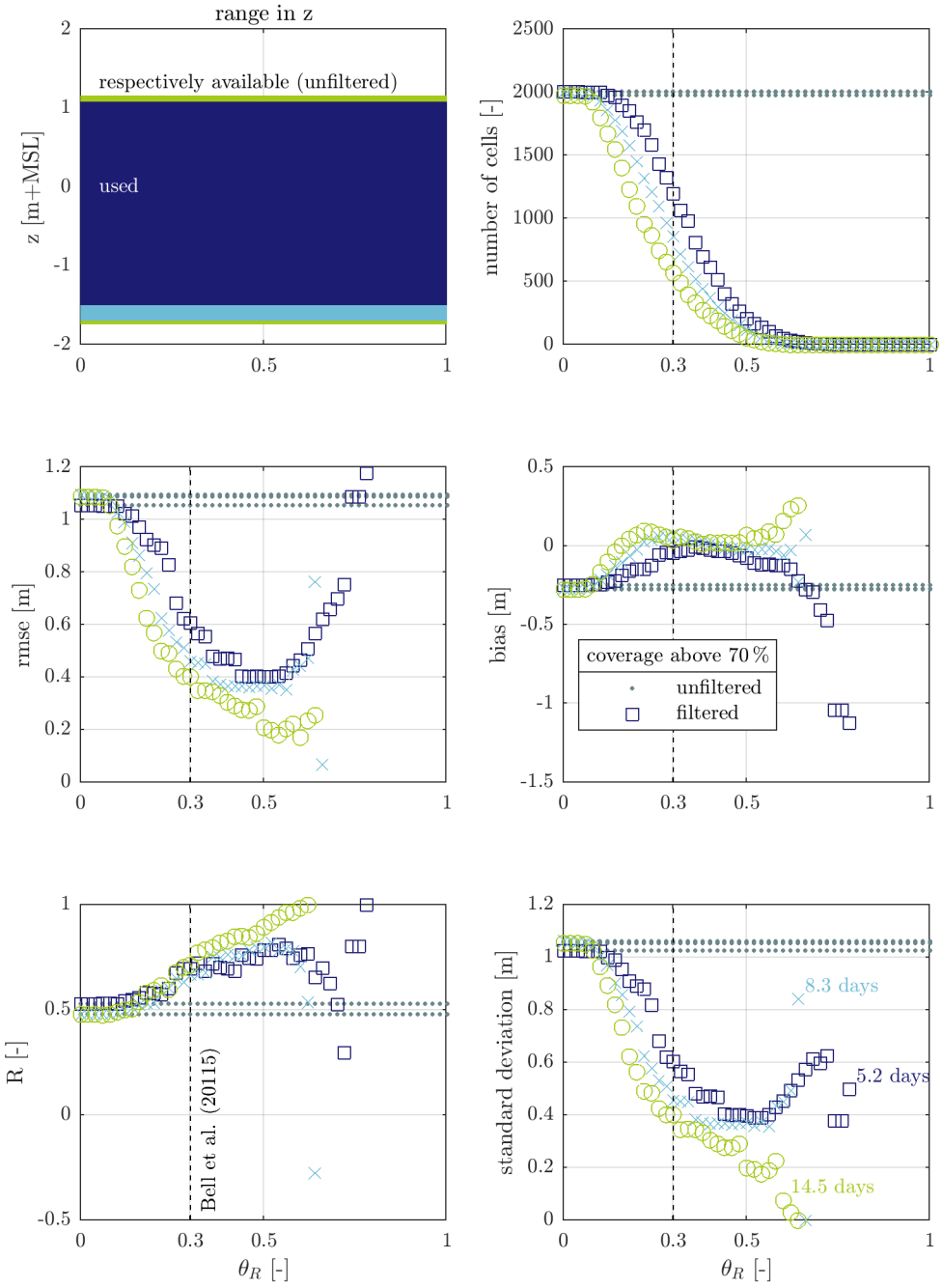

Figure A.18: error measures for increasing θ_R - equal z range **top left:** all RDBs are cut to the same z grid in order to ensure comparability **top right:** with increasing θ_R more cells are filtered. The deviations between the three curves indicate that the overall correlation of one RDB depends on the window length T **coverage:** number of records over possible records (assuming one record each 30 min) in percent **data:** RDB presented in three different window length: 28, 16 and 10 tidal cycles (about 14.5, 8.3 and 5.2 days) around May 16, 12:00, 2018 with maximum period covered from May 9, 6:30 to May 22, 1:30

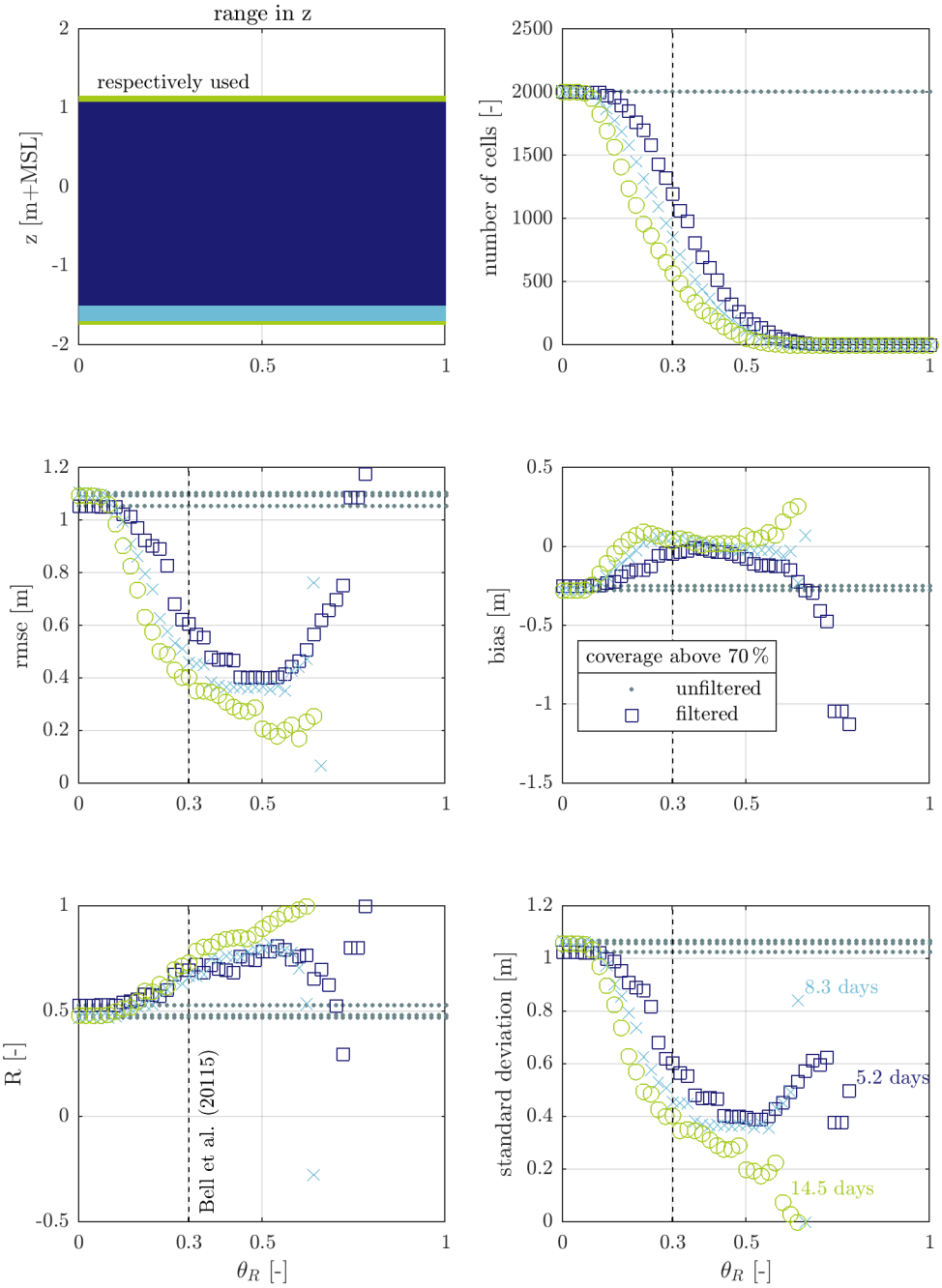

Figure A.19: error measures for increasing θ_R - varying z range **top left:** in this case no z values are cut-off. It makes no difference in comparison to an equal z range as can be seen by the almost unchanged number of cells in the top right frame (as compared to Fig. A.18) **top right:** with increasing θ_R more cells are filtered. The deviations between the three curves indicate that the overall correlation of one RDB depends on the window length T **coverage:** number of records over possible records (assuming one record each 30 min) in percent **data:** RDB presented in three different window length: 28, 16 and 10 tidal cycles (about 14.5, 8.3 and 5.2 days) around May 16, 12:00, 2018 with maximum period covered from May 9, 6:30 to May 22, 1:30

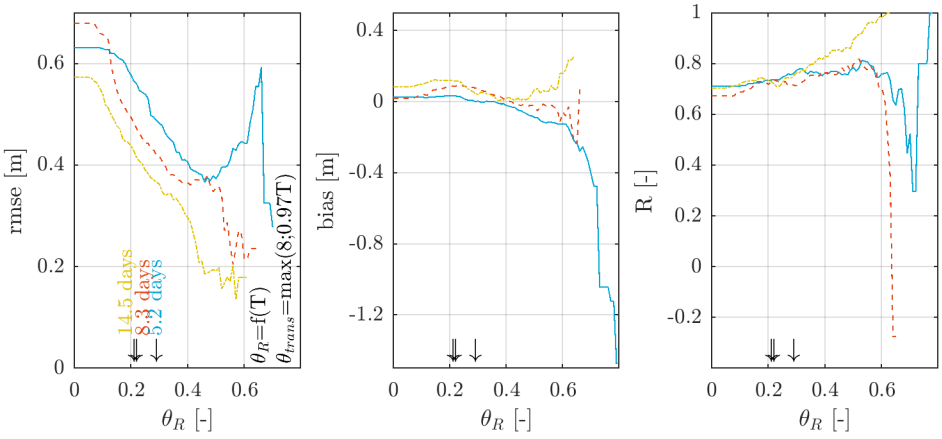

Figure A.20: sensitivity of filtering by correlation without cutting. Lines end where filtering removes all cells. **colors:** length of analysis window **arrows:** indicate maximum correlation found in reference window for estimation of θ_R according to Eq. 4.4 **data:** RDB centered around May 16, 12:00, 2018 with maximum period covered from May 9, 6:00 to May 23, 18:00, 2018

offset [m]:	x	y	z (rmse)
May 15, 2018	19.80	-2.07	5.51 (0.0322)
May 16, 2018	19.48	-1.71	5.49 (0.0805)
May 17, 2018	*no stationary measurement available*		

Table A.5: three-dimensional offsets for sledge data

A.5. Three-dimensional Offset of Sledge Data

The raw sledge data is shifted in space, yet in itself consistent. The recorded tracks cover a period of less than three days, May 15 to May 17, 2018. Offsets in all three spatial dimensions are needed to correct the sledge signal. In horizontal dimensions this is achieved by comparing stationary measurements of the wheelbarrow and the sledge. Mathematically speaking this is the bias between both. Both devices were positioned after each other on the same spot. The horizontal offsets are calculated as the difference of the sample means, thus the bias:

$$\text{offset in x: } \mathrm{bias}(x_s) = \overline{x}_s - \overline{x}_w \tag{A.1}$$

$$\text{offset in y: } \mathrm{bias}(y_s) = \overline{y}_s - \overline{y}_w \tag{A.2}$$

Indices s and w denote sledge and wheelbarrow respectively. The coordinates x and y refer to the local coordinate reference system BH-CRS (see Sec. 3.1). Uncertainties in the vertical direction are larger. Therefore the effort is made to find the vertical offset by minimizing the rmse, instead of sibtracting mean values.

$$\mathrm{rmse} = \sqrt{\overline{(z_s - z_w)^2}} \tag{A.3}$$

The height z is in reference to the MSL geoid. Any sample mean (denoted with an overbar) is calculated as:

$$\overline{x} = \frac{1}{n}\sum_{i=1}^{n} x_i \tag{A.4}$$

The number of samples n is different between sledge and wheelbarrow. For the horizontal offsets the difference in sample size is irrelevant, because both tracks are long enough and sample the same position. But for the vertical offset it is necessary to have the same number of samples. Vertical coordinates of sledge and wheelbarrow are therefore paired in a kind of nearest neighbours approach. This way the rmse can be determined. For each sledge datapoint all datapoints from the wheelbarrow are found that are within a search radius of 0.3 m around the sledge datapoint. Each of the wheelbarrow datapoints is paired with the current sledge datapoint. Related rmse over vertical offset is presented in Fig. A.21. All offsets are summarized in Tab. A.5. The difference in rmse of the vertical offset is related to the datasets. For May 15, 2018 the pairs mainly consist of paths, that the wheelbarrow exactly followed the sledge. It is therefore expected, that the rmse is low. Whereas for the next day, May 16, 2018 the wheelbarrow and sledge data cover the same area, but do not walk on the same paths. This causes a higher rmse, yet it is still good enough for the validation. The offsets are subtracted from the recorded signal of the sledge:

$$\mathrm{sledge}_{\mathrm{corrected}} = \mathrm{sledge} - \mathrm{offsets}$$

Stationary tracks as well as their summary statistics are presented in Fig. A.22 and Tab. A.6. Standard deviations indicate precision.

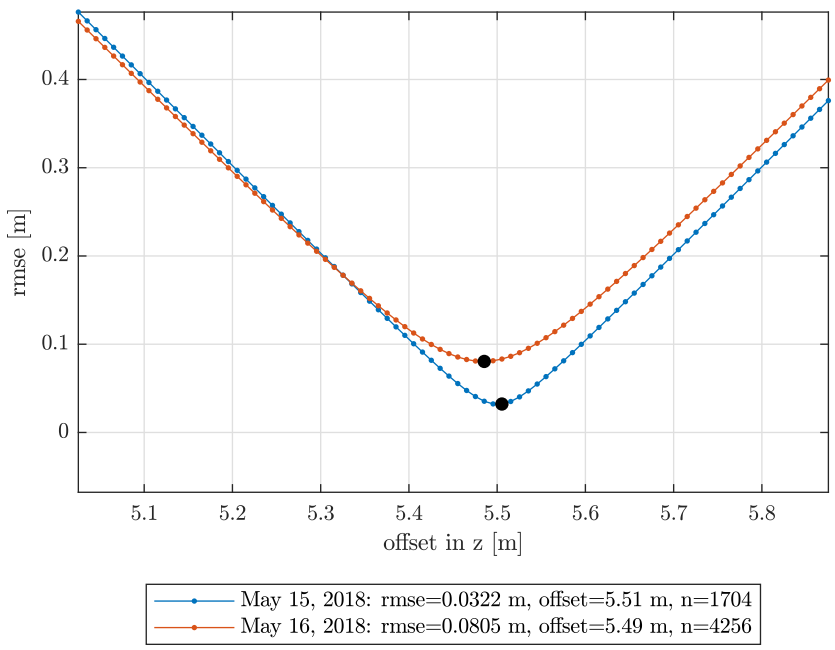

Figure A.21: vertical offset in the sledge data in relation to rmse **data:** May 15 and 16, 2018 as presented in Sec. 3.2

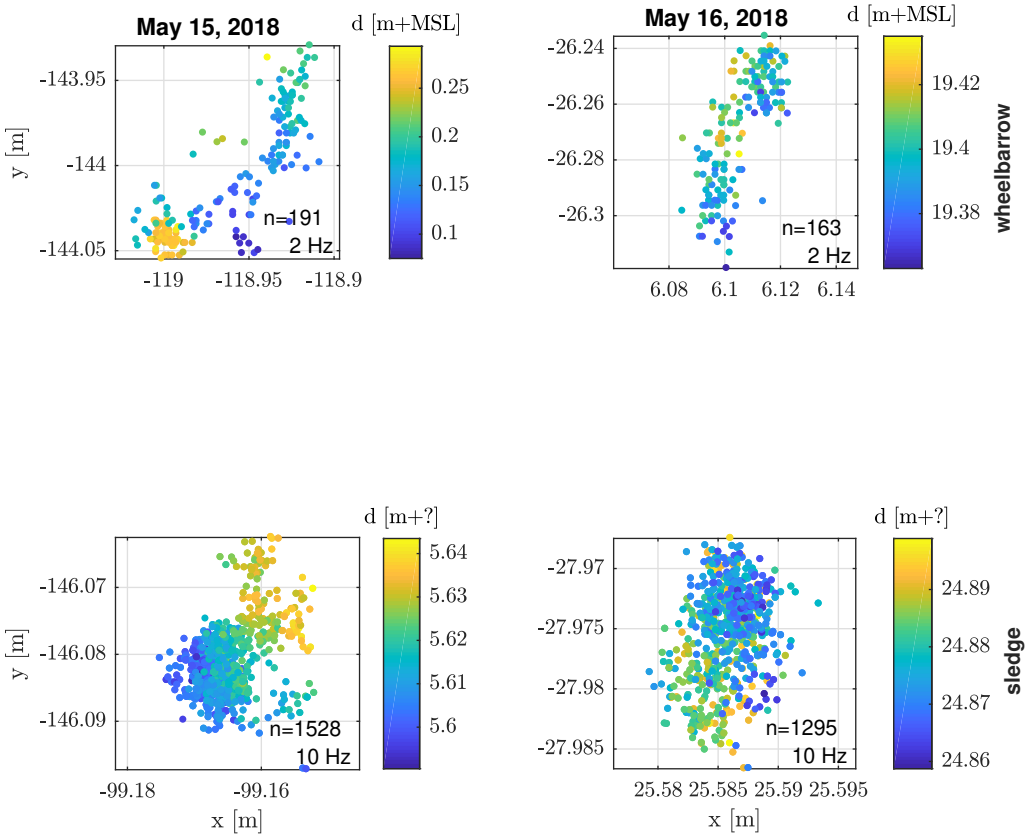

Figure A.22: stationary measurements used for the calculation of sledge offsets **data:** May 15 and 16, 2018 as presented in Sec. 3.2

			May 15, 2018		May 16, 2018	
			wheelbarrow	sledge	wheelbarrow	sledge
x	mean	[m]	-118.962	-99.165	6.106	25.586
	median	[m]	-118.958	-99.166	6.105	25.586
	st. dev.	[m]	0.033	0.004	0.009	0.002
y	mean	[m]	-144.010	-146.081	-26.270	-27.975
	median	[m]	-144.022	-146.082	-26.263	-27.975
	st. dev.	[m]	0.035	0.005	0.020	0.004
z	mean	[m]	0.188	5.613	19.398	24.878
	median	[m]	0.179	5.611	19.397	24.877
	st. dev.	[m]	0.056	0.011	0.013	0.008

Table A.6: summary statistics of stationary measurements used for the calculation of sledge offsets

	min	mean (median)	max	standard deviation
R_2 [m]	0.15	0.42 (0.35)	1.06	0.23

Table A.7: summary statistics of wave related setups R_2

A.6. Input Data for WLM-updated

The choice of data sources as input for R_2 (Eq. 2.3) is guided by decisions described in Blossier et al. [2016]. See Fig. A.23 for reference to the data. Note that the period in the investigated two weeks is more limiting to the range of application than the wave height. Given a constant beach slope in time, it is in general the combination of wave period and height (so-called wave steepness) that indicates validity of the formulation (beach slope and wave steepness yield Irribarren number ξ, Eq. 2.1). During grey shaded periods the stretch of Sylt beach cannot be regarded as intermediate beach and the R_2 should not be calculated with Eq. 2.3. Tab. A.7 lists the summary statistics of the calculated R_2.

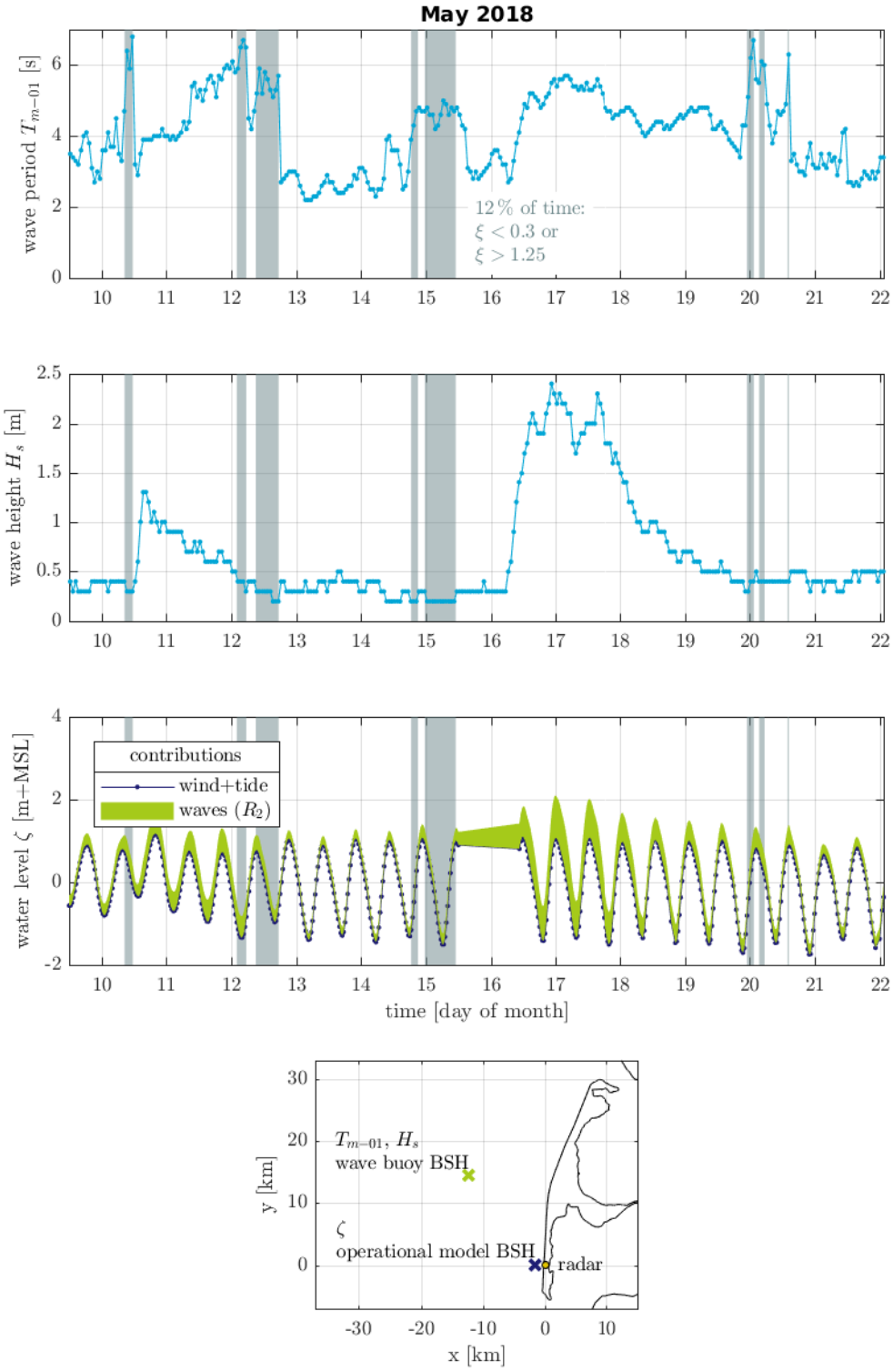

Figure A.23: wave characteristics and water level used in WLM-updated **top three:** wave characteristics and water level **bottom:** map of stations **data:** wave characteristics (at about 14 m depth) and water level from BSH, May 9, 12:00 to 22, 2:00, 2018, map based on openstreetmap.org